SOME ADVANCES IN

OPTICAL CONTOURING OF DIFFUSE OBJECTS USING

MOIRE AND SPECKLE TECHNIQUES

by

Ramon Rodriguez-Vera

A Doctoral Thesis
submitted in partial fulfilment of
the requirements for the award of
Doctor of Philosophy
of the
Loughborough University of Technology

April 1993

Supervisors: Drs. D. Kerr and F. Mendoza-Santoyo
Department of Mechanical Engineering

TO THE MEMORY OF MY MOTHER

MARIA LUISA VERA DE RODRIGUEZ

SYNOPSIS

Optical contouring is a full field, non-contact technique capable of determining shape and deformation data from 3-D surfaces. The data, which are obtained from the optical contouring system, represent the surface geometry at evenly sampled points. The main objective of this thesis is to report some advances achieved by the author in the optical contouring field. Conditions for the design and construction of optical systems to measure object topography and deformation using the same hardware, as well as the optical working methodology and system parameters, are analysed.

The conventional in-plane and out-of-plane optical setups for displacement sensitive ESPI systems are employed to contour. The contour maps are obtained by giving small displacements to optical fibres carrying the object and reference beam illumination. A rigorous mathematical treatment of shape contours generated by ESPI is given. It is experimentally verified that the fringe patterns produced are identical to projected fringe contours, and may be analysed in the same way. Then, practical systems which combine deformation and shape measurement in both in-plane and out-of-plane ESPI configuration are demonstrated.

Comparison is made with shape measurement using two fringe projection moiré techniques. The first moiré technique uses electronic demodulation to obtain the contour maps. This technique encodes and analyses moiré contours by using an electronic system similar to that used for Electronic Speckle Pattern Interferometry (ESPI). Hence automatic fringe detection and contour measurement is possible.

The Talbot effect, where the self imaging of a periodic object is used as second moiré technique. The Talbot image of a linear grating is imaged on the target surface. The grating lines are deformed according to the surface shape. Viewing this deformed grating image through a second reference grating, generates contour maps. A novel on-axis sensor which directly measures distance as a direct colour mapping is introduced.

It is emphasized that all the techniques researched here can be extended to be applied as industrial tools for surface inspection or quality control. Phase-shift measurement and digital image processing are employed for data reduction.

ACKNOWLEDGEMENTS

I would like to express my sincere appreciation to Dr. D. Kerr for his supervision, patience and guidance. His help in resolving many difficulties which occurred during this work and valuable discussions and remarks are highly acknowledged.

I am deeply indebted to Dr. F. Mendoza-Santoyo for his supervision, advice, help and encouragement at every stage during the progress of my research work and in the preparation of the manuscript of this thesis. His invaluable suggestions and comments helped me considerably in the development of the work presented here. He has always been friendly and cooperative and his readiness to assist me at all times has been remarkable.

My special thanks for Dr. J.R. Tyrer, my director of research for his continuous encouragement during the development of this work.

I would like to express my sincere thanks to all Optics Group members of the Department of Mechanical Engineering for their help and cooperation. In particular to Prof. N.A. Halliwell Head of the Group and Head of the Department for his support and help on a number of occasions.

I would like to thank Mr. K. Topley and Mr. V. Scothern for producing the photographic material, Mrs. J. Redman for the line drawings, and Mr. T. West and Mr. B. Cooper for the electronic assistance.

I also want to thank Prof. G. Kaufmann for his friendship and valuable discussions and help.

I wish to thank Centro de Investigaciones en Optica, through its General Director, A. Morales, for granting my study leave and Consejo Nacional de Ciencia y Tecnologia of Mexico for awarding a scholarship to pursue the research programme.

I also wish to take this opportunity to express my gratitude to my father, brothers and sisters for their encouragement and prayerful blessing for my welfare and success. I am deeply grieved for the death of my mother in my absence from Mexico, who had always wished for my higher education but can no longer witness this thesis; my ultimate gratitude.

Early days in England were too hard for me and my family, but with the help and friendship of Mr. Jim Pitts we overcame that situation. I am profoundly grateful to him and his wife Joan.

My wife, Dr. Maria Georgina Cervantes, stood beside me with kindness and love during all aspects of this thesis and during hard times which extended along this work. I will always be indebted and grateful to her.

Finally I would like to apologize to my sons Victor and Miguelito for not having spent the time I should have spent with them. I thank them for not reproaching this to me. This is for them and my wife that this thesis is dedicated.

Introduction

In the last two decades, optical metrology has increased its applications in many fields of science and engineering. Several physical magnitudes may be measured by optical methods. These can be put in two groups: dynamic and static measurements. Examples of dynamic measurements include flow conditions, vibration, and convection. Displacement, torsion, refractive index, and pressure changes are among the static measurements. The measurement is usually made on a fringe pattern which is produced from the interference between two or more wavefronts or by the combination of two periodic structures. This fringe pattern is closely related with a general phase change produced, in some cases, by changing the optical path. Normally, this phase change is connected with the physical magnitude to be measured. A quantitative description of the measurement may be displayed as a wire-frame isometric plot. This must be scaled with reference to some plane fixed in space. However, one major constraint which is at present preventing a more widespread industrial application of the optical techniques, is the inherent complexity of the data produced, creating a requirement for specialised analysis skills in interpretation of fringe patterns. For example, most engineering objects are not flat, but the TV picture produced by the system is a 2-D version of 3-D scene, therefore a perspective shortcoming in the object's field of view is obtained. Some structures (e.g., automobile engines) have disjunctures in their surface where in a part may move independently of the other one making a big problem for fringe analysis. Some interpretation ambiguities are also found when a displacement to be measured is several orders of magnitude larger than the sensitivity interval of the instrument. In order to remove such ambiguities of perspective and disjunctures and relay deformation to position on the

surface, is necessary to have an a priory knowledge of the surface shape. Furthermore, it is advantageous to combine the surface form and displacement measurement capability in a single instrument, where the complete 3-D amplitude vector is determined.

One way to obtain object shape information is by producing a contour map of its surface using optical metrology. Holographic, speckle, and moiré interferometric techniques are well suited for contouring. Together with the opto-electronic equipment for information capture and micro-computers with large data reduction capabilities, these techniques have the potential to be used as quantitative measurement tools.

Contouring is used in a wide range of applications, most of which are distinct from analysis of the physical magnitudes mentioned above. From a contour map, the topographic characteristics of the target are obtained which can be applied in general areas such as On-line inspection, Robotics, Medical diagnostics, and Solid modeling. It is useful to consider current applications of contouring in order to design a modified interferometer for displacement analysis.

The objective of this thesis is to create optical systems with a built-in contouring facility, which may then be used in engineering measurement of diffuse surfaces, or in shape determination, without any optical hardware modifications. Some advances in the optical contouring field are therefore presented. Moiré and speckle contouring techniques are investigated for improving absolute and comparative shape measurement. In order to update the techniques studied, moiré and speckle contour techniques are briefly revised in the first chapter.

A novel approach on moiré techniques for absolute shape measuring is presented chapter 2. This approach is based on the Talbot effect, i.e., the imaging of a periodical structure without using optical systems. A Talbot image of a linear grating is formed on the target surface. The grating lines are deformed according to the surface shape. Demodulation is carried out using a second grating obtaining depth contours. These contours are analysed to determine the shape of the surface. A phase shifting technique is employed for data reduction. It is demonstrated that this technique has a wide depth measurement range, from micrometers to centimeters.

One important characteristic of the last method is the dependence of the Talbot plane position with respect to the wavelength illumination beam. This special feature is employed for associating colour to different depth planes on the target surface. This fact is analysed in detail in the same chapter two. The detection is made by producing a coloured moiré pattern. Then each colour on the moiré pattern correspond to a determined depth on the target surface.

Another contribution made by the author on moiré techniques is dealt in chapter 3. Moiré patterns are obtained using electronic demodulation. This technique has been called Electronic Moiré Contouring (EMC). The novelty of the EMC technique lies in the electronic hardware, which is built up with a A/D converter, a digital storage device, an image subtractor, a D/A converter, a video amplifier, and a band pass filter. Placing all parts together, is constructed a electronic device capable of producing moiré contours when the target surface with projected fringes is compared between two states. Furthermore, plugging the electronic device to a computer with fringe analysis and

phase shifting measurement facilities, the EMC technique gives the possibility of surface inspection with extended application in surface quality and deformation measurements in a quick fashion.

Chapter 4 deals with in-plane and out-of-plane sensitive optical ESPI instruments which are employed to measure shape without alterations to the optical set-up. The shape measurement of three-dimensional diffuse objects is achieved when small displacements to the optical fibres carrying the object and reference beam illumination are introduced. For this, special attention is devoted to the theoretical analysis. An important new interpretation to the generated contours is given by the author. It is demonstrated that the fringe patterns produced are identical to projected fringe contours. The theory is supported by good agreement with experimental results and the fringe contours may be analysed using digital image processing and phase shifting techniques.

Finally, in chapter 5, on the basis of merit and limitations, the work is completed with a discussion of the contributions made to the optical contouring field. General analysis of the techniques studied are given and ideas for future work are recommended.

CONTENTS

APPENDIXES

CHAPTER 1

Survey on moiré and speckle contouring techniques

1.1 Introduction

There are several optical non-destructive testing methods for measuring absolute and comparative surface shape [Varner (1974) and Jones & Wykes (1983)]. These work by generating fringes over the target surface, which are called contours. Contour generation may be separated into 'Grid' and 'Depth' contours. Grid contour are generally sets of parallel fringes superimposed on the image of the target and spatially modulated by the target surface shape. Depth contours represent parallel planes in space perpendicular to the line of sight. They are useful in that they describe areas of constant target surface height, analogous to contour lines on a map. The distinctive advantage of such methods compared with profilers [Creath & Morales (1992)] is the provision of information over the full field of view in one image; overall features of the surface can immediately be assessed in addition to making detailed measurements. Moreover, no physical contact with the target surface is made, and all of the methods work with diffuse surfaces.

Present contouring techniques are studied in this chapter with the objective of evaluating their relative merits and limitations, justifying the choice of the most appropriate systems for shape measuring and adopting for this work and improve them. This first chapter deals then with a survey on optical contouring methods where moiré and speckle techniques are included.

Recently, dramatic advances have been made in the

different ways of capturing and reducing data from these techniques [Malacara (1992)]. These advances have been achieved mainly with the better availability of cheap micro-computers, CCD cameras and digital image processing software for fringe analysis. In order to support the contour fringe analysis method employed in this thesis, a section, where different methods are evaluated, is also included in this chapter.

1.2 Moiré methods

The term "moiré" derives from the French word moiré meaning waved or watered. Moiré patterns are seen in the shimmering silk fabric produced by the Chinese in ancient times. In Japan, moiré fabrics are still used as silk gauze for Summer clothing. Moiré patterns are visible in everyday life; two sets of railings on a bridge may produce a moiré pattern when they are observed from certain direction. On the TV screen a subject which possesses a line pattern motif similar to the TV raster can result in a moiré pattern.

Fig. 1.1 shows the moiré pattern produced by two identical straight line gratings rotated by a small angle θ relative to each other. A dark fringe is produced where the dark lines for one grating fall on top of the corresponding light lines for the second grating. If the angle between the two gratings is increased, the separation between the bright and dark fringes decreases [Nishijima & Oster (1964)].

Moiré metrology is based on the superposition of two gratings. Normally one of the gratings (test grating) is distorted, the distortion being produced by the target under study. Generally the distortion is to an extent

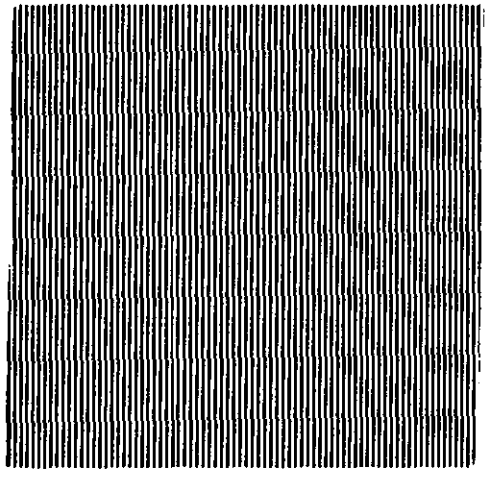

Figure 1.1a
Straight-line grating.

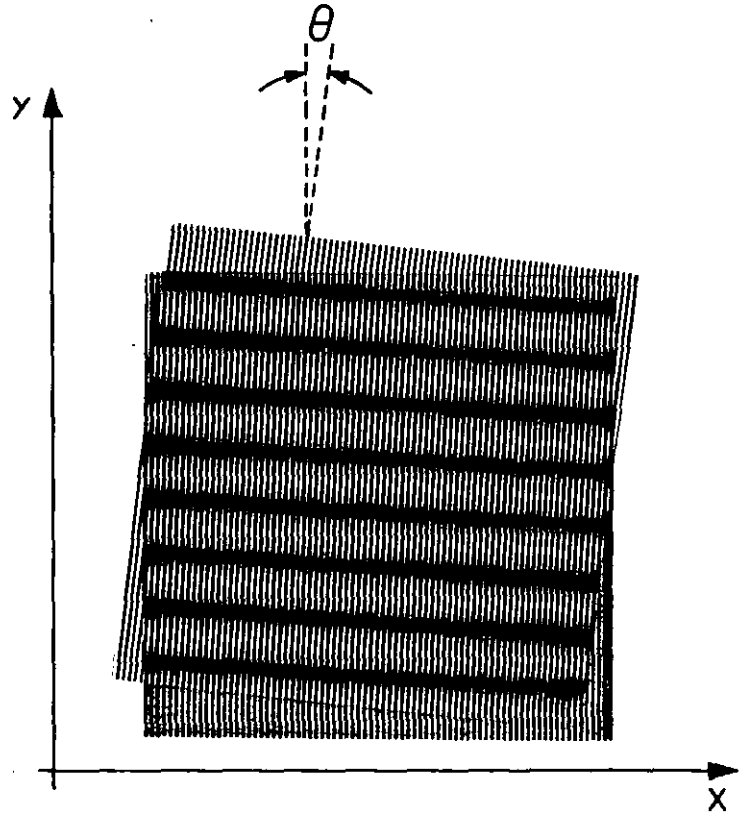

Figure 1.1b
Moire between two straight-line gratings of the same period at angle θ with respect to one another.

linearly proportional to the quantity to be measured. The other grating (reference grating) is undistorted. There are several approaches in moiré metrology. Excellent reviews have been published on the subject [Burch (1963), Theocaris (1969), Durelly & Parks (1970), Reid (1984), and Kafri & Glatt (1990)]. Here, the different contouring moiré approaches will be briefly described, paying particular attention to those techniques which have been applied to absolute and comparative shape and displacement measurement.

1.2.1 Optical interference fringe projection

Using a combination of moiré fringe techniques with interferometric projection offers considerable potential for precision measurement through vision systems. The subject has attracted much attention particularly in a gauging context. Earlier work by Rowe & Welford (1967) and Brooks & Heflinger (1969), describes a possible optical arrangement. An interferometric scheme to illuminate the target with two nearly parallel beams of laser light derived from a single laser source is employed. The area where the two beams overlap represents parallel planes of light in space which coincide with points of constant phase difference between the two beams. The planes for which the beam phases differ by π are planes of reduced intensity and have been named as projected fringe surfaces (like projection moiré contouring) [Shamir (1973)]. A target surface illuminated by the two beams will be intersected by lines of low illumination intensity. Grid contours delineating the lines of intersection between the target surface and the family of planes in space separated by its period may thus be observed. Additional work by other authors has been published [Butters, et al. (1980) and Varman (1984)]. These attempted to adapt the method as a

computer based measurement sensor with a good success.

Varman's technique is used in an on line measuring sensor and compares the contour lines described above with a similar set of contours (the reference pattern) generated on an target of known shape. The reference pattern may be formed optically using a real target or generated numerically from design data, which may be the preferred method for CAD/CAM users [Morshedizadeh & Wykes (1989)]. In either case the reference pattern is stored digitally on a video store, for instance in the case of computer generation by direct data input and in the case of optically generated contours through a television camera interface and digitizer. Next, the target under test is observed using exactly the original illumination geometry. The digitized data is electronically subtracted from the reference pattern producing a system of moiré-type fringes. In the case where the test surface exactly replicates the form and position of the reference surface, no fringes will be observed, a situation which can be used for initial commissioning of the measuring rig. Hence the method operates as a comparator since geometrical data from a real surface is involved.

Recently, phase measuring profilometry through interference fringe projection has been reported [Mercer & Behein (1990), Rosvold (1990), and Chang & Wan (1991)]. Fast and accurate computation of the spatial phase distribution has been done in order to increase the efficiency and accuracy of the technique. However, since collimated beam illumination is employed for fringe projecting, there is a limitation of the technique in respect to the target size to be tested; i.e., it must be at least the same size as the collimated field.

1.2.2 The holographic moiré method

Hildebrand and Haines (1967) worked on a double-exposure holographic method in which the object illuminating beam was tilted between exposures. The fringes appearing on the reconstructed image were equivalent to Young's fringes modulated by the target shape. These fringes represented grid contours. Abramson (1976) used a sandwich hologram with plane-parallel glass plates to obtain depth contours whose reference plane may be arbitrarily chosen. In this method the modulated Young's fringes produced by tilting the illumination beam were demodulated by tilting the sandwich hologram in the reconstruction step, producing moiré-type fringes. Then the contour reference planes can be arbitrarily oriented, just rotating the sandwich hologram. The method requires a lot of care in handling the optical setup and plane plane-parallel holographic plates are required to make sandwich holograms that render expected shape fringes.

Yonemura (1982) and Sciammarella (1982) suggested a double-exposure holographic method that uses a single holographic plate for obtaining depth contours. This double-exposure method includes translation of the illumination source and the holographic plate between exposures. Translation of the illumination beam produces Young's fringes which are modulated by the target shape. Demodulation is made by the translation of the holographic plate.

More recently, Rastogi and co-workers (1984 and 1990) were able to obtain holographic depth contours in real-time by using two symmetrical object illumination beams. The method is based on the principle of four-wavefront mixing

in real- time. Two wavefronts scattered by the surface are recorded on the holographic plate. These are played back during the reconstruction of the hologram. The two wavefronts are due to one illumination each. The other two wavefronts, also due to one illumination each, correspond to the 'live' wavefronts issuing from the target surface and are observed through the holographic plate when the these wavefronts are displaced.

The facility to link opto-electronic devices to a holographic system for data reduction and fringe analysis has followed the development of holographic moiré techniques. The application of modern electronic interference fringe interpolation methods [Thalman & Dandliker (1985)] and digital computers for 3-D object shape measurement by contouring, particularly by using phase-shifting techniques has been described [Creath (1989), Quan & Bryanston-Cross, (1990), and Rastogi & Pflug (1991 and 1992)]. However, holography has been largely confined to laboratory applications. The main reasons for lack of widespread application are excessive sensitivity, high mechanical stability required, and lengthy plate processing with introduction of errors.

Holographic interferometry is sensitive to changes of optical path length of the order of 0.1λ and can measure changes of the order 0.25λ where λ is the illuminating wavelength. If λ were chosen large enough this could be compatible with "normal" engineering tolerances which are usually of the order 0.001 inch or $25\mu m$ [Butters & Leenderz (1971)]. Such wavelengths are in the infra-red part of the electromagnetic spectrum and in the ultra-sonic band of elastic waves in dense materials. In neither case are suitable recording materials available for making holograms

of a quality acceptable for measurement purposes. Holography of appropriate quality is only really practical when photographic emulsions are used as the recording medium. This limits the wavelength range to something like 0.4μm to 0.7μm which, after allowing for system design, is roughly 20 times too sensitive.

The practical confinement to photographic processing giving rise to lengthy chemical processing procedures and accompanying errors arising from emulsion shrinkage during chemical treatment. Dry processing materials such as photochromics have been successfully used for holography, but their high exposure energy requirements allow only small area holograms with application limited to high density data bit storage.

1.2.3 Sticked grating moiré interferometry

In Sticked Grating Moiré Interferometry (SGMI), the moiré phenomena and the gratings are described by physical optics, with an emphasis on diffraction and interference effects [Post (1982)]. The distorted grating is printed on the target surface that is coated with a photo-sensitive material. The surface is illuminated by two interfering wavefronts in such a way that the interference fringes are recorded on the material. By superimposing this distorted grating with a virtual one (which is formed by illuminating the surface by the same two wavefronts employed to produce the specimen grating), the moiré pattern is created. This technique has been used routinely in material testing and fracturing for high sensitivity, full-field measurements of in plane displacements [Post (1985) and Chiang & Williams (1985)].

In order to determine contour lines from derivatives of

displacement, Asundi & Dobbins (1992) proposed a variation of the SGMI technique. Their method uses the generation of moiré contours using two identical moiré patterns: "moiré of moiré". A uniform initial moiré pattern is produced by superimposing the virtual grating rotated with respect to the sticked one. As a result of the subtraction of this pattern with the other obtained after an object deformation, a moiré of moiré is obtained, making it possible to determine strain at certain points of the surface. Several alternative schemes were proposed making use of electronic and digital imaging techniques. One of them uses hardware from standard Electronic Speckle Pattern Interferometers.

SGMI has been employed to extract shape information from contour maps. High resolution moiré contouring using a hybrid technique that combines light and electro-optics was proposed by Robinson (1981). The technique was applied to contour a diamond using a scanning electron microscope to form depth contours over a field diameter of 800 μm and 200 μm deep. Recently, Dai & Chiang (1991) made use of SGMI for determining the topography of a curved target. The technique proposed was double-exposure. After preparing the target surface with the sticked grating, the surface is rotated relative to the virtual grating between the two exposures. Moiré fringes are then produced which reveal topographic contours of the surface with good contrast.

The SGMI gives high quality moiré fringes and its sensitivity can be from the order of one micrometer to that of a millimeter depending on the frequency of the sticked and virtual gratings. The obvious inconvenience of the technique is the target cosmetic preparation in order to form the sticked grating.

1.2.4 Shadow moiré contouring

In Shadow Moiré Contouring (SMC), a linear grating placed close to the target under inspection is illuminated in such a way that the shadow of the grating falls on the target surface and is viewed through the same grating. The shadow and the grating interfere to generate a moiré fringe pattern [Takasaki (1970) and Meadows, et al. (1970)]. The moiré fringes produced describe depth contours on the surface of the target. The technique requires only a grating and a source of light for its implementation. Perhaps due to its simplicity the shadow moiré method has become popular in the visualization and quantitative interpretation of three-dimensional shape. Early work [Pirodda (1982) and Livnat & Kafri (1983)] in this field relied on photography and subsequent manual fringe analysis to provide quantitative interpretation of the contour map; a time consuming task. More recently, digital image processing has opened up the possibility of capture and fringe analysis by using segmentation methods [Cline, et al. (1984)], or phase measurement methods [Reid, et al. (1986), Jin & Tang (1989) and Shapira & Voloshin (1992)]. The limitation of this technique is the size of the target to be tested: it must be at least the same size as the grating employed.

Another interesting point that is important to analyze in SMC is in respect to its sensitivity. The period of the grating has smaller practical limits determined by the loss in definition of the shadow of the grating with increase in the distance from the grating itself. This in turn is caused by diffraction and penumbra effects. The highest sensitivity can be attained with very flat targets whose surface can be placed very close to the grating. An optimum case is the measurement of small deformations of an

initially plane surface, where an overall sensitivity factor of the order of 1/100 mm can be obtained [Pirodda (1982)]. But in most practical cases, however, the limit is considered an order of magnitude higher, i.e., 1/10 mm, which is not good enough for such engineering applications as component inspection.

1.2.5 Projection moiré contouring

The moiré contouring techniques mentioned in the previous sections are very useful for measuring the 3-D surface shape of a relatively small target. The size of the target to be measured is restricted to the grating size and the optical elements in the experimental setup. As an alternative, a shadow grating produced by projecting a grating onto the target may be observed through another grating [Dessus & Leblanc (1973), Murakami & Murakami (1978), Shupe & Gorman (1979), and Doty (1983)]. This projection-type moiré topography eliminates the need for a large grating to produce contour lines on a large target. Another approach to the projection moiré topography was introduced by Miles & Speight (1975). Photographs are taken of two gratings. One is projected onto a target, and the other is an equally spaced line grating. Then, the two gratings are superimposed to generate depth contours. Dessus et al. (1975) have discussed the use of real time video processing to generate moiré fringes. A shadow grating and an electronic filtering technique are utilized to make vibration measurements, deformation, and contour mapping. An arrangement that projects two gratings instead of one [Wasowski (1970), Hovanesian & Hung (1971), and Benoit & Mathieu (1974)] may be used in order to increase the sensitivity of the method. Alternative techniques have been proposed to generate the reference grating using optoelectronic elements such as voltage controlled

oscillators [Homiere & Mathieu (1976)], electronic scanning [Idesawa, et al. (1977)], or the most recent method of computer grating generation [Asundi & Yung (1991a,b), Asundi (1993)].

To produce contours on the surface, an incoherent white-light source illuminates the grating in the projection arm which is in turn imaged onto the test surface. The grating is two dimensional and has not significant longitudinal depth. However, its image has a longitudinal depth that is equal to the depth of focus of the imaging optics, which is chosen to be equal to the maximum depth of the test surface. Hence the image of the projection grating in the vicinity of the test surface consists of dark and light planes that can be, but are not necessarily, parallel to one another. A comparison can be made by viewing the object and reference grids in digital form and adding or subtracting them [Gasvik, et al. (1983), (1986), (1989)].

One of the widely recognized limitations of projection moiré topography is its inability to provide unambiguous data from targets which have discontinuities in their shape. Similar limitations arise when two parts of a target are separated by a region which is in shadow. This feature of moiré topography has limited its use to the measurements of targets which have a continuous surface. Although many variations of projected moiré exist, most of them derive contour maps by working in the **infinite fringe mode**, that means, the lines of the gratings are placed parallel ($\theta = 0$ in Fig. 1.1). In most cases it is found that the **finite fringe mode** is more useful [Reid, et al. (1987)]. One reason is that the contour interval may be increased.

Other problems with projection moiré topography are that the fringe order number is not linear with target height. An equal phase plane of moiré fringes is curved except when special optical geometry is used for which the optical axes of projector and imaging lenses are parallel [Idesawa, et al. (1977)]. There are several alternative methods using computer-aided programing to measure surface profile from moiré fringes. These methods have been used to determine the spatial phase of moiré fringes by heterodyne methods [Indebetouw (1978)] or by phase-stepping methods [Reid, et al (1984), Andresen & Klassen (1986/87), and Halioua & Liu (1989)]. Heterodyning in moiré is achieved by translating the reference grating at a constant speed and detecting the intensity distribution at two or more discrete points. The relative phase difference between these signals can be used to determine the shape information. Sensitivity is claimed to be quite high if discrete photodetectors and a personal computer are used for determining phase differences. However, only depths at discrete locations can be determined. Phase-stepping interferometry can be classed as a discrete heterodyne process. In this process the change in phase intensity at a particular location, which is due to shift of the reference grating by a predetermined step, is used to determine the phase and thus the fringe order at any point. Precise control of the shift of the physical reference grating is required (see section 1.4.2c).

1.2.6 Methods based on the Talbot effect

Talbot interferometry was introduced by Lohmann & Silva and Yokozeki & Suzuki in 1971 as a simple method to measure the derivatives of the wavefront transmitted or reflected by a target. Their system works as a shearing interferometer and uses the Talbot effect or the self-imaging property of a grating without any other

optical component (for a complete theoretical analysis based on diffraction approach, see appendix A). Their original experimental arrangement consisted of two similar gratings under collimated illumination. The gratings are placed parallel to each another and perpendicular to the illumination beam. The self image of the first grating falls onto the second one. By placing a phase target between the gratings, a moiré pattern is formed on the plane of the second grating. This pattern gives information about the collimated wavefront derivative due to the presence of the target. In terms of classical interferometry or optical testing, the wavefront derivative is related with the target's aberrations [Patorski (1989)].

Modifications to the original arrangement have been made in order to determine surface shape of mirror-like surfaces, e.g. liquid surfaces deformed by stationary or variable forces [Andreev, et al (1989)]. Water surface relief produced by ultrasound is illuminated by a linear grating in collimated illumination. The reflected surface-relief-distorted image of the grating in its self-imaging plane is recorded. The shift of the grating elements in this image is used to determine the surface shape.

The method of moiré deflectometry developed by Kafri and co-workers (1985) uses the ray approach (instead of diffraction approach) that maps the change on the moiré pattern produced by the two gratings in presence of the target. In this case the target under test is placed before the first grating.

Typical Talbot interferometers are schematically shown in Fig. 1.2. The gratings G_1 and G_2 are separated by a

Talbot distance Δ_k. In Fig. 1.2a, the sample phase target is placed between the gratings or before them for traditional Talbot interferometry (shown as a continuous line) or moiré deflectometry (dotted line). The modification in the interferometer for the case of mirror-like targets is shown in Fig. 1.2b. In this last case, the surface under test is illuminated by the first grating in collimated illumination. The reflected light from the surface is relayed to a Talbot plane of the first grating. A second grating is placed on that Talbot plane. Again, the moiré pattern formed on the second grating plane gives information of target deviations from a flat one.

Talbot interferometry and moiré deflectometry applied to the test of phase targets and mirror-like surfaces have become useful tools for optical shop testing [Patorski (1989) and Kafri & Glatt (1990)].

Although the methods mentioned above have been widely applied in fields such as strain analysis, flow dynamics, refractive index gradient and temperature measurements, little has been done in the shape determination of diffuse targets. Chavel and Strand (1984), described a method based on Talbot imaging to determine depth information of diffuse targets on specified planes. The property of the periodic change of contrast in quasi-monochromatic diffracted images with the propagation distance was used for this propose. Leger and Snyder (1984), described a real-time optical processor to represent depth information in pseudocolour. Two separated channels are required for pseudocolour coding. They are realized by using as the self-imaging object a cross-type grating with two component linear gratings of different spatial periods. A liquid crystal light valve is used as an intermediate device to send the

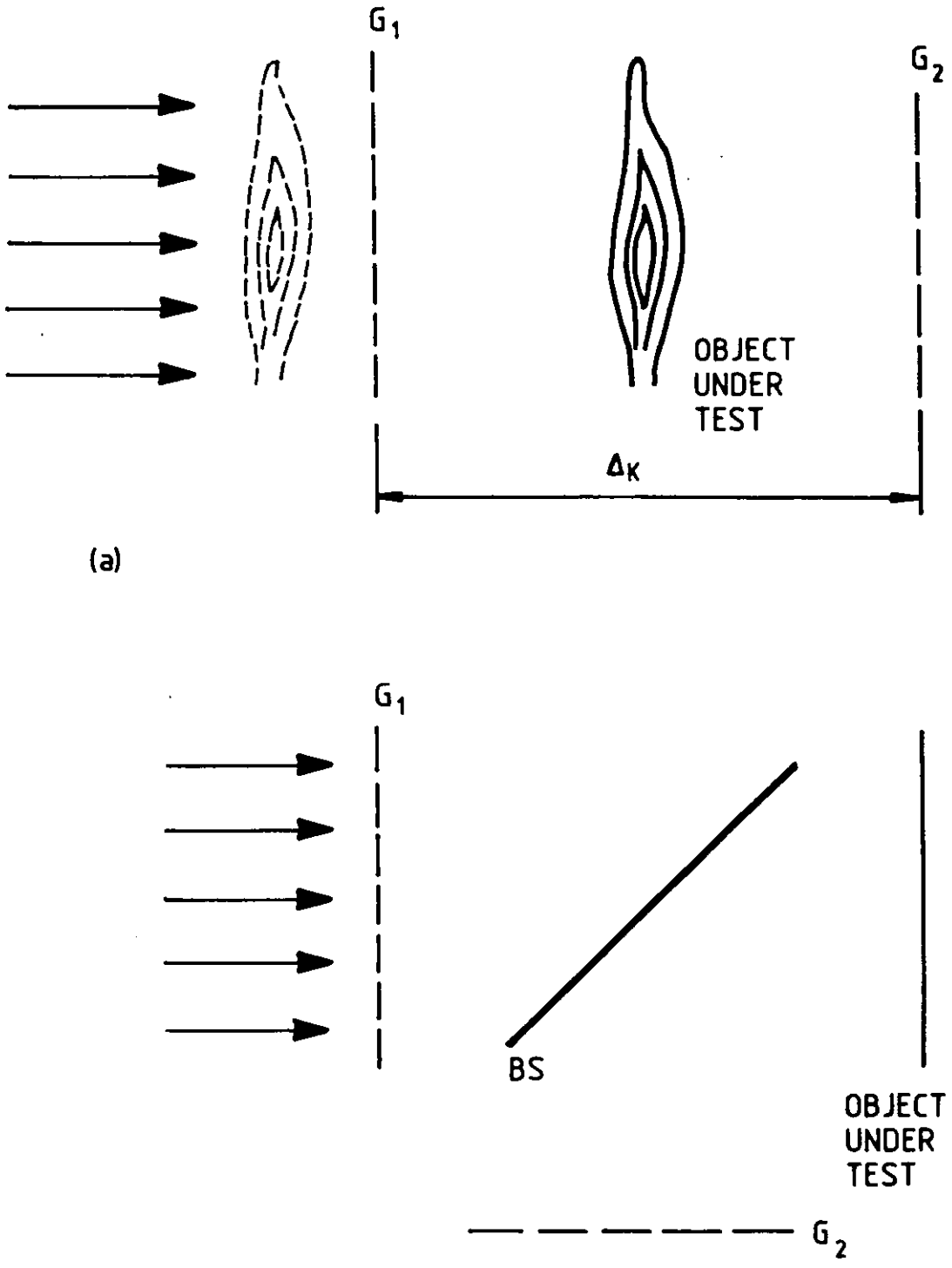

Figure 1.2
Typical Talbot-based interferometers employed for (a) transparent objects and (b) mirror-like surface testing.

depth signal from a monitor to a coherent white light processor. The two depth channels are filtered to produce different colour images such that the hue of the combined image is a function of depth. Livnat and Kafri (1983), have reported a finite fringe shadow moiré technique for fringe slope mapping of diffuse targets. Their system projects the shadow of a grating on the diffuse target. With a photographic camera placed at a certain angle with respect to the normal of the test target, a photograph of the distorted grating is taken. To obtain a contour map the target is removed, and a second exposure of a flat background is taken. However, the technique does not work in real time, this being a disadvantage.

1.3 Speckle methods

The granular appearance seen on a rough surface illuminated by coherent light, for example a laser, is known as the speckle effect. The physical origin of speckle is quite simple. Each point on the surface scatters some light to the observer. Because of its high coherence, the laser light scattered by one surface point interferes with the light scattered by each of the other surface points. The randomness is caused by the surface roughness because the phase of light scattered will vary from point to point in proportion to the local surface height.

Speckle correlation interferometry is a non-contact technique that allows measurements to be made on targets with optically rough surfaces. The method, developed by Leendertz (1970) at Loughborough University used photographic recording techniques. Subsequent developments by Butters and Leendertz (1971) in UK and Macovski, et al. (1971) in USA, enabled measurements to be made using a television camera and electronic recording in place of the

photographic film, thus coining a name for this method of Electronic Speckle Pattern Interferometry (ESPI).

There is a close analogy between contouring methods using holographic interferometry (HI) and those proposed in the literature for the speckle pattern fringe approach [Montgomery (1987)]. The main difference with ESPI is the increased noise sensitivity of the resulting fringes, which can rapidly lead to decorrelation and loss of resolution.

There are several methods of contouring with speckle when using photographic recording: white-light speckle [Forno (1975)] and laser speckle [Jaisingh & Chiang (1981) and Aggarwal, et al. (1984)]. These techniques involve double-exposure photography of speckle interferograms. A technique that involves displacement of the illumination beam produces grid contours on the target surface. Jones & Wykes (1983 pp. 266-268) have reported the phenomenon to compensate for rigid body tilt and rotation.

Nowadays two contouring approaches using ESPI methods are the most important. These are dual-frequency (also refered as dual wavelength) contouring and dual-source contouring.

1.3.1 Dual-frequency method

Research work concerned with the comparative geometry of two nominally identical objects was carried out by Butters & Leendertz (1974) and Jones & Butters (1975). The goal was to apply dual-frequency speckle techniques for component inspection. Photographic recording was employed. Later, an adaptation of this technique to ESPI was carried out [Jones & Wykes (1978)]. The principle of the technique is based in the illumination of a non-specular target with a smooth

'master wavefront' at a specific wavelength. The interferogram formed between the speckle image of this target and an in-line reference beam is subtracted from the pattern observed at a second wavelength. These Speckle pattern correlation fringes define differences between the target under study and the master wavefront. Master wavefronts of complex geometries are reconstructed by holographic elements which initially record the light field reflected from a specular master component or a diffuse target [Denby, et al. (1975)]. This field is reconstructed to form the required illumination wavefront by re-illuminating the hologram with a wavefront of identical geometry to the recording reference wavefront, but propagating in the opposite direction.

More recently Tatam, et al. (1990) have incorporated a laser diode with monomode optical fibres to bring the development of contouring by switching between two laser wavelengths, thus obtaining contour intervals from 0.5 to 5 mm. These contours were generated by modulating the current of the laser diode. Although good experimental results have been obtained with the laboratory prototypes, the technique is far from being applied in industrial environments, due to instability and chaotic laser output irradiance.

1.3.2 Dual-source method

Contouring by projected fringes produced by object beam translation or dual-source, was first proposed by Winther & Slettemoen (1984) as part of a strain measurement analysis system. The authors used a single mode fibre to deliver the object beam. By mounting the fibre end in a micropositioner, the object beam could be given a known, small translation. ESPI subtraction electronics produced

grid contour fringes superimposed on the image. The contour height of the surface could be deduced from this pattern as a function of the number of fringes, laser wavelength, and the coordinates of the fibre position with respect to the surface analysis point.

The accuracy of determination of the fringe interval depended on the number of projected fringes across the surface, and resolution increased with the angle between illumination and viewing axes. The fringe interval was therefore controlled in terms of resolution and reference plane orientation. One major drawback was that the grid fringes were not easily understood, and quantitative analysis involved knowing the fringe order and the use of curve fitting routines to interpolate the data. The authors discovered that by adding a small rotation to the target following the above fibre translation, more conventional contour depth fringes were produced. These fringes were qualitatively understood and produced a further increase in measurement accuracy. More recently, depth contours based in this small rotation of the target have been reported [Ganesan & Sirohi (1988) and Joenathan, et al. (1990)].

The idea that the illumination change relates to the target surface shape as if the target cuts a projected grid was proposed by Berquist & Montgomery (1985). Several ways of changing the illumination direction in order to obtain better empirical interpretation of the contour fringes were proposed by Montgomery (1987). Both authors called this technique Electronic Speckle Contouring (ESC). However, the mathematical interpretation was not completely developed.

1.4 Fringe analysis applied to contouring techniques

In previous sections, moiré and speckle contouring

techniques have been considered. Contour maps must be expressed in such a way that non-specialists can comprehend them or in such a way that they may be combined with other physical measurements. Contour maps therefore must be interpreted representing them in a required numerical or graphical format. To do it, contour maps must be analyzed.

In this section, developments with respect to automatic contour fringe analysis will be reviewed. Since contour fringe pattern image analysis procedures are essentially unaffected by the mechanism of contour fringe generation [Reid (1986/87)], the intensity distribution $I(x,y)$ of a contour fringe pattern can be expressed by

$$I(x,y) = A(x,y) + B(x,y) \cos [2\pi f_f x + \phi(x,y)], \qquad (1.1)$$

where $A(x,y)$, $B(x,y)$, $\phi(x,y)$, and f_f represent the background intensity, amplitude, phase, and spatial frequency of the contour fringes, respectively.

When evaluating contour fringe patterns, two possible approaches can be distinguished. The first approach is a comparison between an ideal contour fringe pattern and a real contour fringe pattern. The second approach is feature extraction, where the contour fringe pattern will be decomposed in such a way that its phase is obtained. Because to evaluation of fringe in all type of contouring techniques studied in this thesis are based on phase extraction, the second approach will be reviewed.

When the phase of the contour fringe pattern at a point (x,y) and its meaning are known, the desired features such as stress or physical dimensions can be determined. Methods to determine the phase of contour fringe patterns can be

divided in two categories: static and dynamic methods.

1.4.1 Static methods

Static contour fringe evaluation methods, i.e. methods which use one contour fringe pattern in the evaluation process, can be further divided in three separate groups:

a) Contour fringe tracking,
b) Fourier domain techniques
c) Spatial domain techniques

1.4.1a. Contour fringe tracking

Perhaps the most obvious approach to contour fringe pattern analysis involves identifying and subsequently tracking fringes across an interferogram [Robinson (1983)]. This approach is broadly applicable, since it requires little or no prior knowledge of the fringe pattern characteristics, and it has the important feature of allowing simple verification of the fringe tracking algorithm by comparing a graphical representation of the tracked fringes with the original interferogram.

A number of fringe tracking methods have been proposed. Although these methods differ in detail, they usually rely on the following procedure [Reid (1986/87)]:

+ Filter the image
+ Either (i) fit curves to the intensity data with a view to interpolating between the fringe centers, or (ii) identify and track the intensity maxima and/or minima with the goal of skeletonising the pattern and thereby minimizing the amount of data which must be subsequently processed.
+ Number the fringes iteratively or automatically

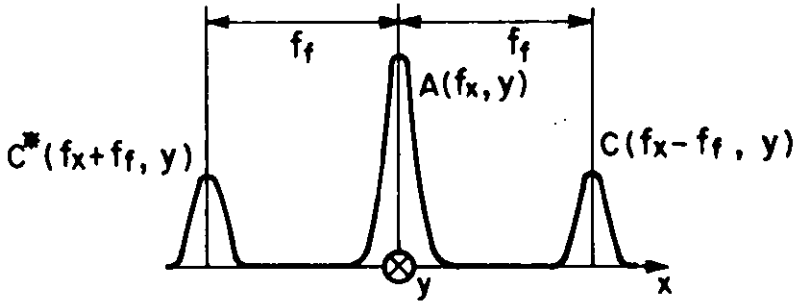

Figure 1.3
Separated Fourier spectra of a fringe pattern

+ Calculate the measurement parameter from the fringe pattern data.

1.4.1b. Fourier domain techniques

The phase from an image of a deformed grating projected on an target may be directly analyzed without the use of a reference grating. A deformed grating pattern is regarded as a phase modulated pattern with a constant spatial carrier. To retrieve the phase modulation, the acquired data are sinusoidally fitted using a phase detection algorithm similar to that used in communication techniques [Yoshino, et al. (1976) and Toyooka & Iwaasa (1986)]. Takeda, et al. (1982 and 1983), proposed an excellent method called Fourier Transform Profilometry (FTP). Interference fringes with a tilted reference wave or an image of a grating projected on the target are scanned by an electrooptical imaging device perpendicular to the fringes. Phase values are determined by calculating the Fourier transformation of acquired intensity data, filtering in the spatial frequency domain, and calculating an inverse Fourier transformation [Tang & Hung (1990), and Suganuma & Yoshizawa (1991)].

In order to switch to the Fourier domain, Eq. (1.1) is rewritten as [Takeda (1982)]:

$$I(x,y) = A(x,y) + C(x,y)\ \exp(2i\pi f_f x) + C^*(x,y)\ \exp(-2i\pi f_f x) \qquad (1.2)$$

with, $C(x,y) = \frac{1}{2} B(x,y)\ \exp[i\phi(x,y)]$. The symbol * denotes the complex conjugate.

Taking the Fourier Transform $\mathcal{F}\{\}$ of $I(x,y)$ with respect

to x, it is obtained

$$\mathcal{F}\{I(x,y)\} = \hat{A}(f_x,y) + \hat{C}(f_x - f_f,y) + \hat{C}^*(f_x + f_f,y) \qquad (1.3)$$

where the symbol ^ over the letters represents Fourier spectra and f_x represents the spatial frequency in the x-direction.

Assuming that A(x,y), B(x,y), $\phi(x,y)$, have frequencies which are much lower than f_f, then Eq. (1.3) will take the form shown in Fig. 1.3. The function $\hat{C}(f_x - f_f,y)$ can then be isolated by a filter which is centered on f_f and the function can be translated to the origin of Fig. 1.3 giving $\hat{C}(f_x,y)$. Taking the inverse Fourier transform of $\hat{C}(f_x,y)$ with respect to x, we get C(x,y). The phase can be calculated then by

$$\phi(x,y) = \arctan\left[\frac{\text{Im }\{C(x,y)\}}{\text{Re }\{C(x,y)\}}\right], \qquad (1.4)$$

where Re {C(x,y)} and Im {C(x,y)} represent the real and imaginary parts of C(x,y), respectively.

1.4.1c Spatial domain techniques

The analysis is started from Eq. (1.1) [Womack (1984) and Mertz (1983)]. A reference pattern r(x,y) is generated by, and stored within, a computer:

$$r(x,y) = \cos(2\pi f_f x). \qquad (1.5)$$

Obtaining the product of (1.1) and (1.4) yields:

$$I(x,y)r(x,y) = A(x,y)\cos(2\pi f_f x) + \frac{B(x,y)}{2}\cos[\phi(x,y) + 4\pi f_f x]$$

$$+ \frac{B(x,y)}{2} \cos [\phi(x,y)]. \qquad (1.6)$$

Applying a low pass-filter to the product of Eq. (1.6) generates a function of the form

$$M_1(x,y) = \frac{B(x,y)}{2} \cos [\phi(x,y)]. \qquad (1.7)$$

Introducing a phase shift of $\pi/2$ in the reference pattern $r(x,y)$ a second function is generated:

$$M_2(x,y) = \frac{B(x,y)}{2} \sin [\phi(x,y)]. \qquad (1.8)$$

The phase at point (x,y) now can be calculated using (1.7) and (1.8):

$$\phi(x,y) = \arctan \left(\frac{M_2(x,y)}{M_1(x,y)} \right). \qquad (1.9)$$

While the analysis of static contour fringe pattern has benefited from computerization, it suffers from the need to find fringe centres and the resulting trade-off between precision and number of data points. Data is collected only along the fringe centres, and most analyses need the data on a regular grid, therefore requiring interpolation. With a static contour fringe pattern, an additional piece of information is also required to determine the sign of the surface.

1.4.2 Dynamic methods

One of the major advantages of dynamic fringe evaluation methods is that the sign of the fringe pattern is resolved unambiguously. Dynamic methods, i.e., methods which use several fringe patterns in the evaluation process, can be

divided into three groups:

a) Heterodyne technique
b) Phase-locked technique
c) Phase-stepping

1.4.2a Heterodyne technique

By modulation of the phase in a fringe pattern, (directional) order numbers can be assigned to the fringes. The intensity of the fringe pattern is written as:

$$I(x,y) = A(x,y) + B(x,y) \cos [2\pi Vt + \phi(x,y)], \qquad (1.10)$$

where V is the translation speed in cycles/second and t the time.

The phase difference $\Delta\phi$ between two points is obtained by measuring the propagation time t of a fringe from one point to another given by

$$\Delta\phi = 2\pi t \qquad (1.11)$$

The heterodyne method allows considerable simplification of the fringe analysis software. Since the values of phase are largely unaffected by stationary noise and variations in fringe contrast and since the phase values increase or decrease in sympathy with an increasing or decreasing fringe order number, many elements of a conventional fringe analysis are unnecessary. Furthermore, since phase values can often be obtained with an accuracy approaching $2\pi/1000$, heterodyne fringe analysis can provide an improvement in accuracy of between two or three orders of magnitude over conventional systems.

1.4.2b The phase-locked technique

By modulating the phase of the fringe pattern with a small amplitude it is possible to determine the phase of the fringe pattern. The intensity of the fringe pattern in point (x,y) at time t is given by

$$I(x,y) = A(x,y) + B(x,y) \cos [\alpha(t) + \phi(x,y)], \qquad (1.12)$$

where $\alpha(t) = A \sin(\omega t)$ the time dependent phase, ω is the oscillation frequency and A the amplitude.

The method transforms the change in phase into areas of maximum or minimum intensity fluctuations. These can be located by directly studying the intensity in time but also by studying the frequency of the intensity signal [Moore & Truax (1979)].

1.4.2c The phase-stepping method

One of the most important developments in automatic fringe analysis was the advent of the phase-stepping or quasi-heterodyne method. By introducing discrete shifts in the position of the fringes, this technique allows the a.c. signal required for the phase measurement to be acquired from a number of discrete measurements. The bandwidth requirement for each measurement is in this manner low enough to allow the data to be acquired by a television camera [Reid (1986/87)].

The fringe pattern intensity $I_i(x,y)$ of sample i at point (x,y) is obtained as

$$I_i(x,y) = A(x,y) + B(x,y) \cos [\phi(x,y) + \alpha], \qquad (1.13)$$

where α is the discrete-phase-shift. Particularly, taking

three values for α the phase $\phi(x,y)$ can be resolved, since there are three equations and three unknown parameters, $A(x,y)$, $B(x,y)$, and $\phi(x,y)$. If a phase shift of $-(2/3)\pi$, 0, and $+(2/3)\Pi$, corresponding to -120°, 0° and 120°, the three pattern intensity measurements become

$$I_1(x,y) = A(x,y) + B(x,y) \cos [\phi(x,y) - (2/3)\pi], \qquad (1.14)$$

$$I_2(x,y) = A(x,y) + B(x,y) \cos [\phi(x,y)], \qquad (1.15)$$

$$I_3(x,y) = A(x,y) + B(x,y) \cos [\phi(x,y) + (2/3)\pi]. \qquad (1.16)$$

For these intensity measurements the phase is

$$\phi(x,y) = \tan^{-1} \left(\sqrt{3} \, \frac{I_3(x,y) - I_2(x,y)}{2I_1(x,y) - I_2(x,y) - I_3(x,y)} \right) \qquad (1.17)$$

The phase image has a number of highly desirable characteristics. Firstly, the phase values are insensitive to changes in contrast of the fringes so that uneven illumination of the target or uneven scattering or reflection light from the target has little effect on the phase calculations. Secondly, the phase values provide an unambiguous indication of the fringe number. According to the conventions used during the phase calculations, the phase values may advance as the fringe number increases and retard as the fringe number decreases. Thirdly, since phase values are available at each pixel location, the measurement parameter (e.g. shape or deformation) which is evaluated after the analysis of the fringes will be available at a regular mesh of points and not only along the loci of the fringe centres.

1.5 Conclusions

Optical Contouring techniques based on moiré methods and the speckle effect have been reviewed. From this, the following may be concluded:

1. The range of measurements and sensitivities covered by the techniques show a significant degree of overlapping, and therefore complement each other. For example, it is possible to make measurements from the order of a fraction of the wavelength to several millimeters, thus encompassing most of the engineering tolerances.

2. The potential of the techniques to overspread applications ranging from industrial and medical diagnostics, to scientific and academic ones.

3. Talbot interferometry has been used just to test transparent and mirror-like targets.

4. Techniques like Optical Interference Fringe projection, SMC and SGMI are confined to test small objects, i.e., as small as the collimated light illumination or grating size.

5. Widely recognized limitations of projection moiré contouring are its inability to provide unambiguous data from targets which have discontinuities in their shape and fringe order number is not linear with the target height.

6. The photographic process in holographic techniques gives rise to lengthy chemical processing procedures and accompanying errors arising from emulsion shrinkage during chemical treatment. Furthermore, high mechanical stability is required.

7. The mathematical interpretation of the Electronic Speckle Contouring (ESC) was not completely developed.

8. Todays applications include fast computers for data reduction from information captured by CCD cameras, together with facilities for digital image processing and fringe analysis. The main trend being the phase-measurement techniques.

In order to solve the problems encountered in the different reviewed techniques, the author describes, in the following chapters of this thesis, several innovations and improvements in the optical contouring field. In this way, a Talbot-based interferometer is employed to obtain shape information for engineering surfaces. The technique is also used as a means to discriminate between hills and valleys of the target by using white light illumination This is achieved by associating a different colour Talbot plane with a different plane on the target.

The limitation in target size and ambiguous data of the moiré techniques analyzed are removed using a projection system with capability of image subtraction by an electronic device. Computer generated gratings have shown usefullness to elude shadows on target discontinuities.

Avoiding the lengthy holographic process, but witholding the holographic measure range, the author gives an account of some novelties in contouring with ESPI. A new theoretical interpretation of the fringe contours gives a solution to the interpretation of ESC as moiré line projection, being capable of analyzing the fringes in the usual way.

Finally, because of their high accuracy and automatic sign determination, phase-stepping techniques are used for data reduction in throughout this thesis.

CHAPTER 2

The Talbot-projected moiré method

2.1 Introduction

In this chapter Talbot fringe projection, a moiré technique, is applied to three-dimensional contouring of diffuse targets for absolute shape measurement. The basic system relies on depth encoding the test surface by projecting onto it the Talbot image of a linear grating using monochromatic light. A second grating, similar to that used for the Talbot image, is employed to obtain the moiré fringes. These fringes represent surface contours of equal depth. Using a phase measurement technique and digital image processing algorithms, the surface shape information is obtained from the contour maps.

As an extension of the Talbot-projected moiré method, the possibility of encoding the depth information with colour is considered. White light illumination is employed to achieve different projected Talbot planes on the diffuse target surface. The dependence on λ (see appendix A) is noted in the relationship describing the separation along the axis between the Talbot planes and hence the possibility of moiré colour reproduction is obtained. Each colour on the moiré pattern is associated with a different Talbot plane and hence with a different depth of the surface. Experimental results, merits and limitations of the techniques are discussed.

2.2 Talbot projected moiré topography (TPMT)

As it was mentioned in one of the conclusions of chapter one, Talbot interferometry has been used to test only mirror-like and transparent targets. Basically this

interferometer consists of two identical gratings separated by a Talbot distance, Δ_k, and illuminated by a collimated beam as shown in Fig. 2.1. If the lines of these gratings are rotated a small angle, a straight fringe moiré pattern is formed on the second grating plane, without transparent object (Fig. 2.1a). When the illuminated beam is not collimated or a transparent object is placed, the moiré pattern is modified as shown in Fig. 2.1b or 2.1c, respectively. Moiré fringe deviations from the straight ones are measured in order to map ray deflections, and then the object's refractive index [Servin, et al. (1990)].

This section is devoted to describe an alternative approach of the Talbot interferometer developed by the author [Rodriguez-Vera (1991a) and (1991b)]. This approach works by imaging a Talbot plane on a diffuse target surface instead of a transparent or specular one.

2.2.1 Depth encoding by the Talbot effect

A detailed description of the Talbot effect theory can be found in appendix A. Any periodic object with an amplitude distribution $g(x',y')$ will also be periodic in the direction of light propagation (z' in Fig. 2.2). One simple periodic target is a cosine grating of period p. If the grating is illuminated by a plane wavefront of wavelength λ, positive identical reproductions of the original grating are formed at multiple distances of a fundamental distance $2p^2/\lambda$. Halfway between each positive Talbot plane there is a Talbot plane with maximum negative reproduction, forming an image of the original grating with a phase shift of 180°. The method of demodulation used here is insensitive to the phase of the carrier, so the positive and negative Talbot images look identical. Then, without loss of generality, the equation for the Talbot planes can

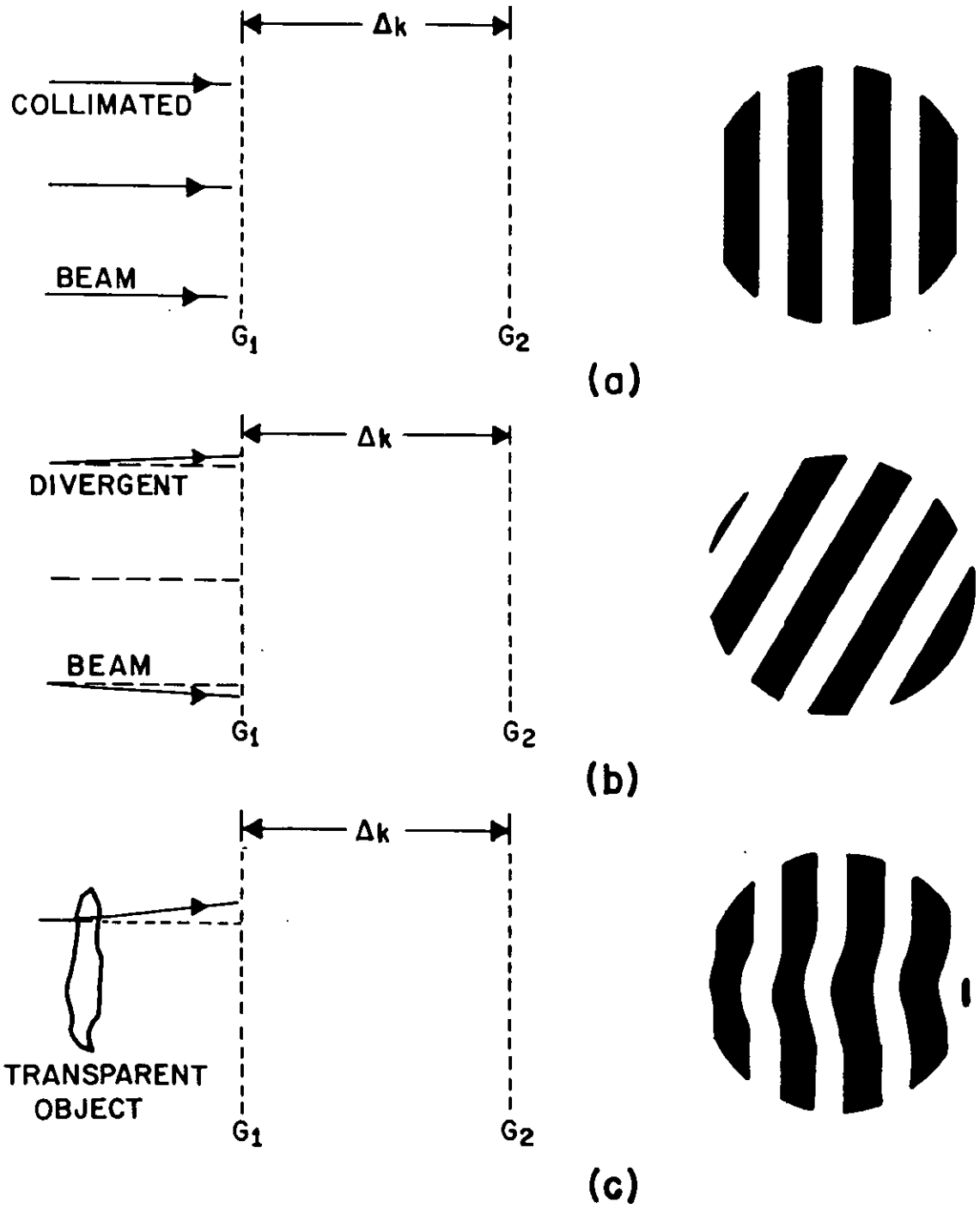

Figure 2.1
Talbot interferometer. (a) Without phase object, (b) Slightly uncollimated illumination beam, and (c) With phase object.

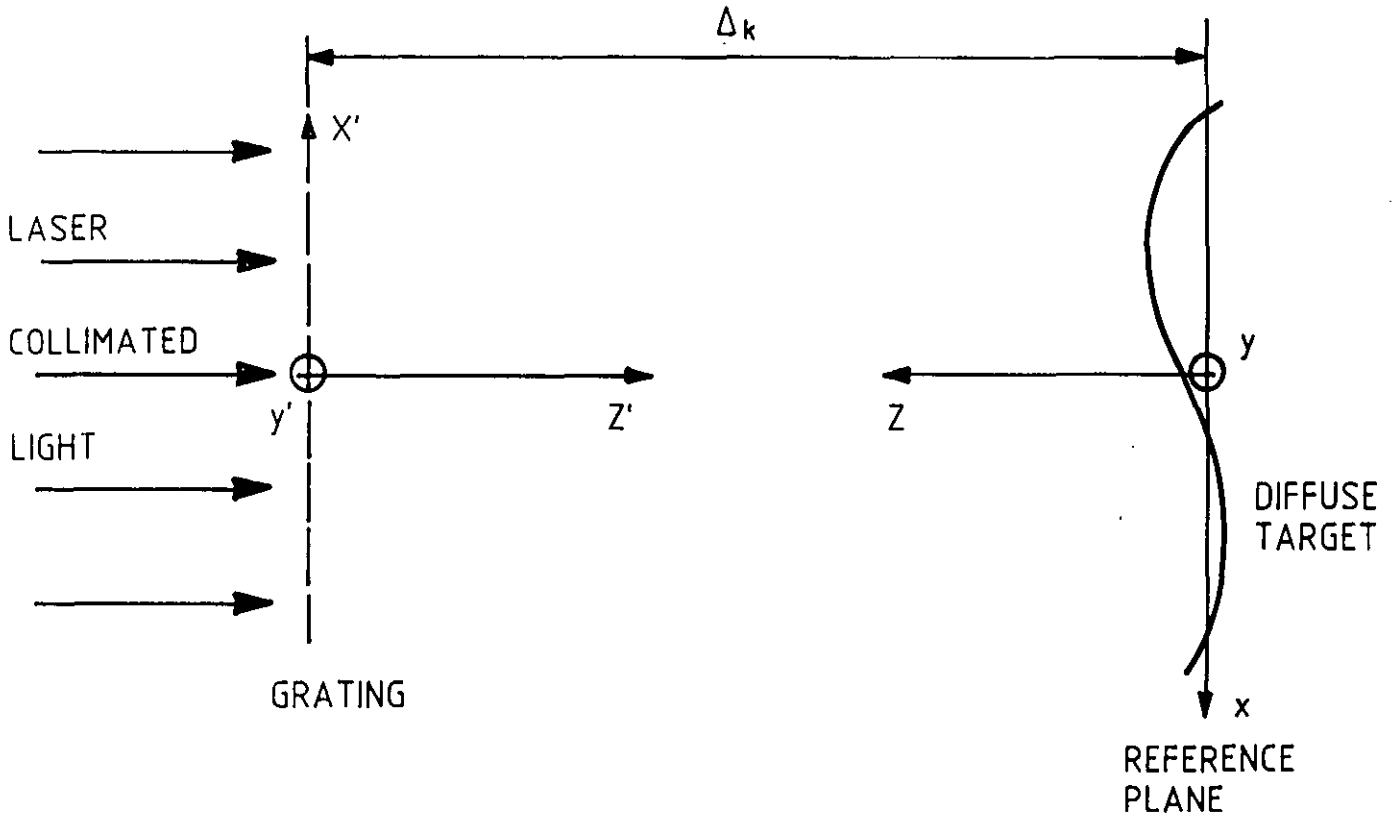

Figure 2.2
Talbot fringe formation on the target surface.

be written as

$$\Delta_k = k \frac{p^2}{\lambda}, \qquad (2.1)$$

where k is a positive integer. An odd integer k gives negative Talbot images and an even integer gives positive Talbot images.

Now consider the target surface being illuminated by the Talbot image, as shown in Fig. 2.2, where the the grating lines are perpendicular to x'-z' plane. Also, consider the target surface to be described by a function z = f(x,y). Then the amplitude distribution in the vicinity of the target surface is given by

$$O(x,y) = R(x,y,z)\ g(x,y), \qquad (2.2)$$

where R(x,y,z) is the reflectivity function characteristic of the target surface. It is seen from Eq. (2.2) that the target surface is depth encoded in amplitude by a carrier frequency corresponding to the original grating frequency. This property is the most important in Talbot interferometry because it can determine a contour map by decoding the information using a second grating.

2.2.2 Contour generation by the TPMT method

Figure 2.3 shows the TPMT approach. Collimated laser light is used to illuminate the grating G_1 whose self-image will fall on the target surface. The lens L of focal length f is placed in such a way that an image of the object, encoded by G_1, is formed on the second grating G_2. Unit magnification is chosen. Gratings G_1 and G_2 are identical and with period p. The optical axis where the lens L is

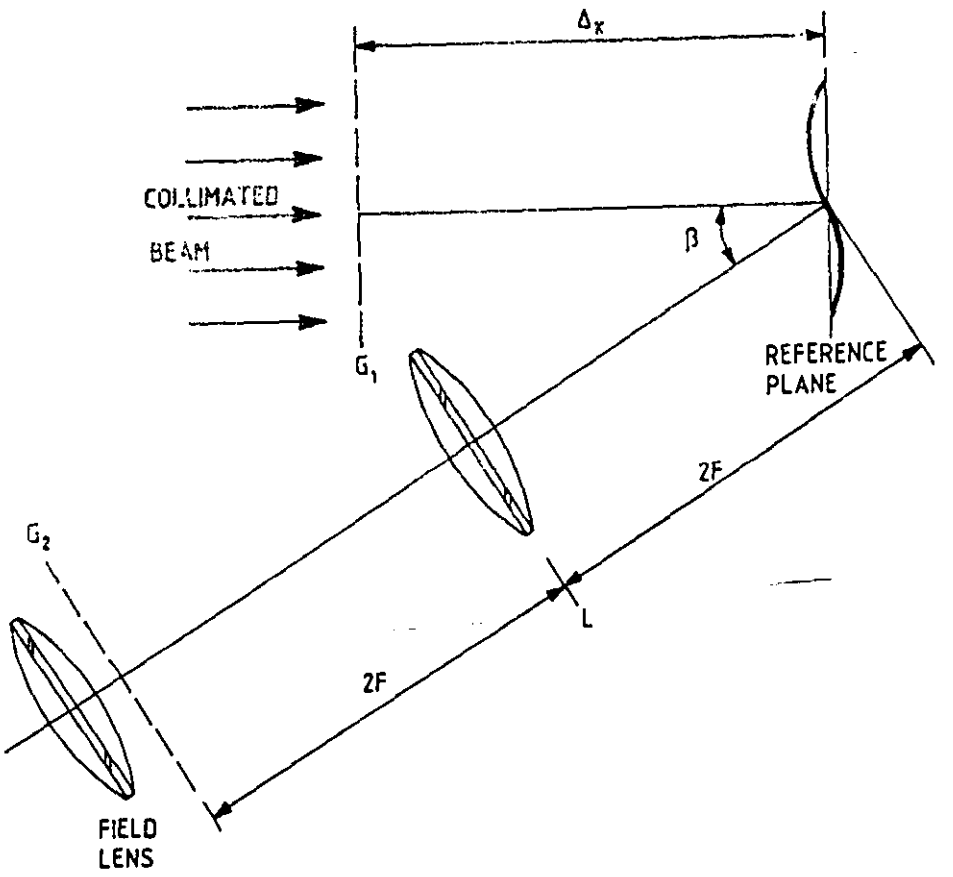

Figure 2.3
Experimental setup for the Talbot-projected moire topography method.

placed is at an angle β with respect to the perpendicular (z) of the grating G_1. The intensity distribution of the encoded surface on the G_2 plane is given by

$$O(x,y) = A + B \cos \frac{2\pi}{p_x} \left(x - z \tan \beta \right), \qquad (2.3)$$

where A and B are constants related to the reflectivity of the target surface, the background intensity and fringe contrast, and $p_x = p / \cos \beta$. This image is overlapped on a similar (demodulating) grating whose lines are shifted by an angle θ with respect to the projected ones. The grating G_2 has an intensity distribution given by

$$g_2(x,y) = c + m \cos \frac{2\pi}{p} \left(x \cos \theta - y \sin \theta \right), \qquad (2.4)$$

where c and m are constants related with grating bias level and modulation index, respectively. The total intensity distribution in the G_2 plane is given by the product $O(x,y)g_2(x,y)$, which results in a fringe pattern. Low frequency fringes obtained from this result, correspond to a moiré pattern given by

$$I_m = Ac + Bm \cos \frac{2\pi}{p} \left(x \cos \theta - y \sin \theta - x \cos \beta - z \sin \beta \right). \qquad (2.5)$$

hence, the moiré fringe formula is given by the indicial equation [Yokozeki (1982)]

$$y = \frac{(\cos \theta - \cos \beta)}{\sin \theta} x + \frac{\sin \beta}{\sin \theta} z + \frac{np}{\sin \theta}, \qquad (2.6)$$

where n is the indicial integer number. The inter-fringe distance in this pattern represents an absolute measure of

the target variation in depth (z direction), and is equal to

$$\Delta z = \frac{1}{\nu \sin \beta}, \qquad (2.7)$$

where $\nu = 1/p$ is the grating frequency.

2.2.3 Absolute shape measurement

The experimental arrangement is shown in Fig. 2.3. A 10 mW and $\lambda = 0.6328$ μm He-Ne laser is used as the source. The collimated beam illuminates the grating G_1 whose frequency is 3.9 lines/mm. The target surface is placed in the third Talbot plane from G_1 [$\Delta_3 = 306$ mm, see Eq. (2.1)]. The illumination field is 20 mm in diameter. The scattered light from the target surface is collected by a 50 mm diameter, 150 mm focal length lens (L). This is placed in such a way that the target surface is imaged onto the plane of the second grating G_2 (identical to G_1), with unity magnification. The lens optical axis is displaced by $\beta = 22^\circ$ with respect to the normal to the G_1 plane. The second grating G_2 is located in a holder with a micrometer screw. The lines of the G_2 grating can be shifted angularly by θ with respect to the G_1 ones, like in Fig. 1.1. In this case $\theta = 3^\circ$. A CCD camera linked to a computer is focused at the plane G_2. In this way a record of the moiré patterns is kept.

The target contours can be obtained from the position of the moiré fringes using equation (2.5). The moiré fringe patterns can be represented in a general form by (see section 1.4.2c)

$$I(x,y) = a(x,y) + b(x,y) \cos \left[\phi(x,y) \right], \qquad (2.8)$$

where the phase $\phi(x,y)$ contains the desired shape information and $a(x,y)$, $b(x,y)$ represent irradiance variations arising from non-uniform light reflection by the test target.

There are several methods used to retrieve the phase $\phi(x,y)$ term. One of them is the phase-shifting method, a review of which may be found in Reid, et al, (1984), where particular emphasis is placed on moiré topography. Phase calculation may use three contour patterns stored in the computer: one at 120^0, the second at 0°, and the third shifted $+120^\circ$. This shifting can be realised by moving the reference grating G_2 using a micrometer controlled transverse screw, in its own plane (x,y), by -1/3 , 0, and +1/3 of the grating pitch. Thus, three intensity values I_1, I_2 and I_3 at each pixel location are obtained and used to compute the phase ϕ of the contour pattern from the relation (1.17)

$$\phi = \tan^{-1} \frac{\sqrt{3}\ (I_3 - I_2)}{2I_1 - I_2 - I_3}. \qquad (2.9)$$

By evaluating equation (2.9) at every pixel location, the three contour patterns are transformed into a grey level modulo 2π phase distribution which is directly related to the shape of the surface.

Application, made by the author, of Eq. (2.9) to three particular cases gave the results shown in figure 2.4. 3-D shape information was obtained from flat, cylindrical and spherical diffuse targets. Each photograph contains the three shifted contour maps at -120°, 0°, and $+120^\circ$ with their respective phase maps. The high frequency noise on

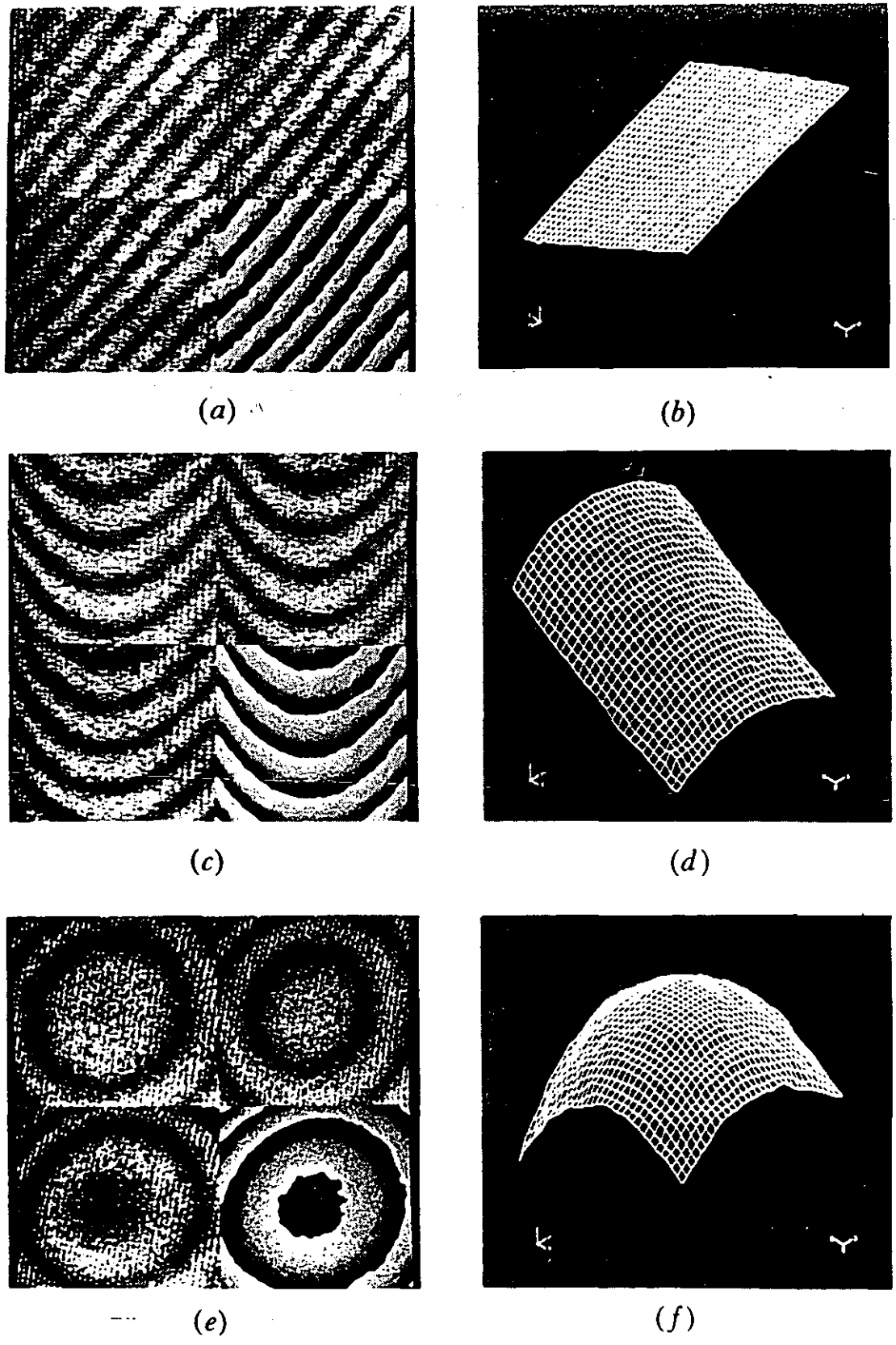

Figure 2.4
Experimental results. Photographs showing contours, phase map and normalized shape information respectively for: (a) and (b) flat; (c) and (d) cylindrical; and (e) and (f) spherical target surface.

the contour maps was removed by passing twice a 7X7 mask filter on each one.

2.2.4 Evaluation of the technique

Equation (2.7) shows that there is no apparent limit to the sensitivity of the TPMT method, i.e. Δz falls to zero when the frequency of the modulation grating goes to ∞. However, it is necessary to consider the image forming system (L in Fig. 2.3), which limits (due to its finite size) the actual resolution of the grating pitch, as well as the target depth range. The resolution limit of an optical system is defined as the minimum distance between two points such that the Airy disk generated by one point falls on the first zero of that generated by the second point [i.e., the Rayleigh criterion, Goodman (1968) pp. 129]. Hence, the minimum resolvable separation of the projected grating is the separation between the borders of two lines of the grating, i.e. $p_x/2$,

$$\frac{p_x}{2} = \frac{1}{2\nu \cos \beta} = 1.22 \lambda 2 \left(\frac{f}{D} \right), \qquad (2.10)$$

where f is the focal distance of the image forming system, D its aperture diameter, λ the wavelength of the light employed, and ν the grating frequency.

The depth of field ε of a diffraction limited lens is given by [Goodman (1968)]

$$\varepsilon = 2.44 \lambda \left(\frac{f}{D} \right)^2. \qquad (2.11)$$

The depth of field of the viewing lens limits the physical depth of the target being observed in that this must not exceed the depth of field of the viewing lens if fringes

are to be observed over the whole surface at once, this means that we can choose $\Delta z \cong \varepsilon$. Thus combining Eqs. (2.10) and (2.11) we obtain

$$\Delta z = \frac{1}{9.76\ \lambda\ \nu^2\ \cos^2\beta}, \qquad (2.12)$$

which is interpreted as the maximum depth detected when the minimum frequency is resolved.

A closer examination of the sensitivity limit for the TPMT method, i.e. the contour interval Δz, is shown in Fig. 2.5 where equations (2.7) (continuous lines) and (2.12) (dotted lines) are plotted with the frequency ν as a parameter. The curves are limited to the geometrical range $0 < \beta \leq \pi/2$. From the figure it can be seen that the theoretical sensitivity limit Δz approaches 0 when a high frequency grating is employed. However, the projected grating on the target surface has to be resolved by the imaging lens. The f-number ($f^* = f/D$) is a parameter that characterises all lenses. From Eqs. (2.10) and (2.11) it can be seen that high f^* give better resolution for the depth of field and that low f^* give better resolution of the grating frequency to be detected. There is then a compromise between these two parameters. A practical value for the resolving power of a lens, if the grating is to be imaged, with good contrast, with a medium quality photographic objective lens, can be set to $f^* \sim 2\text{-}3$. This gives a readable frequency of 100-170 lines/mm. From Fig. 2.5 and the curves corresponding to 150 lines/mm, it may be seen that these give a sensitivity limit Δz of about 11 μm when $\beta = 36^\circ$. A measure of the sensitivity of the TPMT method may be expressed as a ratio of the sensitivity limit to the target dimension (in one direction). Thus, using

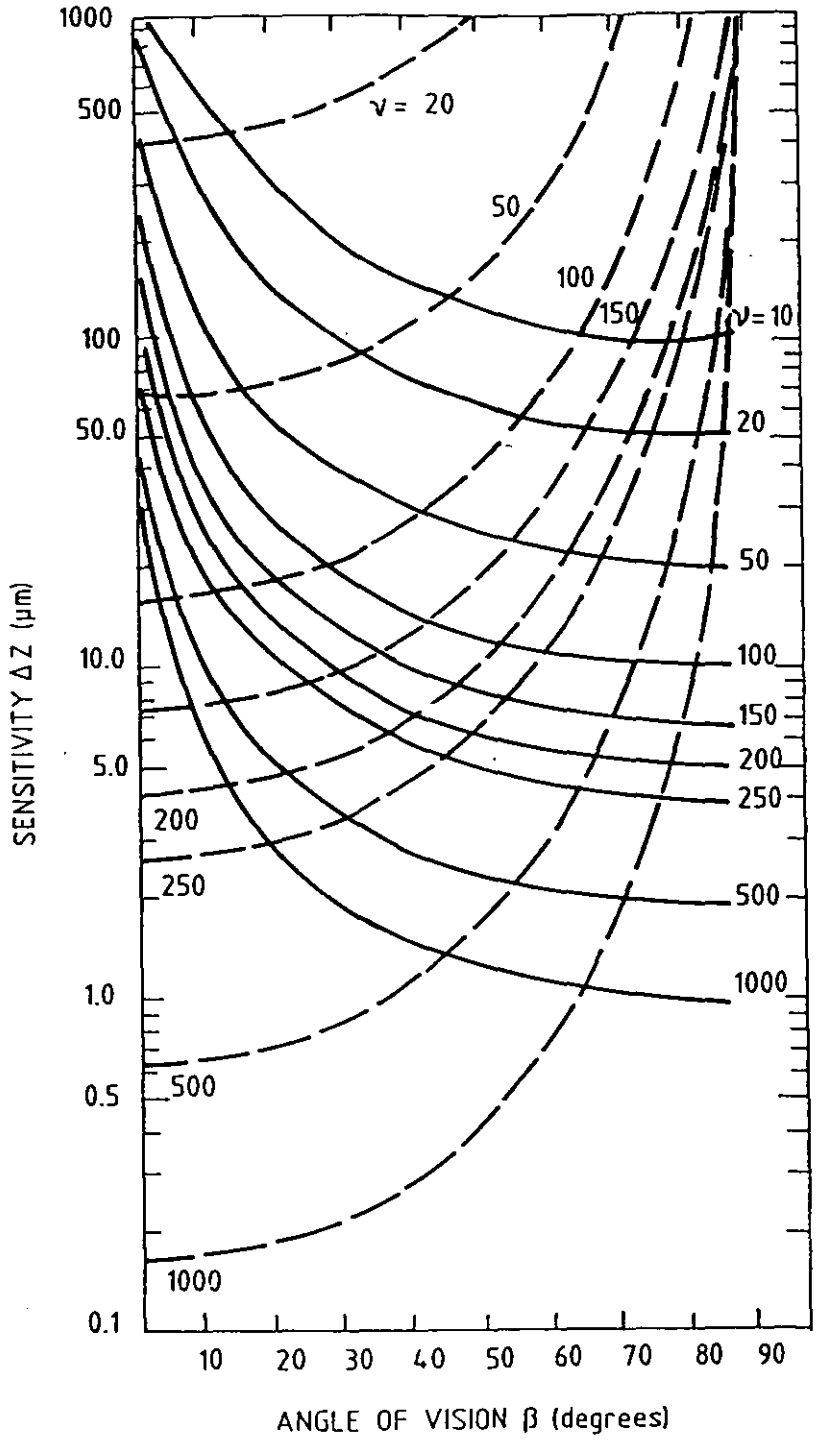

Figure 2.5
The sensitivity against the angle of vision with the grating frequency as a parameter.

this value on the grating G_2 (Fig. 2.3) and with a maximum field size of 20 mm, it is found that

$$\frac{\Delta z}{w} = \frac{11\ \mu m}{20\ mm} = 5.5\ X\ 10^{-4},$$

where w is the target dimension measured in the y-direction (see Fig. 2.3). This ratio illustrates the sensitivity of the TPMT method. In particular, the ratio shown is one order of magnitude less than that reported for the interference projected fringe method [Gasvik (1983)].

We have not yet considered limitations with respect to the Talbot plane, which is another parameter that needs to be analysed. Fig. 2.6 shows a plot of Eq. (2.1) for the separation between Talbot planes against the grating line frequency. It can be seen that the measurement of depth must not vary more than half the distance between a positive and negative Talbot plane, because the Talbot image then disappears. As was mentioned by Leger and Snyder (1984), this unambiguous range could be a limitation, but if one is interested in only a specific range interval, this may not be a problem. There is therefore a compromise between the resolution ability of the imaging system and the separation of the Talbot planes. For instance with a grating of 150 lines/mm the Talbot plane separation is 70 μm and the imaging system depth resolution would be 11 μm for $\beta = 36^{\circ}$. Hence the sensitivity of the TPMT method will be set at the lower depth limit, i.e. 11 μm.

The TPMT method has been employed to test real objects with extremely good results. For example, Fig. 2.7 shows experimental results for a golf ball used as the target surface. The photographs were taken under similar conditions as those of Fig. 2.4. The contour and phase maps

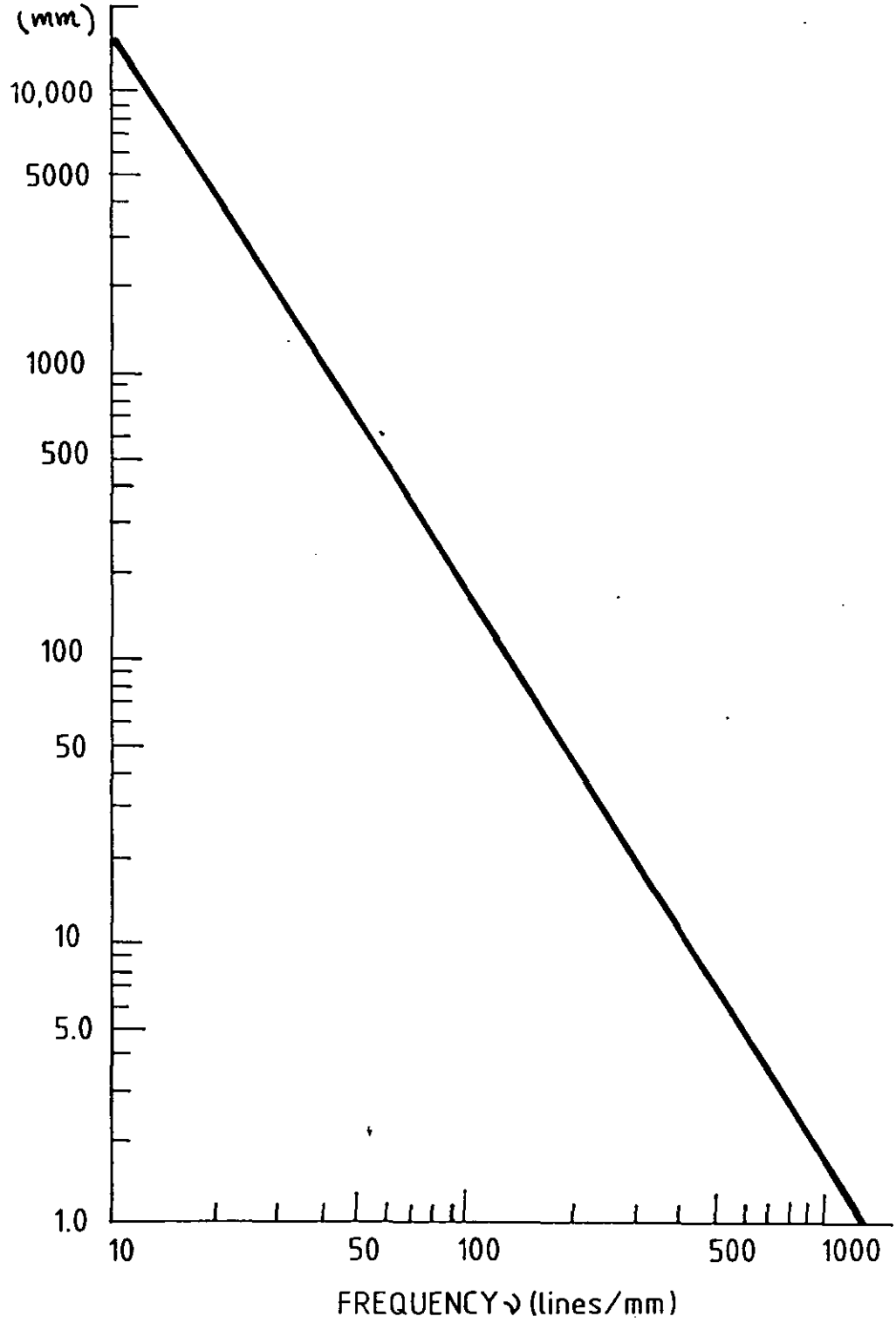

Figure 2.6
Plot of equation (2. 1) which shows the separation between positive and negative Talbot planes against the grating frequency (1/p).

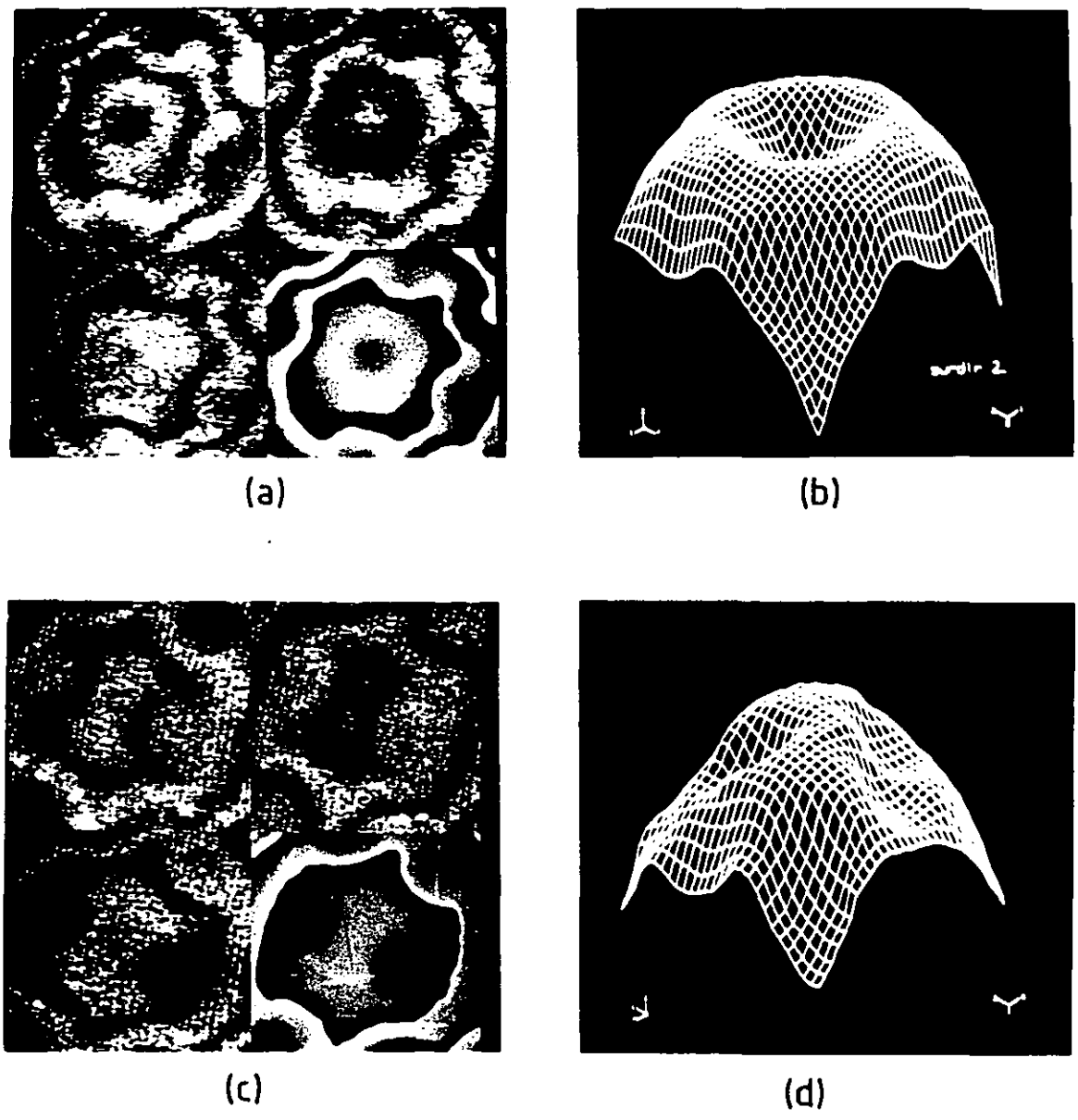

Figure 2.7
Photographs showing phase map and normalized shape information for a golf ball for two different views. The indentation on the surface of the ball are clearly seen.

are shown in the left column, and a three-dimensional plot of the target surface in the right column. These photographs were recorded from the monitor for two different positions of the target separated by a small rotation about an arbitrary axis through it.

As with shadow moiré contouring the TPMT method is limited to testing small targets, e.g. as small as the size of the optical aperture or diameter of the collimator lens and the grating. However, Talbot planes may also be obtained with divergent beam illumination, so it may be possible to apply this technique using magnified Talbot planes [Joyeux & Sabban (1982)].

2.3 Depth colour encoding

Another interesting possibility to use Talbot projected fringes is by using white light illumination. In this case the author has put into practice a Talbot interferometer as depth sensor in colour to test diffuse targets.

The use of white light as the illuminating source produces wavelength separated Talbot planes, and real-time colour-coding of surface depth is thus possible. Colour Talbot images are generated at different distances [see Eq. (2.1)] when white light is used, i.e. the colour of the Talbot image contains information on depth variation. Fig. 2.8 shows this situation. A surface reflecting the Talbot images has the depth information encoded in colour at the observation plane. Therefore, a direct colour-coding of depth can be achieved by using a white-light Talbot interferometer [Jutamulia, et al (1986)].

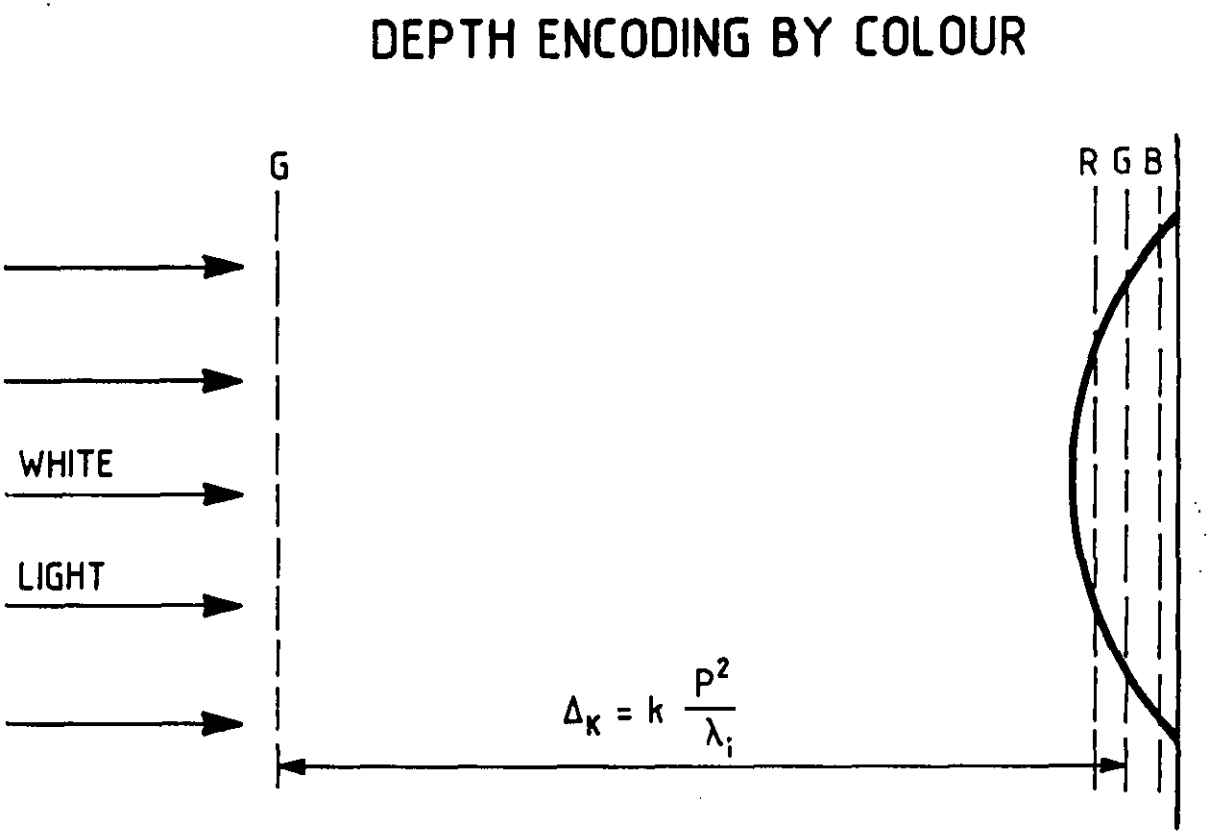

Figure 2.8
Depth encoding of a diffuse surface by colour Talbot planes.

2.3.1 Coloured Talbot planes

If the grating in Fig. 2.9 is illuminated by a collimated white light source, a set of Talbot colour planes appear. They are separated in space according to Eq. (2.1). This shows that Talbot planes will be further away from the grating for small wavelengths. A lens is used to image the Talbot planes onto a target surface, where different coloured planes may be observed. To retrieve the colours corresponding to different planes on the target, a second grating is required. Using unity magnification, the image of the encoded target is made to fall onto a second grating, and coloured moiré fringes are obtained. Each colour in the moiré pattern represents a particular Talbot plane. Subsequent interpretation of these colours allows the selection of a discrete set of contour planes, which suggests the possibility of profile measurement without using conventional fringe and phase analysis techniques.

Quantitative feasibility of this method is based in modern advances in the digital image processing area. Scientific applications of colour frame grabber boards are now available. These boards acquire colour frames, storing them in onboard memory, and displaying them on a colour monitor at real-time video rates. These modern boards convert between the video-standard **RGB** (red, green, blue) colour space and the processing-optimized **HSI** (hue, saturation, intensity) colour space. The hue-saturation-intensity model is a far more natural way of describing colour than traditional RGB. HSI components convey important information directly: hue is the colour itself (blue, yellow, purple); saturation is the depth of colour (pink or red); and intensity is the overall brightness or darkness.

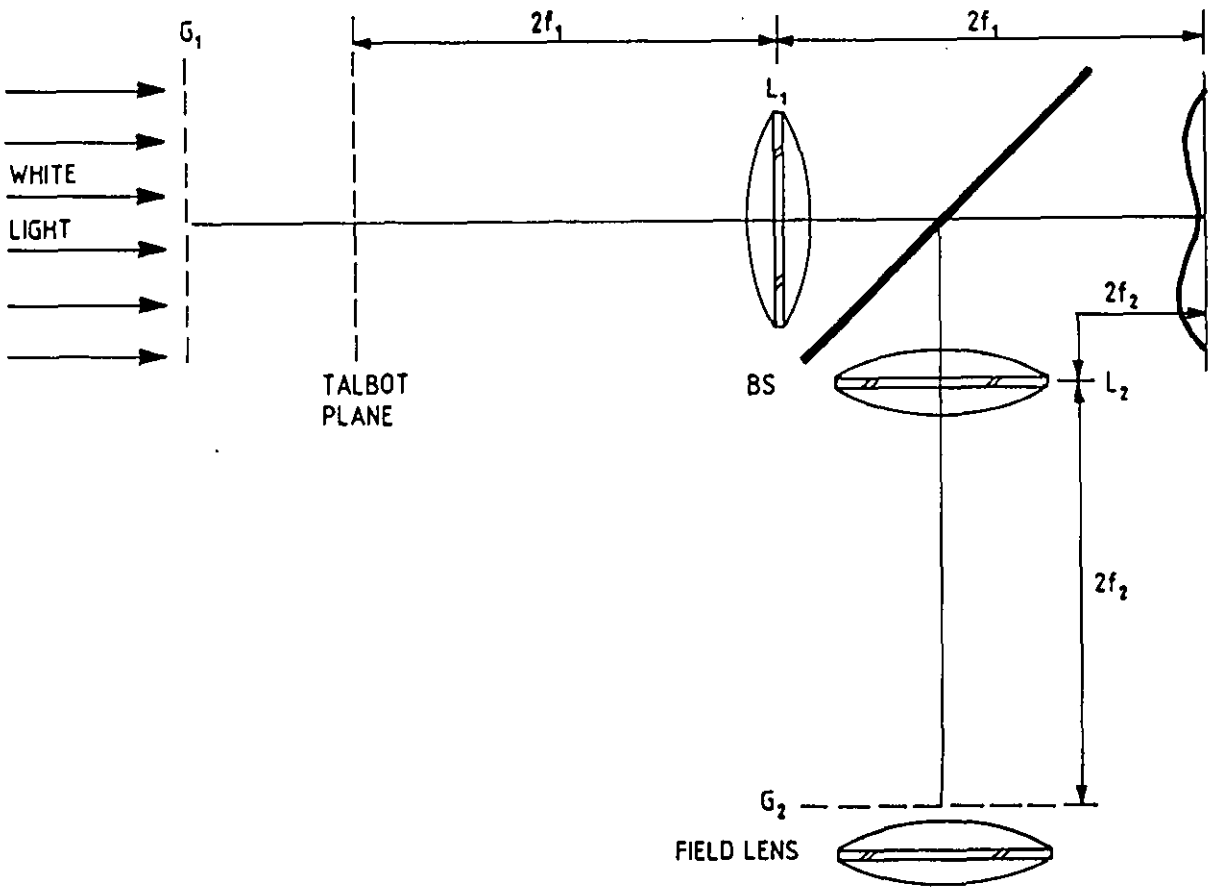

Figure 2.9
Talbot interferometer for colour depth encoding of a diffuse target.

HSI saves processing time because for most applications one only has to examine one component-RGB almost always requires one to examine all three. For example, to check the colour of an apple or a car door, look at the hue value. Examine the saturation value to separate pale blue from deep blue. Since the intensity value exactly corresponds to the monochrome version of an image, one can use it directly with any of dozens of monochrome-only processing algorithms.

2.3.2 Experimental results

Depth colour information is seen using the experimental arrangement shown in Fig. 2.9. A 35 W, 6 V tungsten-halogen incandescent lamp is used as the source. The beam is collimated and illuminates the grating G_1 whose frequency is 3.9 lines/mm. The first Talbot plane formed at 102 mm from G_1 is imaged (with unity magnification) by a 150 mm focal length lens, L_1, on the target. The illumination field is 40 mm in diameter. The scattered light from the target surface is collected (via combiner **BS**) by a 50 mm diameter, 150 mm focal length lens (L_2). L_2 is placed so that the target surface is imaged (with unity magnification) onto the plane of the second grating G_2. The optical axes of the lenses are collinear. The lines of the G_2 grating can be shifted angularly in its plane by using a micrometric rotary stage (not shown in the figure). A field lens is placed in front of the second grating through which the coloured moiré patterns can be observed.

In order to prove the method, various diffuse surfaces were used. Fig. 2.10 shows the set of objects tested. Each target was sprayed with white paint to avoid specular reflections. Fig. 2.11 shows a set of colour photographs of the experimental results corresponding to those of Fig.

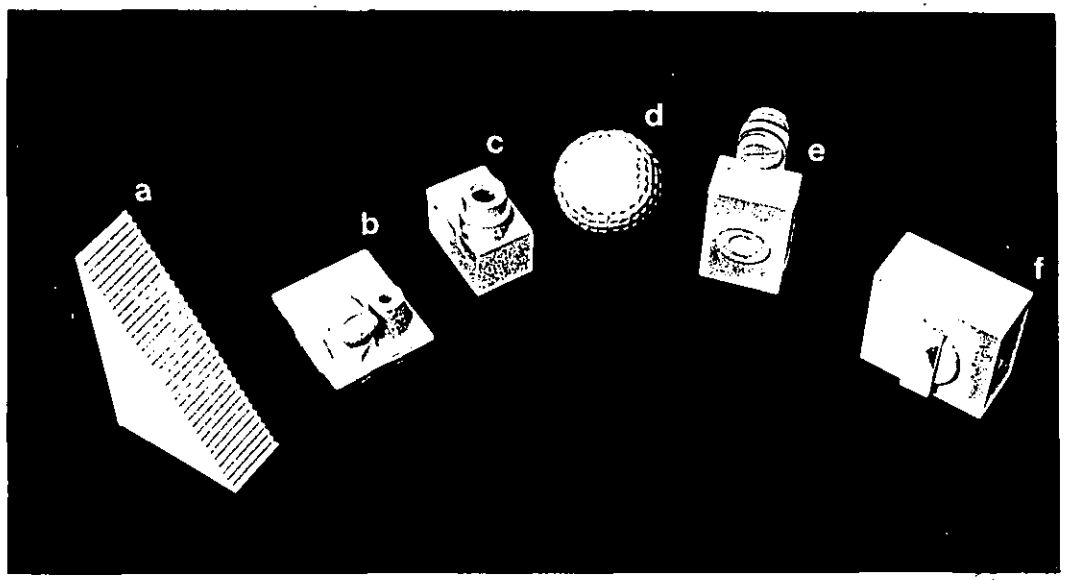

Figure 2.10
Diffuse objects to be tested under the coloured Talbot projected images.

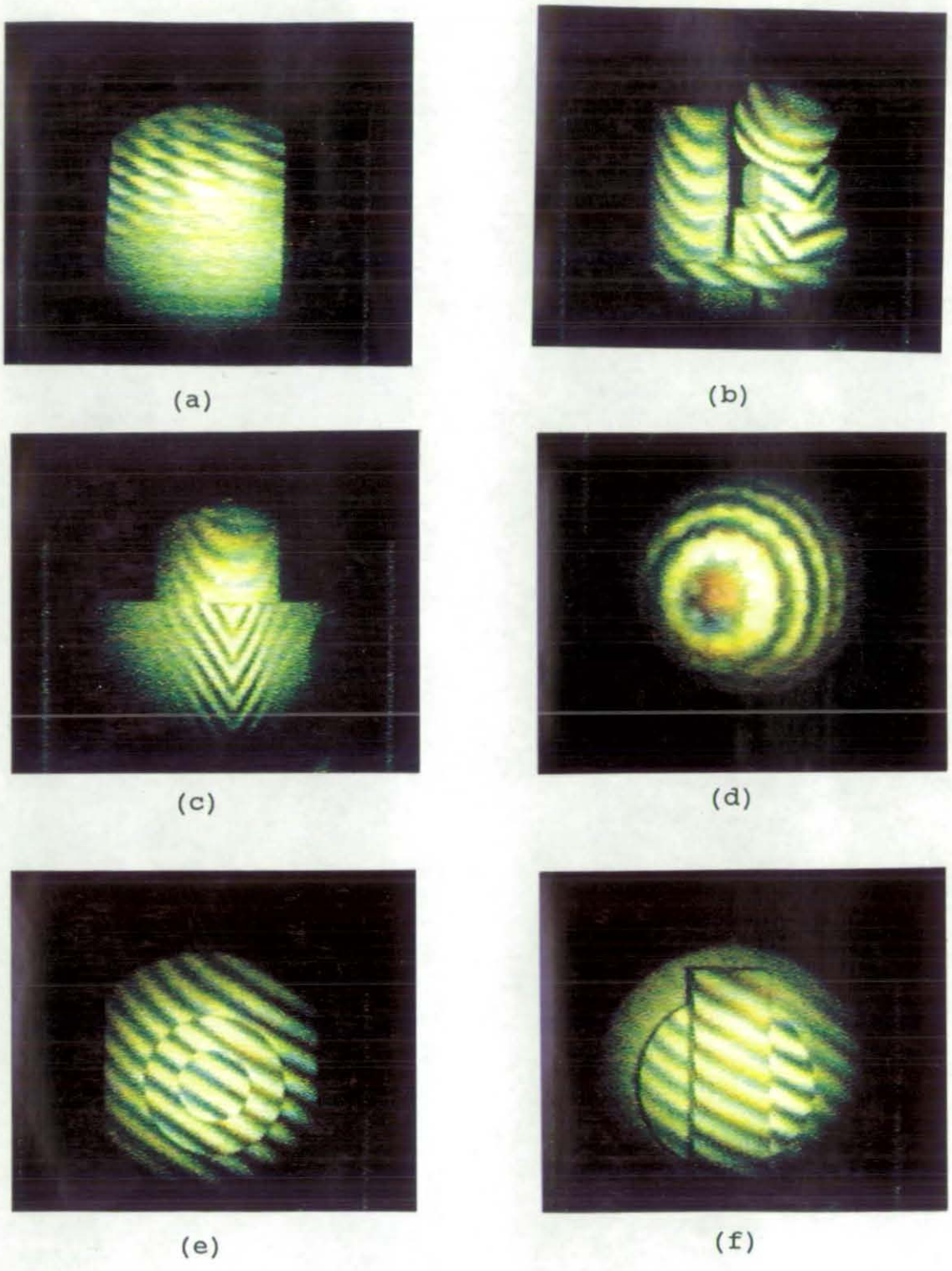

Figure 2.11
Coloured moiré fringes corresponding to the objects shown in figure 2.10.

2.10. Colour moiré fringes were observed due to the angular separation between the grating orientations. Fig. 2.11a corresponds to coloured moiré fringes for Fig. 2.10a, a target which is made up of steps 1.5 mm deep by 2 mm in height. Colour fringes may be observed: from red at the top (nearest plane from G_1 in Fig. 2.9) to blue at the bottom (on the furthest plane). Outside this colour fringe interval, Talbot planes are not formed and colour fringes disappear. In order to show continuous colour moiré fringes, surfaces in Fig. 2.10b-d were tested. The moiré pattern consists of gradually varying colours. Fig. 2.11b-d shows the experimental results from these targets. It was observed that the colours of the moiré pattern gradually changed from red (nearest plane from G_1) to blue (farthest plane from G_1). Two surfaces with two different and sharp depth variations are tested, see Fig. 2.10e,f. The depth difference is 1 mm and 3 mm, respectively. Fig 2.11e,f shows the moiré images of the two surfaces. It should be pointed out here that the fringes observed were mainly orange; red in the nearest part and blue in farthest. The main difference between these pictures is the hue from the blue colour.

In order to obtain quantitative information from a coloured moiré pattern is necessary to know the colour differences point to point of the fringes. Then the HSI model should be the more useful for fringe analysis.

Since several editions of video recordings were made before taking the photographs shown in Fig. 2.10, the results presented are of poor quality. However, when the fringes are seen directly in the experimental setup, several bright colour combinations are observed.

This method is not suitable for measuring relief that is substantially larger than the repetition period of the self-imaging planes.

2.4 Conclusions

The possibility of using Talbot-projected fringes to determine 3-D contouring of engineering targets is demonstrated in this chapter. The principle is based on the encoding of the target surface by a Talbot self-image of a linear grating. The decoding process is carried out by the image formation of the deformed grating onto a reference grating. This produces moiré patterns that correspond to a contour map. Two applications of this phenomenon are demonstrated. One uses laser illumination to obtain the moiré pattern, which is transformed to phase information by using the phase-stepping method. The phase map contains the shape information of the target. The second uses white light illumination to produce different coloured Talbot planes, thus obtaining coloured moiré fringes. Each colour is associated with a different plane on the target.

As was demonstrated, the sensitivity of the TPMT method depends strongly on the grating frequency. The highest sensitivity can be attained with very flat targets whose surface can be placed on a Talbot plane. An optimum case is the measurement of small deformations of an initially plane surface, where an overall sensitivity factor of the order of 11 μm can be obtained. This is an advantage of the method, compared with shadow and projection in which the sensitivity limit is of the order of 100 μm [Pirodda (1982)].

The fact that collimated illumination is employed means that correction to the depth contour equation is not

necessary, eliminating the dependence in z of the grating period. Also, compared with holographic and speckle interferometry, high mechanical stability is not required.

However, there are some limitations inherent in the present methods. As with shadow moiré contouring and sticked grating, the techniques are limited to testing small targets, i.e. small as the size of the optical aperture of the collimator lens or the grating. However, Talbot planes may also be obtained with divergent beam illumination, so it is possible to apply this technique using magnified Talbot planes.

CHAPTER 3

Electronic moiré contouring

3.1 Introduction

In this chapter, an alternative approach to moiré contouring is presented. The method investigated is based on the projection moiré contouring technique, but with the variation that electronic demodulation is used to obtain the contour maps. It is here called Electronic Moiré Contouring (EMC). This technique encodes and analyses moiré contours by using an electronic apparatus similar to that used for ESPI. Experimental results indicate that the technique may be extended as an industrial tool for quality control, or as feedback data in flexible manufacturing systems [Rodriguez-Vera & Kerr (1992a,b)].

In order to evaluate the EMC technique, fringe analysis was carried out by comparing fringe subtraction between reference and specimen gratings using the ESPI electronic hardware and proprietary image processing equipment in a personal computer. As before, a phase-stepping technique has been employed for data reduction, towards the full automation of the technique.

3.2 The electronic moiré contouring method

Since EMC is based on the electronic hardware of ESPI, this will now briefly be illustrated (for a detailed description see chapter 4).

Electronic Speckle Pattern Interferometry (ESPI) works using a process of video signal subtraction or addition. In the subtraction process, a television camera video signal corresponding to the interferometer image-plane speckle

pattern of a undisplaced object is stored electronically. The object is then displaced and the live video signal, as detected by the television camera, is subtracted from the stored waveform. The output is then high-pass filtered and rectified and displayed on a television monitor where correlation fringes may be observed live. Fig. 3.1 shows a diagram of a typical ESPI system. The frame store block of this figure is the most important part in ESPI. Tasks such as Analogic/Digital (A/D) and Digital/Analogic (D/A) conversion, storage, subtraction ($\sum$) band pass filtering (BPF), and rectification (R) of the video signal are performed by the frame store. It can read out again at video rate. A flow diagram illustrating each one of steps followed by the video signal until it appears on the monitor screen is shown in Fig. 3.2.

Electronic Moiré Contouring (EMC) uses an opto-electronic configuration similar to that used in conventional ESPI but modified for moiré work. Such modification is based on the projection of a fringe pattern produced by interference of two plane wavefronts [Varman (1984) and Morshedizadeh & Wykes (1989)] or by imaging a projected grating with a conventional slide projector [Gasvik (1983)]. An image of a reference surface with projected fringes on it is stored in the memory of a video frame store and then subtracted in real time from subsequent images. In this way, absolute and comparative shape measurement as well as deformation measurements can be achieved. Based on this analysis method, an extension of the EMC technique is reported in this chapter. White light illumination and phase-stepping algorithms for data reduction may be used, with a view to full automation of the method.

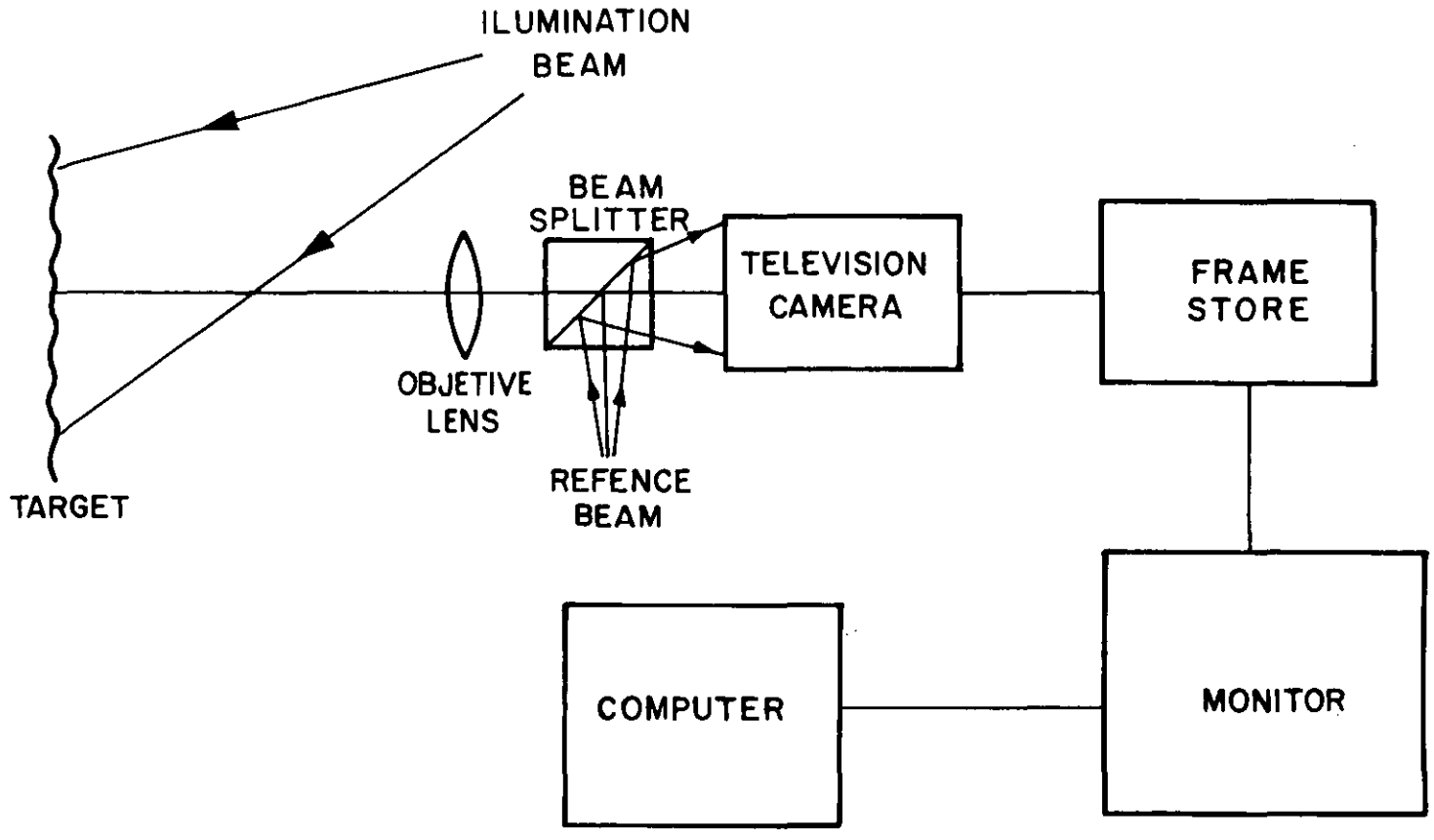

Fig. 3.1
Typical out-of-plane sensitive ESPI system.

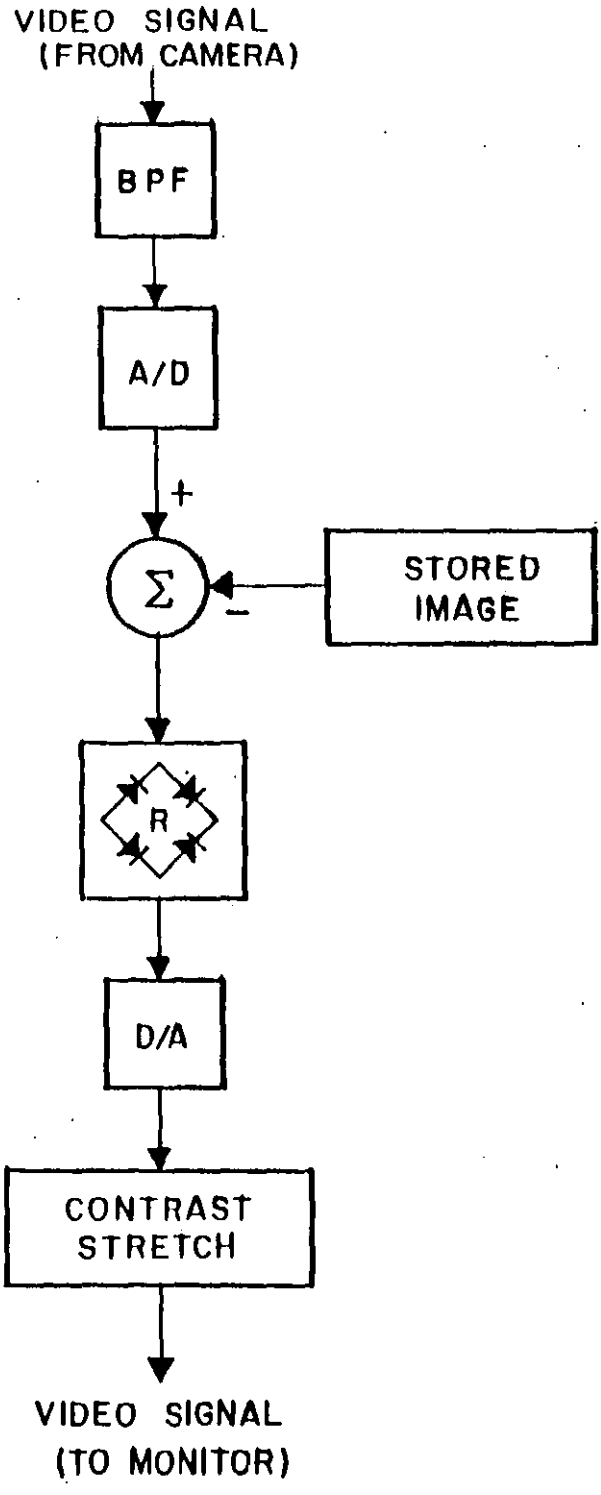

Figure 3.2
Flow diagram of the frame store.

3.2.1 The EMC system

Consider an target surface described by $z_1 = f_1(x,y)$ (Fig. 3.3). A linear grating whose rulings are perpendicular to the plane of the paper is projected on the surface. If the angle between the projection and viewing axes is β, the intensity distribution on the image plane is described by [Hovanesian and Hung (1971)]:

$$I_1(x,y,z) = A + B \cos \frac{2\pi}{p} [x \cos \beta - z_1 \sin \beta], \qquad (3.1)$$

were A and B are constants and p is the grating period.

Consider a second target surface function $z_2 = f_2(x,y)$, which may represent a deviation from z_1 or the real target surface under test if z_1 is a flat, reference surface. Its intensity is

$$I_2(x,y,z) = A + B \cos \frac{2\pi}{p} [x \cos \beta - z_2 \sin \beta]. \qquad (3.2)$$

These intensity distributions, represented by voltage signals V_1 and V_2, are proportional to I_1 and I_2 respectively. The resulting processed video image is proportional to

$$V_1 - V_2 \propto |I_1 - I_2|$$

$$= B \cos \frac{2\pi}{p} [x \cos \beta - z_1 \sin \beta]$$

$$- B \cos \frac{2\pi}{p} [x \cos \beta - z_2 \sin \beta]$$

$$\cong K \sin \left[\frac{\pi}{p} (z_2 - z_1) \sin \beta \right] \sin \left\{ \frac{2\pi}{p} \left[x \cos \beta + \frac{z_2 + z_1}{2} \sin \beta \right] \right\}, \quad (3.3)$$

where K is a constant. Equation (3.3) represents the original projected fringe (except for a slight difference in phase) amplitude modulated by the factor

$$K \sin \left[\frac{\pi}{p} (z_2 - z_1) \sin \beta \right].$$

This modulation function corresponds to the moiré fringes and has a minimum wherever

$$\frac{\pi}{p} (z_2 - z_1) \sin \beta = n\pi,$$

where n is an integer, hence

$$\Delta z = (z_2 - z_1) = n \frac{p}{\sin \beta}. \quad (3.4)$$

The result is a moiré pattern representing a contour map of the surface $z_2 = f_2(x,y)$ with reference to the surface $z_1 = f_1(x,y)$, and with contour intervals given by equation (3.4). In the case where z_1 represents a flat surface the resultant moiré pattern will be a depth contour map of the surface z_2.

In order to use spherical illumination (which is used in practical conditions for big object testing), it is necessary to make some corrections to Eq. (3.4). This was introduced by Gasvik and Fourney (1986) and is given by

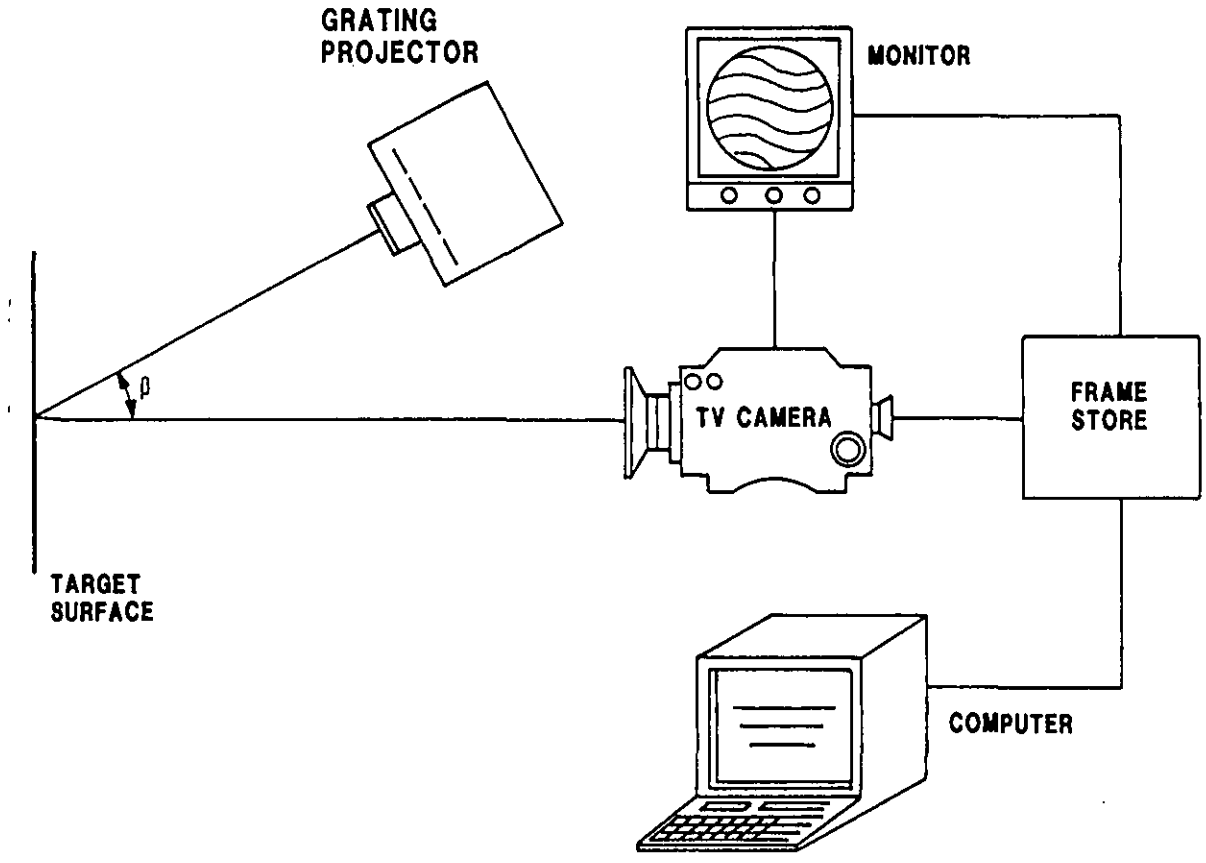

Figure 3.3
Layout of the electronic moire contouring geometry.

$$\Delta z = \frac{p_o}{\sin \beta_o} \sqrt{\left(\sin \beta_o + \frac{x}{l_p} \right)^2 + \cos^2 \beta_o} \qquad (3.5)$$

where p_o is the p value in the centre of the target surface which is the origin of the coordinate system, β_o is the projection angle to the centre of the target and l_p is the distance from the centre of the projection lens to the centre of the target. x is the distance along the target measured from the origin. It can be seen that for $x = 0$ or $l_p >> x$, equation (3.5) reduces to equation (3.4), in agreement with the given theory.

Fig. 3.3 shows the experimental layout of the EMC system. A linear grating of period p is imaged obliquely at an angle β with respect to the viewing axis. A TV camera images the target with the projected fringes; the result can be observed on a TV monitor connected to the frame store output. The main components of the frame store, a FOR.A FM60 Digital modified at Loughborough University of Technology by Mr. T. West, are shown in Fig. 3.2. This device is fed with a video signal from the TV camera which views the target surface and captures a first image of it. Subsequent images are subtracted from the first one at TV frame rate (25 Hz). The projector employed is a MP-1000 Newport Moiré Projector, which is mounted on a stage with a micrometer controlled transverse arrangement. The grating is fixed in the projector. The resultant image displayed on the monitor is an image of the target with moiré fringes superimposed upon it.

3.3 Some Applications

In the following sections, some applications of the EMC system will be described. These applications were simulated

on real targets like plastic bottles, and thin plastic plates.

3.3.1 Example 1: Shape measurement

For shape measurement of a target, an image of a known, flat surface superimposed with projected fringes is captured in the frame store. A 40 mm diameter spherical target is then replaced for the flat surface and its image is subtracted from that of the flat surface without altering the fringe projection layout. Fig. 3.4a is a photograph from the monitor of the contour map. In order to obtain the phase map and isometric plot from the contour map, as before, the phase-stepping method is used. Three contour patterns are captured: one at -120°, the second 0° and third shifted with respect to the last one by $+120^{\circ}$. This is achieved by translating the projection system transversely with the micro-positioner. The translation is perpendicular to the projection axis, by 1/3 (120°) of the grating pitch. Three intensity values I_1, I_2, and I_3 at each pixel location are used to compute the phase of the contour pattern from the relation [Viz. Reid, et al. (1984)]

$$\phi = \tan^{-1} \frac{\sqrt{3}\,(I_3 - I_2)}{2I_1 - I_2 - I_3}. \qquad (3.6)$$

Evaluating Equation (3.6) at every pixel location transforms the three contour patterns into a modulo 2π (wrapped) phase distribution which is directly related to the shape of the surface. Fig. 3.4b and 3.4c show the phase map and isometric plot respectively.

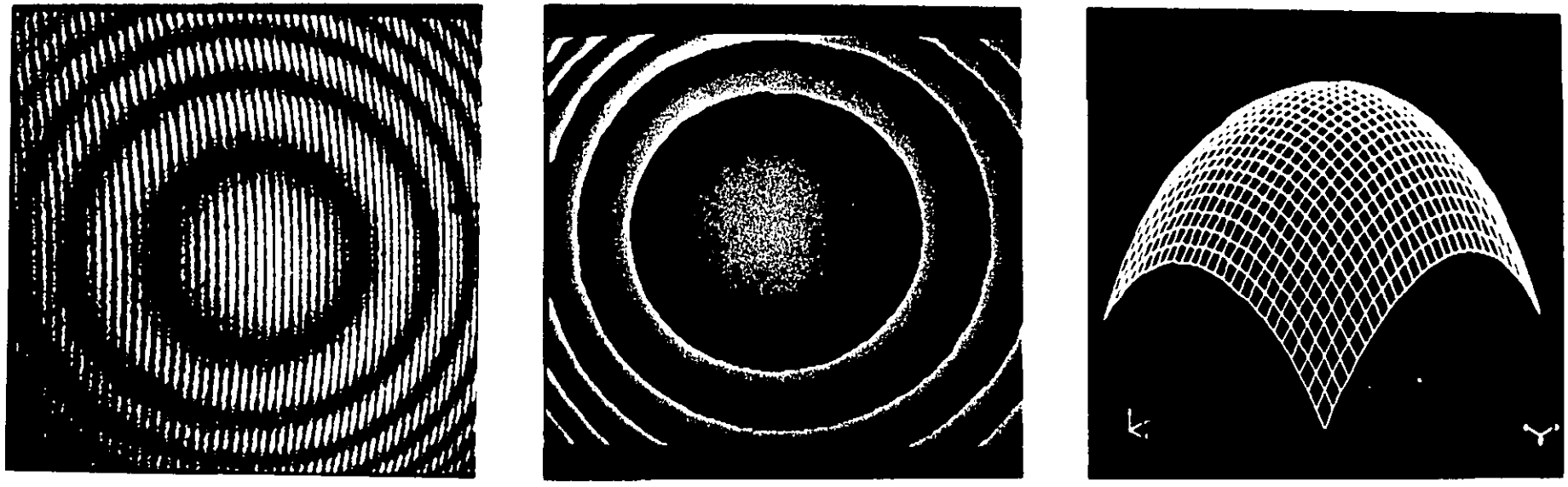

Figure 3.4
Experimental results for absolute shape measuring by EMC: (a) contour map, (b) unwrapped phase map, and (c) shape information.

3.3.2 Example 2: Surface inspection

Using the EMC system, surface defects can be detected and quantified. For quick inspection, a linear grating projected on a flat surface is stored. Replacement with the target under test and subsequent subtraction from the flat surface without altering the fringe projection layout, produces a contour map on the monitor. If a defect exists on the surface under test, the contour map will show it. Sudden changes on smooth contour fringes give an account of the defect. Fig. 3.5 shows this situation for a 2 litre plastic bottle where the depth interval, Δz, was 3 mm. The physical difference that makes figures 3.5a and 3.5b different is a dent on the the target surface. Obviously the surfaces under test may be continuous in order to detect the sudden changes on the fringe contours.

A quantitative analysis of defects may be achieved using the phase-stepping method. Following the same procedure as for shape measurements, a phase map and isometric plot are obtained and shown in Fig. 3.6. In this case the grating pitch on the target was 0.83 mm and $\beta = 32^{\circ}$. The defect was identified as a 15 x 10 mm dent on the bottle surface with variable sinusoidal shape whose maximum depth was 2 mm.

In order to use the EMC method in on-line inspection, which may be useful to adapt in go/no-go controllers, other alternative surface inspection is describe. This alternative makes possible qualitative comparisons between a 'master' surface and a test specimen. A reference surface without defect and with superposed projected fringes is stored. The test surface is replaced at the same position without altering the projected fringe geometry. If this surface is free of defects, a dark field is seen on the monitor. If a defect exists or the surface is not identical

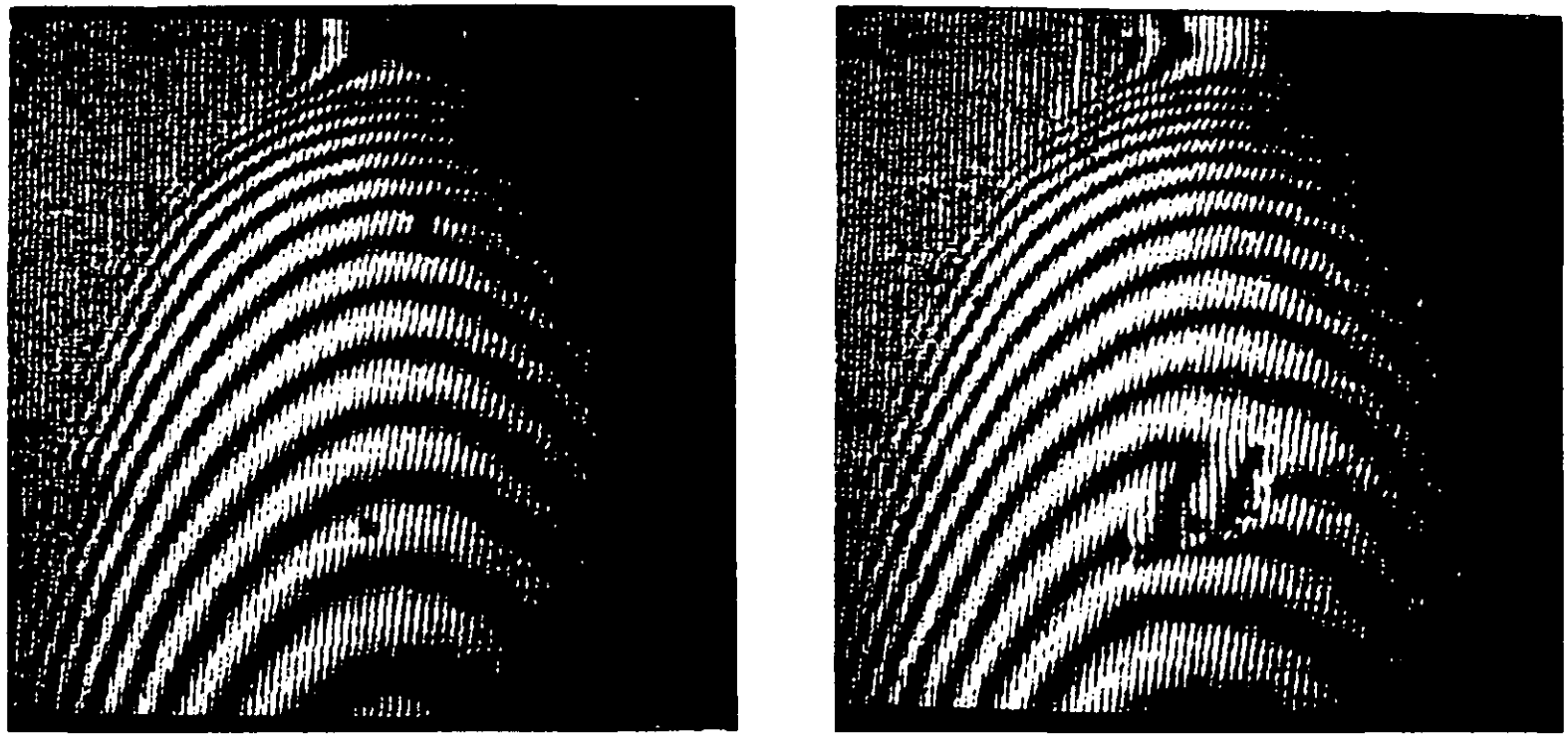

(a) (b)

Figure 3.5
Defect detection for quick surface inspection. Contour maps obtained from a 2 litres plastic bottle: (a) without defect and (b) with defect.

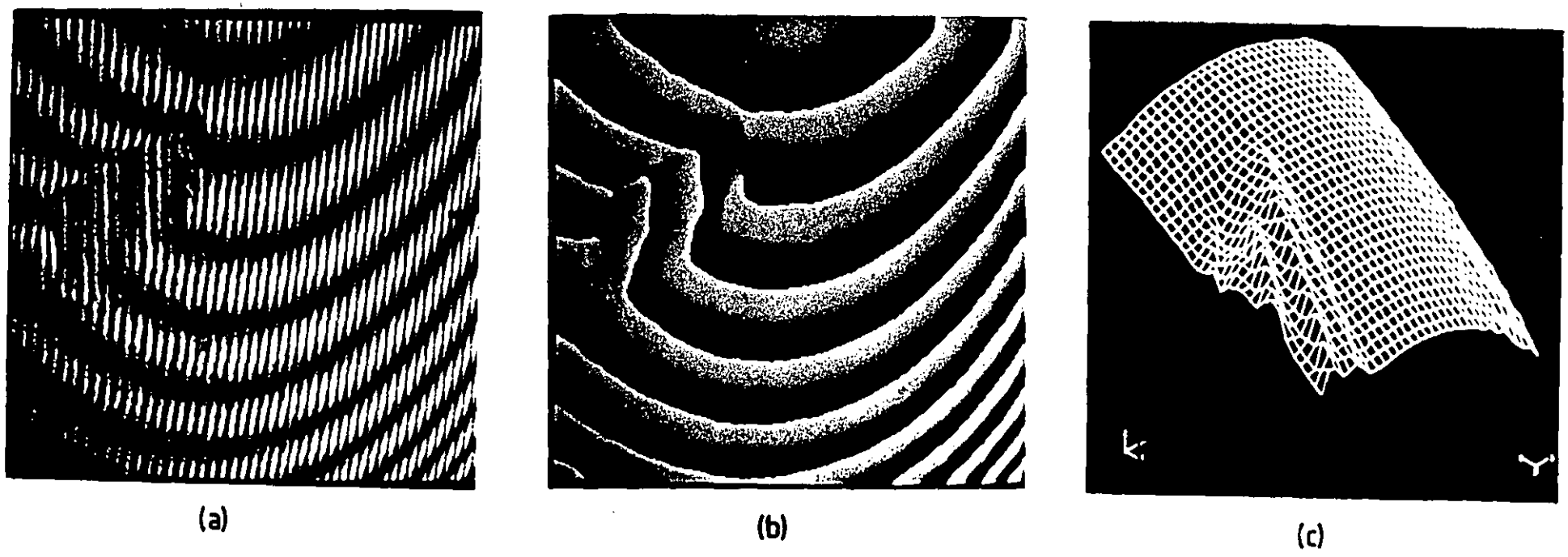

Figure 3.6
Quantitative results for defect measuring: (a) contour map, (b) unwrapped phase map, and (c) wiremesh isometric.

to the reference one, the result is a moiré pattern showing this deviation. Fig. 3.7 shows the comparison between two plastic bottles with and without a defect. The result is clearly seen. The field around the defect is not dark because the reposition is not good enough. However, for a quick practical qualitative comparison, the result shown on the monitor screen is suitable.

It is necessary to mention that both alternatives for surface inspection described above, are very useful in industrial environments. However, care will be necessary during the last alternative, since accurate repositioning of the test surface on the master one is essential.

3.3.3 Example 3: Deformation measurement

In order to demonstrate the possibility of extending the EMC technique to deformation measurement, a thin plastic cylindrical surface was tested. The dimensions of this cylinder are shown in Fig. 3.8 left, where initially the surface is of 50 mm in radius and 60 mm in length. An image of this initial state of the shape with projected fringes on it is stored. A load P is applied to the middle part of the surface which produces a deformation depicted in Fig. 3.8 right. Deformation contours appearing over the surface can be seen on the monitor. By using the usual phase-stepping procedure, the final acquired shape of the deformed target is obtained as seen in Fig. 3.9. In this case the contour interval is 2.5 mm which indicates that the larger deviation (centre of the target) from the original undeformed is 5 mm.

3.4 Evaluation of the technique

In order to obtain the required information, the depth of field of the viewing system in the EMC setup must be

Figure 3.7
Result obtained by comparing two bottles with and without defects.

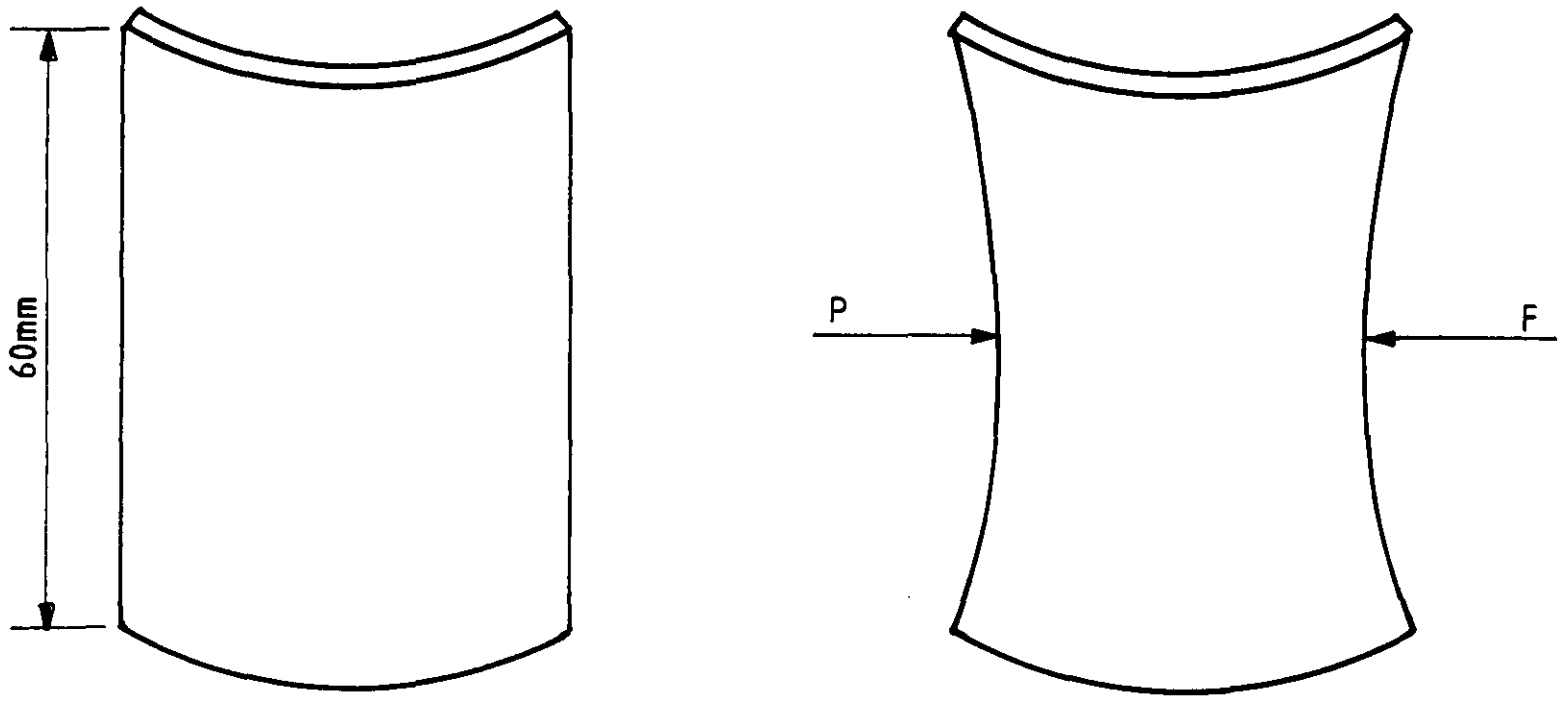

Figure 3.8
A thin plastic surface. Left, initial cylindrical form, and right, surface shape acquired by applying a load P.

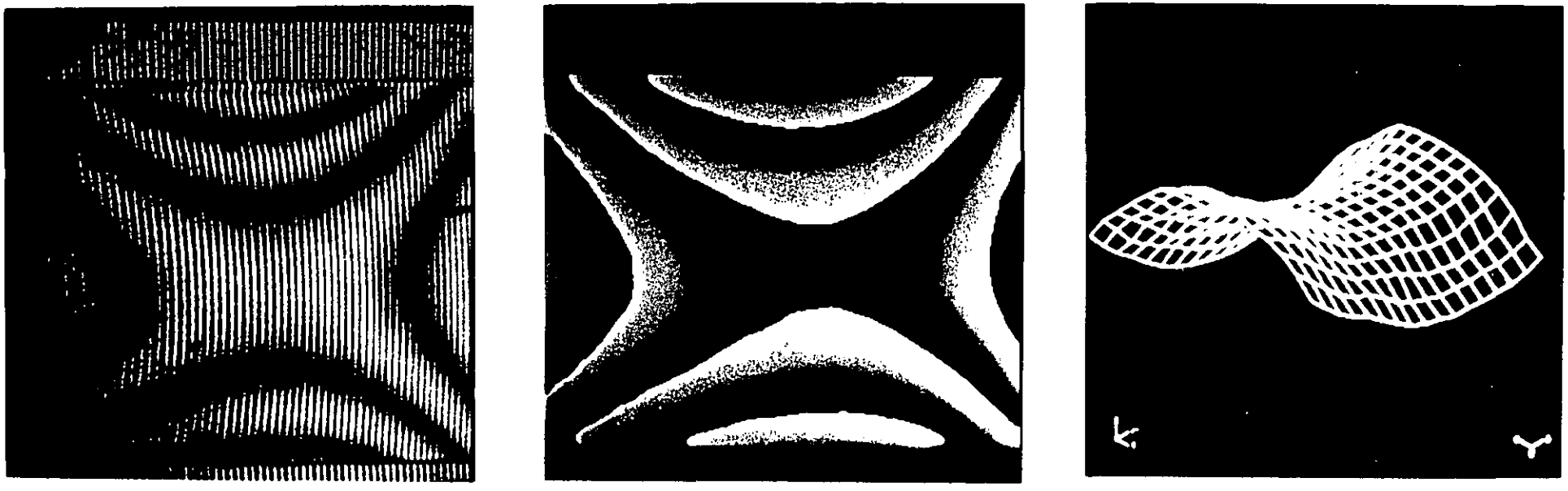

Figure 3.9
Final deformation result after the surface is loaded. (a) contour map, (b) unwrapped phase map, and (c) final surface form.

sufficient to cover the depth of the target surface. This is achieved by reducing the aperture of the viewing lens. However, the image of the grid contour is degraded by diffraction effects when the aperture is closed down. Also, the amount of light reaching the camera is less, then the signal to noise ratio is lower. The EMC technique was evaluated in terms of its visibility of the fringe contours. Image subtraction achieved by the electronic device of the EMC was compared with image subtraction carried out directly with a digital image processing card, the ITI FG100, which sits on the pc buss. Also a comparison was made on the basis of the variation of the aperture of the vision system and the practical considerations of the television camera.

Figure 3.10 shows the intensity profile of a Ronchi grating projected on a flat surface. The images are captured for different aperture diameters (f-numbers) via the frame store (Fig. 3.10a) and without it, in direct form by the computer (Fig. 3.10b). The effect of the electronic device in EMC is noticed, in the truncation of the peaks in Fig. 3.10a. This is due to the electronic processing applied to the video signal. Since the electronic device is designed to work with speckle, it converts a variation of speckle contrast to a variation in mean intensity improving the contrast in the output signal.

The band pass filter in the electronic device (Fig. 3.2), is centered in 1.1 MHz and is used in order to minimize the random variations of the speckles in ESPI. In the case of EMC, this band pass filter helps to eliminate, in part, the carrier fringes. Also, included in the frame store are the rectification and contrast stretching steps. In particular the rectification step produces a

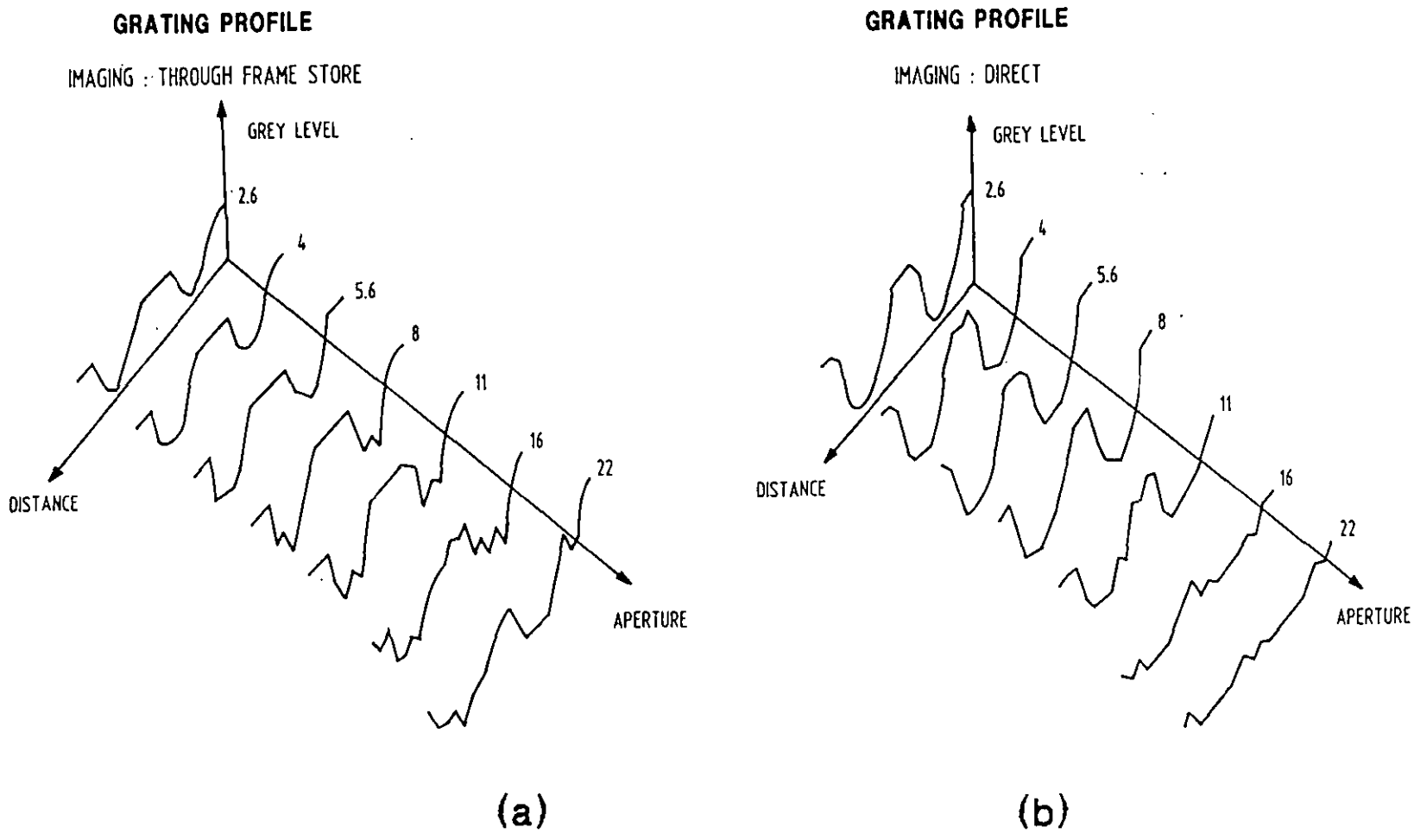

Figure 3.10
Image profile of a Ronchi grating projected on a flat surface. Captured images for different aperture sizes via: (a) frame store and (b) direct.

doubled carrier frequency. Grid contours obtained by projecting a grating on a flat and spherical target are shown in figure 3.11a and b respectively. Depth contours in Fig. 3.11c correspond to a direct subtraction by the computer of the grid contours and 3.11d shows the depth contours obtained through the frame store. Clearly it is noticed in this last result how the electronic device nearly erases the doubled carrier frequency producing a better fringe contrast.

An often adopted way of analyzing the contrast of an image is by measuring the standard deviation from its histogram. The standard deviation was measured for each contour map by varying the aperture size. A graphical comparison is shown in Fig. 3.12. for depth contours obtained through the frame store and directly by the computer. A higher contrast is found when electronic subtraction is performed compared to direct computer subtraction.

Solid state detector arrays, such as Charged Coupled Devices (CCD's) cameras, are more frequently used for the image acquisition of fringe patterns. They consist of an accurate geometric screen containing light sensitive elements (pixels). The intensity incident on a pixel can be digitized and stored in discrete values in a computer memory. Normally intensity values are from 0 to 256. CCD's are chosen because the response at each pixel shows good linearity with the incident intensity.

Due to the finite number of intensity levels, a discrete sampling error may be made. Normally this discrete sampling error does not significantly influence the performance of the phase-stepping method. However, problems can arise when the contrast in the moiré fringe pattern is low. Then, with

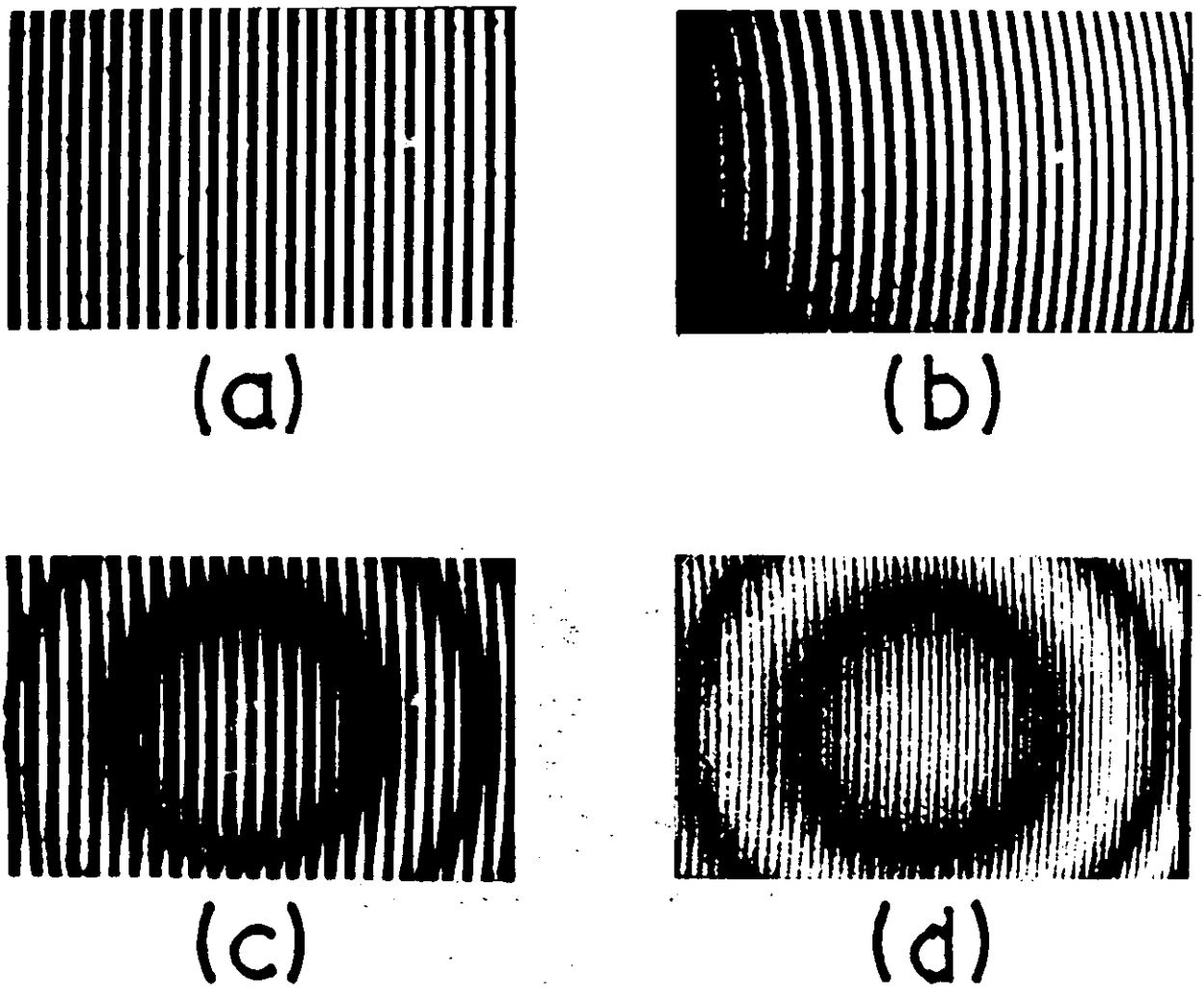

Figure 3.11
(a) and (b) grid contours generated by projecting a linear grating on a flat and spherical object, respectively. Depth contours generated by subtracting the above grid contours via: (c) direct and (d) frame store.

CONTOUR CONTRAST ANALYSIS

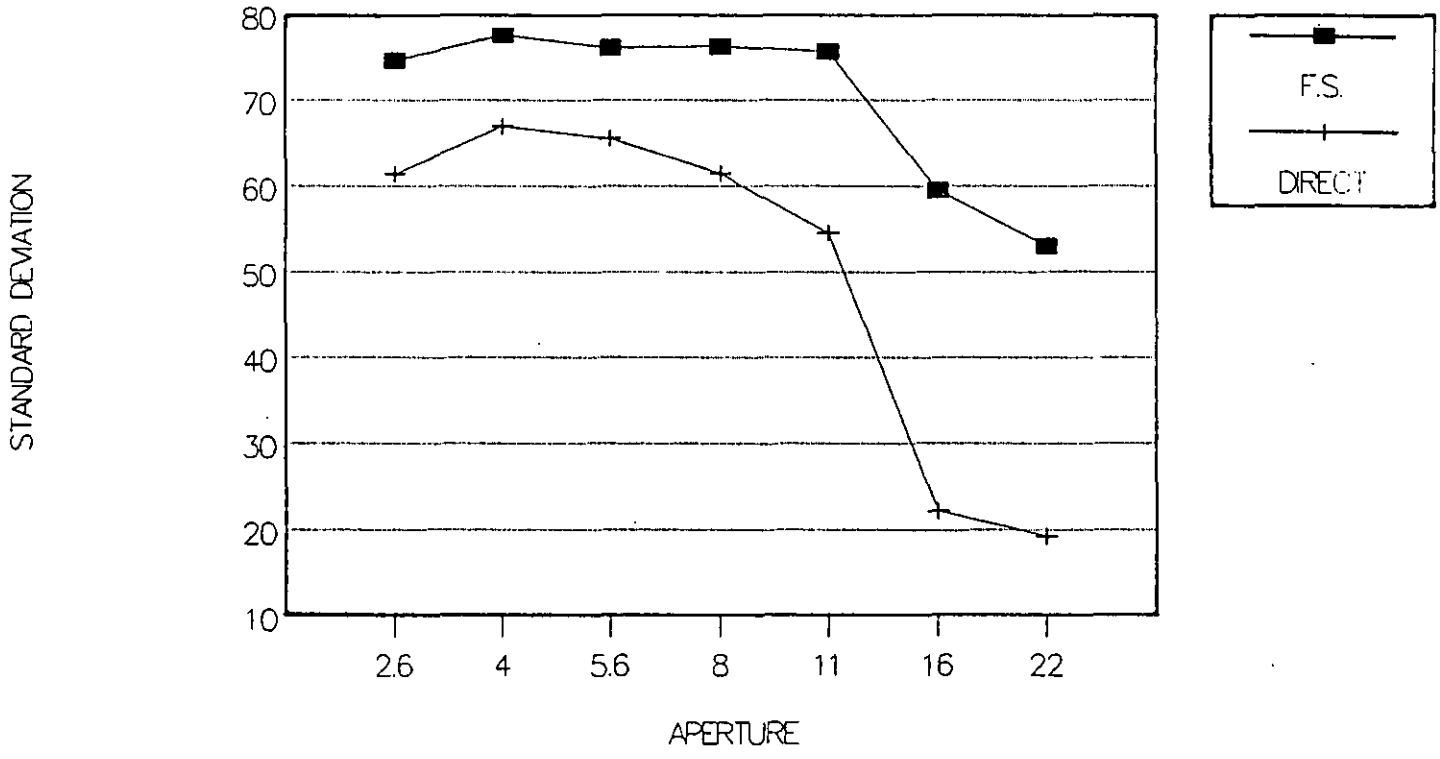

Figure 3.12
Contour contrast comparison produced (▪) electronically and (+) using the computer.

the electronic device, this situation is alleviated in an inherent manner.

From Eq. (3.6) the phase $\phi(x,y)$ can be obtained. As a result of using the arctan function the phase always lies between $-\pi$ and π. Since surfaces under consideration are supposed to be continuous, the continuous phase is obtained after compensating the phase jumps. To distinguish phase jumps from the object dependent phase difference in adjacent pixels theoretically more than two pixels per fringe must be acquired [Greivenkamp & Bruning (1992)]. In the EMC case this situation applies. The grid contours captured by the CCD must be separated by at least two camera pixels, bearing in mind the camera lens resolution.

3.5 Computer generated gratings

As a follow up of the EMC work, the possibilities of producing the grating phase change by computer, as well as computer generated gratings, were explored. The primary advantage is that only one contour frame needs to be digitized instead of the three required by the conventional method. Also, repeatability and accuracy of the phase shift is fixed. One image of the contour map can achieve better results than those using three or more images, where small fluctuations in the shape of the target can not be avoided (such as when measuring biological specimens or parts of the human body). Further, computer generated fringes may be exactly specified in terms of their profile to allow matching.

In order to generate a grating in a computer it is necessary to have a precise knowledge about the profile of the grating projected on the target. It has been demonstrated by Yokozeki (1982) that one can have better

visibility in moiré patterns when the profile of the grating is closely similar to that projected on the target. Then the computer generated grating should be matched in profile to the projected grating. The periodic computer generated grating is built up by assigning each picture element (pixel) of the image processor system memory a number between 0 and 255. These numbers correspond to a grey level. The grating profile, period, bias, and positioning can be chosen using a simple computer program. Fig. 3.13 shows a graph of the grid contour profile (white spots) trying to match with the computer generated grating profile (black spots).

This situation was tested on a car body panel. By using the EMC system, a grating was projected on the target surface. Having matched first the profiles between grid contours and the computer generated grating, the subtraction was made. Fig. 3.14 shows (a) grid contours, (b) computer generated grating, and (c) contour map. In the same figure (d) and (e) shows the rotated computer generated grating and the subtracted contour map, respectively. This last result shows the possibility of varying the contour interval avoiding ambiguous discontinuities on the target surface [Reid, et al. (1987)].

3.6 Conclusions

The potential of Electronic Moiré Contouring linked to the phase-stepping method has been demonstrated experimentally. Absolute and comparative shape measurements have been carried out, in a simple and quick way to capture and retrieve information. Extension of EMC to surface deformation has shown that the technique can be used in a similar way to that of ESPI, with a reduced sensitivity.

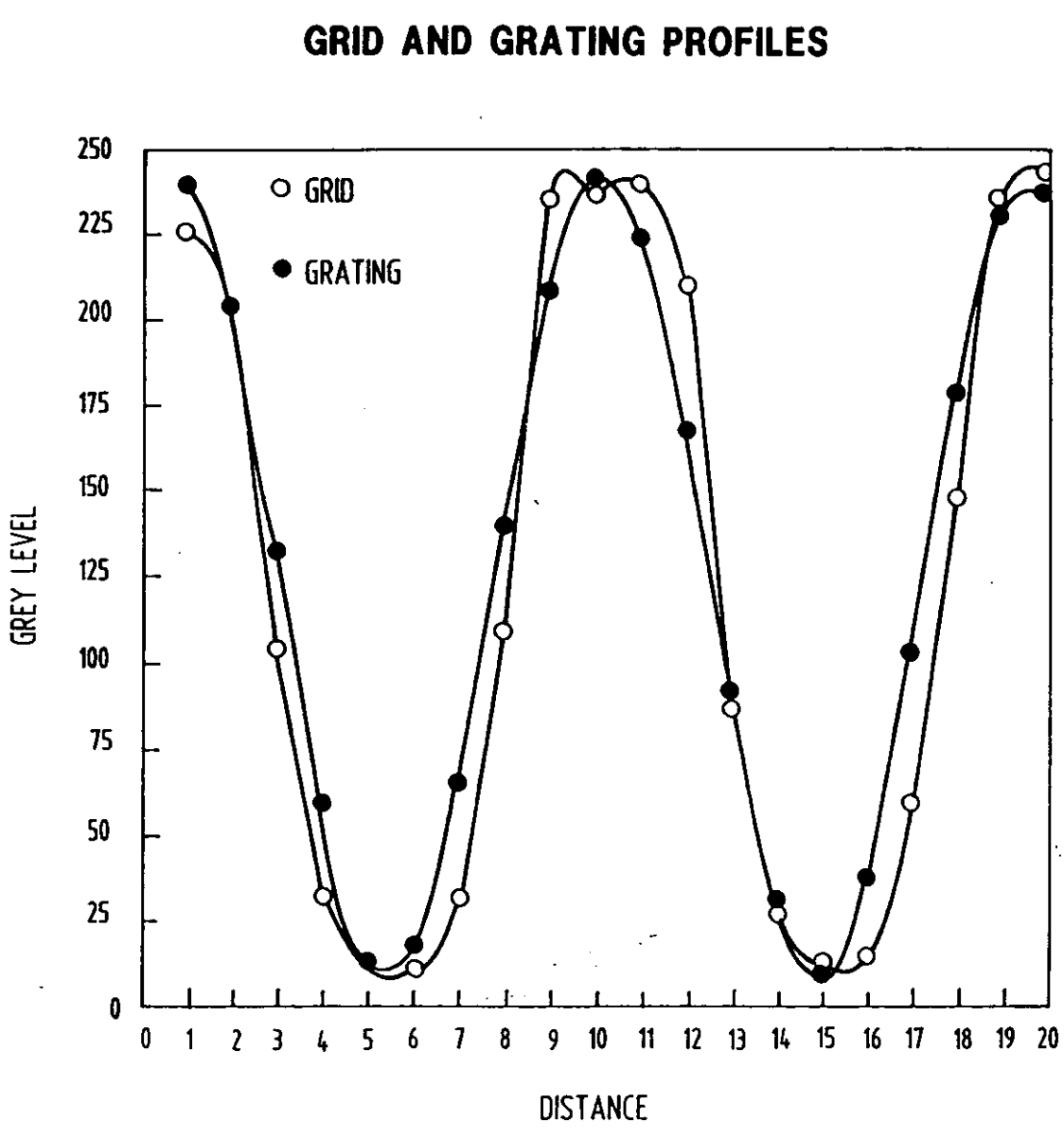

Figure 3.13
Matching grid contour and computer generated grating profiles.

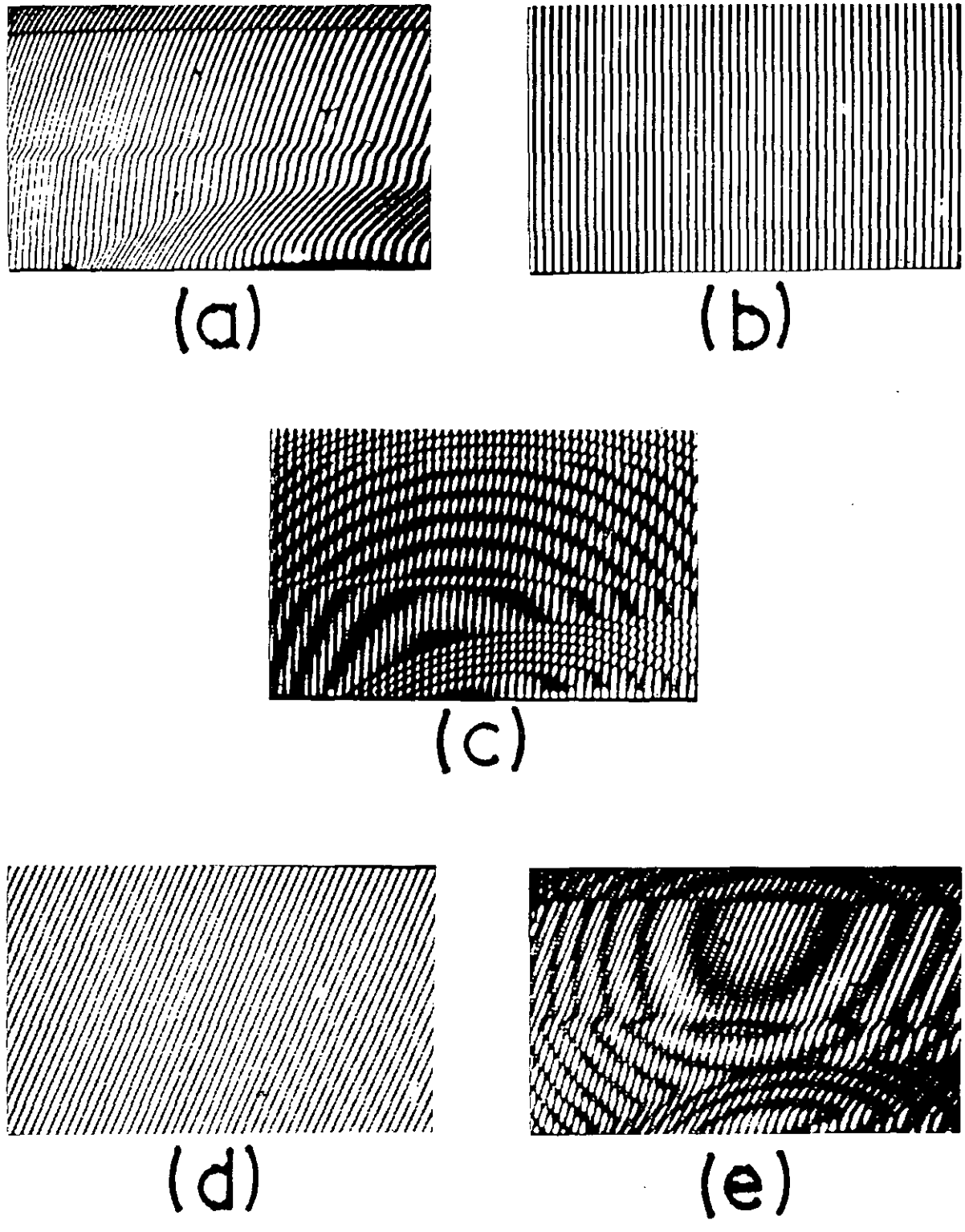

Figure 3.14
(a) Grid contour on a car body panel, (b) computer generated grating, (c) depth contour generated by combining (a) and (b). (d) Computer generated grating rotated and (e) contour generated by combining (a) and (d).

This is useful when measurement of large displacement or the shape of big targets is desired.

This method is very suitable for comparing the shape of different targets and therefore offers a powerful means for measuring the surface profile difference between a product specimen and a master target in real time. This is obtained by subsequent recording of the master and the product, resulting in a moiré pattern which maps the difference between the two targets due to, for example, manufacturing defects.

The use of computer generated gratings linked to the phase-stepping technique is proposed. This can be useful to simplify the procedure in data reduction. The main advantage of this approach is that only a single image of the specimen grating is required, unlike in the conventional approach, which requires three images of the specimen grating. This approach thus avoids the need to have precisely controlled mechanical shifts of the generating contours to get the multiple images needed in the conventional phase-stepping method.

Finally it is necessary to mention that with conventional holographic or ESPI systems, the contour interval obtained is of the order of λ, the wavelength of the light employed. Sometimes it is not necessary to use such a high sensitivity. For example, if big targets are tested, like car body panels, where defects of 1-5 mm on an area of 1 square meter or more exist, the EMC technique is far better for carrying out such testing.

CHAPTER 4

Electronic speckle contouring

4.1 Introduction

Although in recent years, numerous applications of Electronic Speckle Pattern Interferometry (ESPI) to the measurement of target deformations have been described, some long-existing limitations have essentially restricted its use to a laboratory type environment.

Among those limitations, rigid body motion is undoubtedly one of the most severe. The double exposure method measures the change in optical pathlength between exposures with very high sensitivity. Rigid body motion usually accompanies object deformation in practical engineering structures. The resulting interferometric fringe pattern may yield mostly undesired displacement information due to this rigid body motion. Furthermore, rigid body motion may degrade or even completely destroy the resultant speckle fringe pattern due to decorrelation.

A quantitative description of the measurement may be displayed as a wire-frame isometric plot. This must be scaled with reference to some plane fixed in space. However, one other major constraint which is at present preventing a more widespread industrial application of the ESPI techniques, is the inherent complexity of the data produced, creating a requirement for specialised analysis skills in interpretation of fringe patterns. For example, most engineering objects are not flat, but the TV picture produced by the system is a 2-D version of 3-D scene, therefore a perspective shortcoming in the object's field of view is obtained. Some structures (e.g.,

automobile engines) have disjunctures in their surface where a part may move independently of another making a big problem for fringe analysis. Some interpretation ambiguities are also found when a displacement to be measured is several orders of magnitude larger than the sensitivity interval of the instrument. In order to remove such ambiguities of perspective and disjunctures and relay deformation to position on the surface, it is necessary to have an a priory knowledge of the surface shape. Furthermore, it is advantageous to combine the surface form and displacement measurement capability in a single instrument, where the complete 3-D amplitude vector is determined.

Electronic Speckle Contouring (ESC) is concerned with shape measurement using 'fringe projection' techniques in ESPI. This chapter shows the advances made by the author in the contouring field using ESC. The aim is to provide both deformation and shape data from one instrument for combination in fringe analysis. In-plane and out-of-plane displacement sensitive ESPI instrumentation are employed for contouring without alterations to the optical hardware. The contour maps of three-dimensional diffuse targets are obtained by small shifts of optical fibres carrying the object and reference beams illumination.

In this chapter, a novel theoretical approach is also described for ESC fringe. It is theoretically demonstrated and experimentally verified that ESPI fringes produced by wavefront shift are equivalent to a set of projected interferometric fringes, and also to results obtainable from projection grating moiré topography. Considering the latter, it is then possible to discuss a simplified analysis, and to transfer the experimental knowledge

directly to the ESC apparatus. Phase measurement and digital image processing are employed for quantitative data reduction.

4.2 In-plane sensitive system

The grainy appearance of an object when illuminated by coherent light is referred to as the speckle effect. The speckle pattern, caused by the random interference of light scattered from various points on the target surface, acts as a grid naturally printed on the target surface [Hung (1978)]. A number of techniques have been reported on the utilization of this speckle pattern for measuring surface deformation. The speckle effect may be used to obtain information along the **x**, **y** and **z** target axes. Depending on the illumination and viewing direction, in-plane and out-of-plane sensitive systems may thus be created.

The in-plane sensitive system, was introduced by Leendertz (1970) and more recently investigated by others [Joenathan, et al. (1990), Mendoza-Santoyo, et al. (1991), and Zou, et al. (1992)]. This method requires the specimen to be illuminated by two coherent beams at equal angles with respect to the optical viewing axis. The sensitivity of the method depends on the geometrical parameters of the optical arrangement. This will be shown in the next section.

4.2.1 Contour generation

The brightness of ESC fringes seen on the monitor screen are described by the same expression used to describe normal ESPI fringes. For example, subtraction fringes [Jones & Wykes (1983) pp. 168] follow a sine function:

$$B = K \sin(\Delta/2),$$

where **B** is the fringe brightness on the monitor screen and **K** is a constant.

In the case of ESC, the phase change Δ arises from the displacement of the object and reference illumination sources. The theoretical derivation of Δ for the general case of moving source illumination is given in appendix B and in the paper by Rodriguez-Vera, et al. (1992). Fig. 4.1 shows the optical geometry for the case of the in-plane sensitive system, where the symmetrically placed illumination sources, S_1 and S_2, make an angle β with respect to the viewing axis and are at distance **l** from the target surface. From the general equation **(B.16)**, and making $l_1 = l_2 = l$ and $\alpha = -\beta$ the position of fringe **n** is

$$\frac{x}{\lambda l}\left(\Delta S_1 - \Delta S_2\right)\cos\beta - \frac{z}{\lambda l}\left(\Delta S_1 + \Delta S_2\right)\sin\beta = n, \qquad (4.1)$$

where ΔS_1 and ΔS_2 are the transverse displacements of the sources S_1 and S_2 respectively, and λ is the wavelength of the light employed. Equation **(4.1)** represents a set of fringes which appear to the observer as if two linear gratings had been projected onto the target surface.

A special case will now be considered where just one source is displaced. For instance, for symmetrically located illumination sources, only one source, e.g. S_2, is translated. This means that the displacement ΔS_1 is equal to zero. The fringe equation **(4.1)** now becomes:

$$x\left(\frac{\Delta S_2}{\lambda l}\cos\beta\right) - z\left(\frac{\Delta S_2}{\lambda l}\sin\beta\right) = n. \qquad (4.2)$$

The above equation represents a grating projected onto the

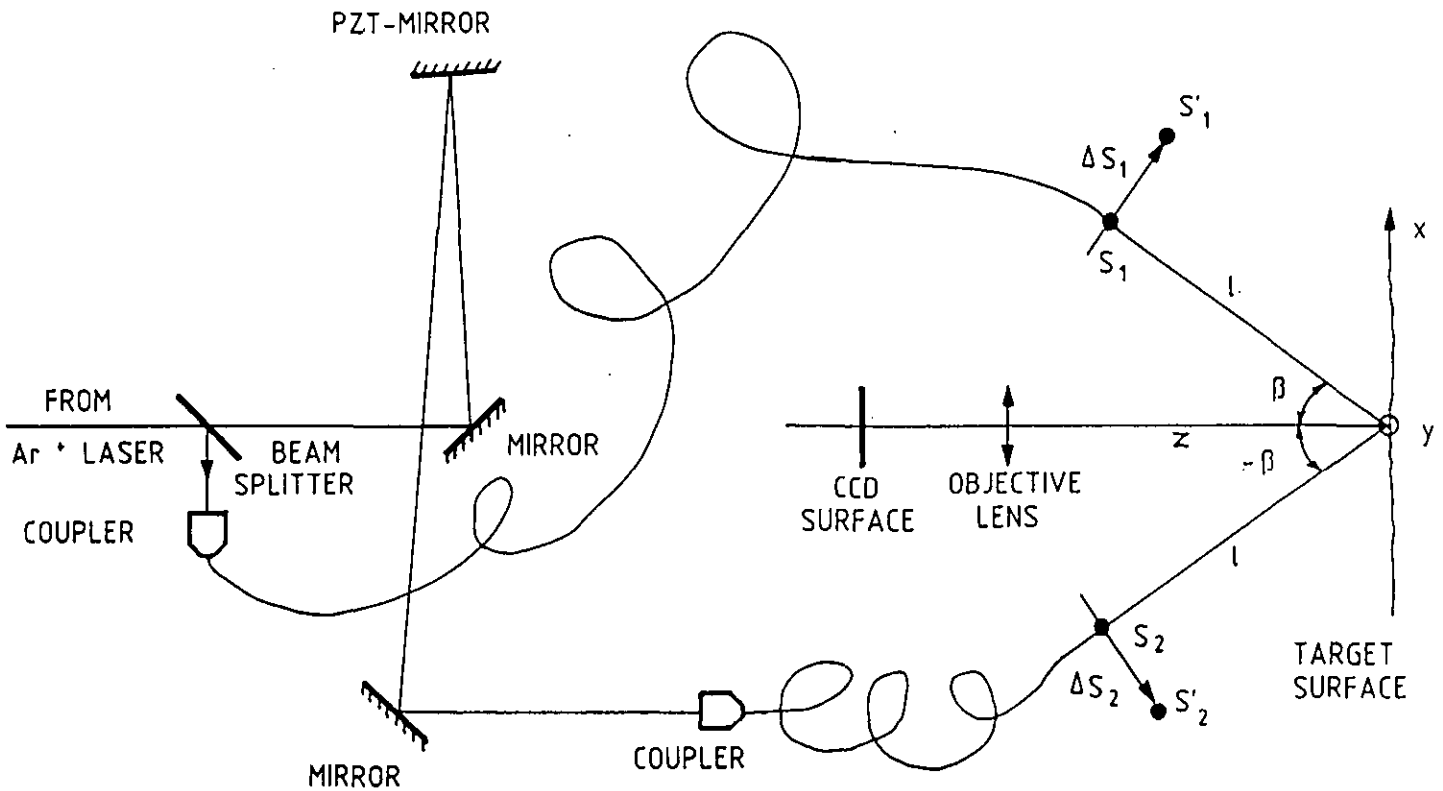

Figure 4.1
Experimental setup of the in-plane sensitive ESC system.

target surface as in traditional fringe projection. The depth or 'contour' interval is given by

$$\Delta z = \left(\frac{\Delta S_2}{\lambda l} \sin \beta \right)^{-1}. \qquad (4.3)$$

It is important to note that the fringe interval Δz is inversely proportional to the optical source displacement ΔS_2. Thus, the fringe interval can be controlled according to the source translation. For a flat surface the fringes correspond to vertical parallel lines with period p given by

$$p = \frac{\lambda l}{\Delta S_2 \cos \beta}, \qquad (4.4)$$

and frequency ν given by

$$\nu = \frac{\Delta S_2 \cos \beta}{\lambda l}. \qquad (4.5)$$

The direct proportionality between fringe frequency and the transverse displacement ΔS_2 is apparent.

4.2.2 Generalization of movement for the illuminating sources S_1 and S_2

So far, we have assumed that the sources moved only in the x-z plane. A similar theoretical treatment can be applied for the case of vertical source displacements. Assuming two orthogonal displacements (one in the x-direction and the second along the y-direction), using only one moving source and a flat target (see Fig. 4.2) equation (4.2) can be rewritten as

$$x \left(\frac{\Delta S_x}{\lambda l} \cos \beta \right) + y \left(\frac{\Delta S_y}{\lambda l} \sin \beta \right) = n, \qquad (4.6)$$

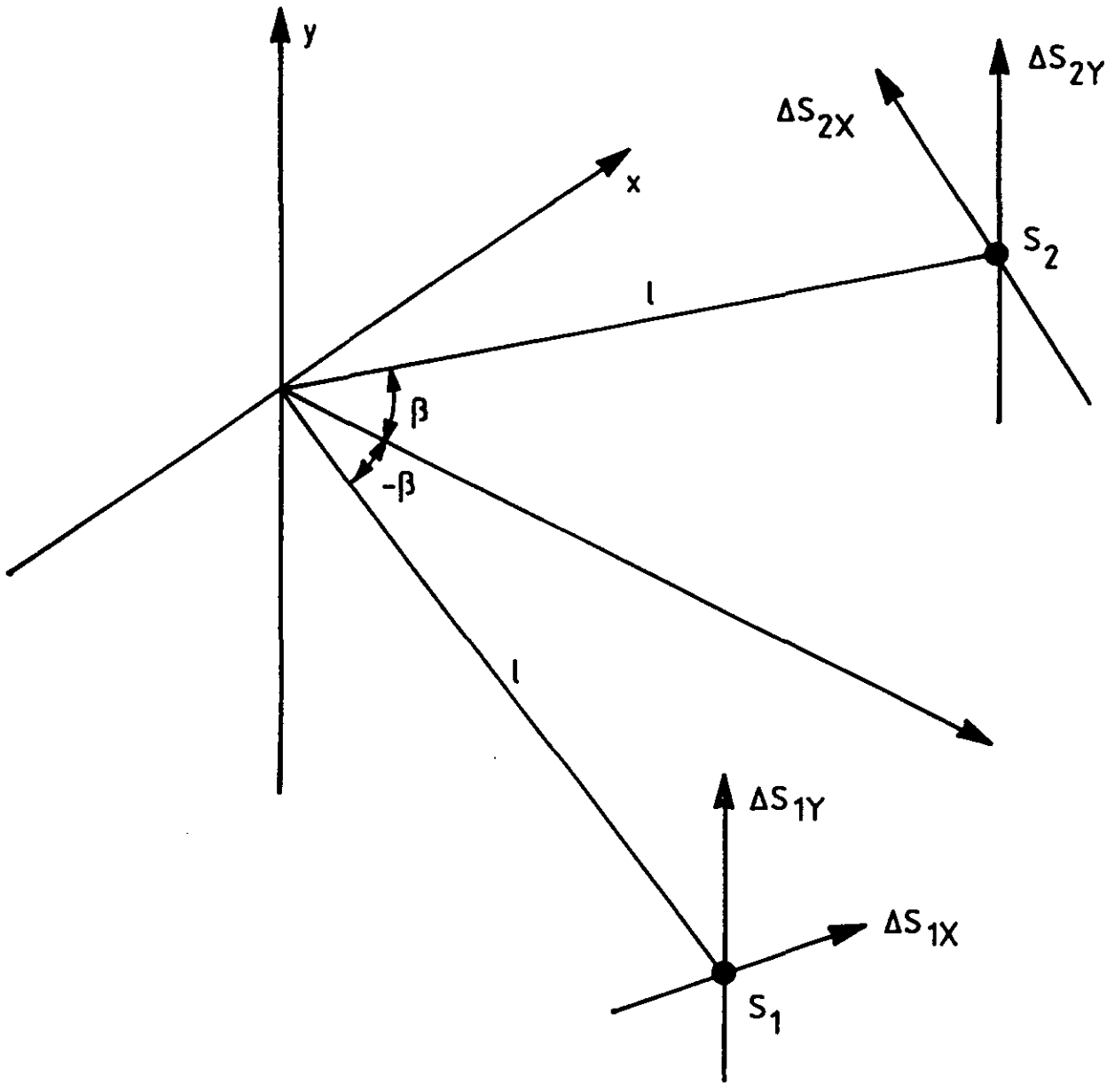

Figure 4.2
Simplified geometry for the in-plane sensitive ESC system.

where ΔS_x and ΔS_y are the displacements of S_1 along x and y-directions. Equation (4.6) represents sets of parallel, inclined fringes whose slope is given by

$$\tan \theta = \frac{\Delta S_y}{\Delta S_x}, \qquad (4.7)$$

where θ is the angle of inclination with respect to y-z plane.

The above theoretical treatment was verified using the apparatus shown in Fig. 4.1. An argon ion laser working at λ = 514 nm was employed. The two illuminating target wavefronts were delivered by optical fibres mounted in micro-position stages at angles $\pm \beta = 24^\circ$ to the viewing axis and l = 460 mm. Fig. 4.3 shows experimental results for a flat target surface. The source movements were:

for image	ΔS_{1x} (μm)	ΔS_{1y} (μm)
4.3a	100	0
4.3b	0	120
4.3c	50	100
4.3d	-50	100

The measured angle θ of the fringes in Fig. 4.3c and 4.3d, agrees with the predicted value given by equation (4.7) to within 1%. Source S_2 remained unmoved in all cases, and the fringes produced may be seen as grid contours.

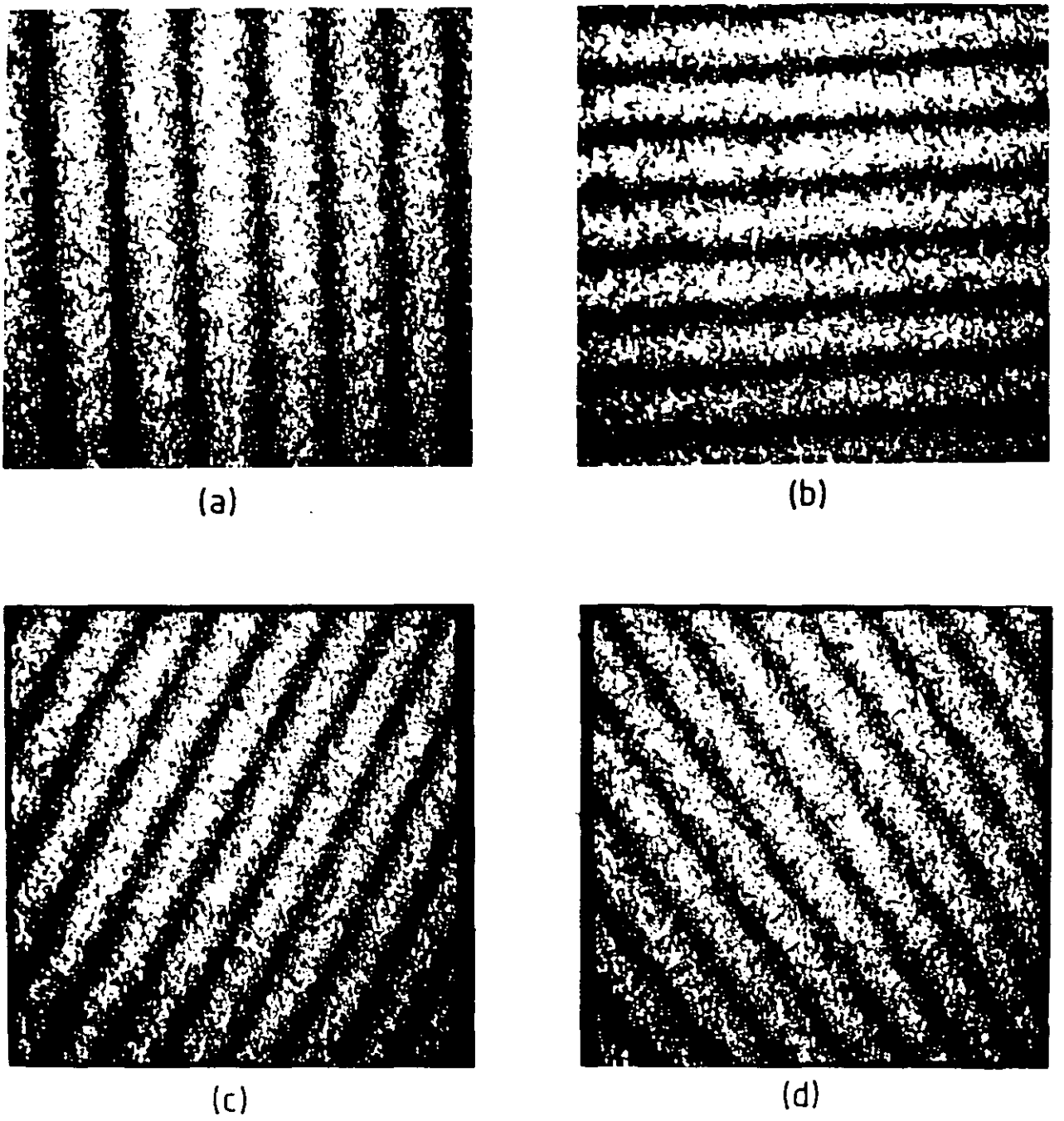

Figure 4.3
Grid contours on a plane surface by single source displacement using in-plane sensitive ESC system.

Call now for a quotation

0800 DIRECT 277377

Lines are open from 8.00 am to 8.00 pm, Monday to Friday, (excluding Bank Holidays), and from 10.00 am to 2.00 pm on Saturdays.

FOLD HERE

1

Midland Direct
FREEPOST
PO Box 421
SOUTHAMPTON
SO15 1XF

New year resolution?

0360

If you would like a quotation when your existing policy comes up for renewal, please fill in this slip and return it to us. We'll call you back nearer the time.

Title [illegible] Initials

Surname

Address

Postcode

Contact telephone number (including dialling code)

Day Evening

Best time to call

We will only telephone you concerning your quote for your home insurance.

Branch Sort Code 4 0 – – –

Please supply the date and month of renewal (approximately).

Date Month

Do you have an existing Midland Home Insurance or Homeplan Policy? Yes ✓ No

Policy Number

Customer Information Service: Midland Bank is a principal member of the HSBC Group*, one of the world's largest banking and financial services organisations. We will not pass information about you to any companies in the Group for marketing purposes without your consent. However, we may send details of our services and those of other members of the Group, which we feel may interest you. If you would prefer not to receive such information, please let your branch know.

*The HSBC Group comprises HSBC Holdings plc, its subsidiaries, including Midland and Associated Companies and their various businesses and departments.

MOISTEN HERE

MOISTEN HERE

Figs. 4.4a and 4.4b show grid contours on a 50 mm diameter spherical surface. The source displacements were:

for image	ΔS_{1x} (μm)	ΔS_{1y} (μm)	ΔS_{2x} (μm)	ΔS_{2y} (μm)
4.4a	60	0	0	0
4.4b	0	0	60	0

To obtain depth contours, the second source should also be displaced, and the fringes in Fig. 4.4c and 4.4d are then obtained. Source displacements were:

for image	ΔS_{1x} (μm)	ΔS_{1y} (μm)	ΔS_{2x} (μm)	ΔS_{2y} (μm)
4.4c	60	0	60	0
4.4d	100	0	100	0

The contour interval is deduced from Eq. (4.1), by substituting the above data. For this case Δz = 3 mm.

A plot of the frequency equation (4.5) is shown in Fig. 4.5. This plot also shows results taken from experiments with the setup of Fig. 4.1. It may be seen from this plot that good agreement exists between the theoretical and experimental data. It should be noted that the arrangement of Fig. 4.1, with both sources fixed, would also function as an in-plane displacement sensitive ESPI device.

4.3. Out-of-plane sensitive system

To transfer this version of the ESC technique into one capable of out-of-plane displacement and shape measurement,

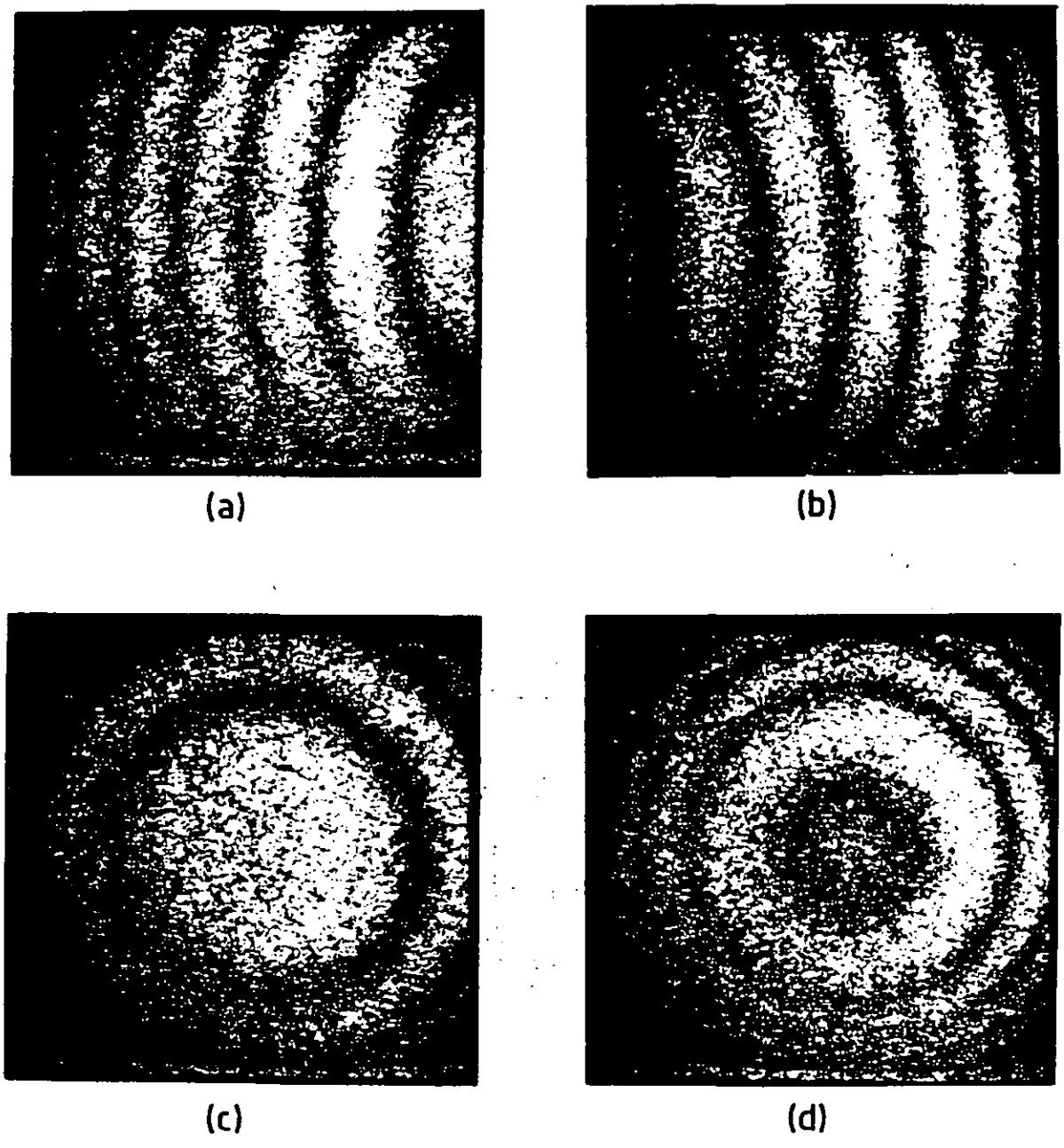

Figure 4.4
(a) and (b) grid contours on an spherical surface with one source displaced; (c) and (d) depth contours on the same surface with both sources displaced in the in-plane sensitive ESC system.

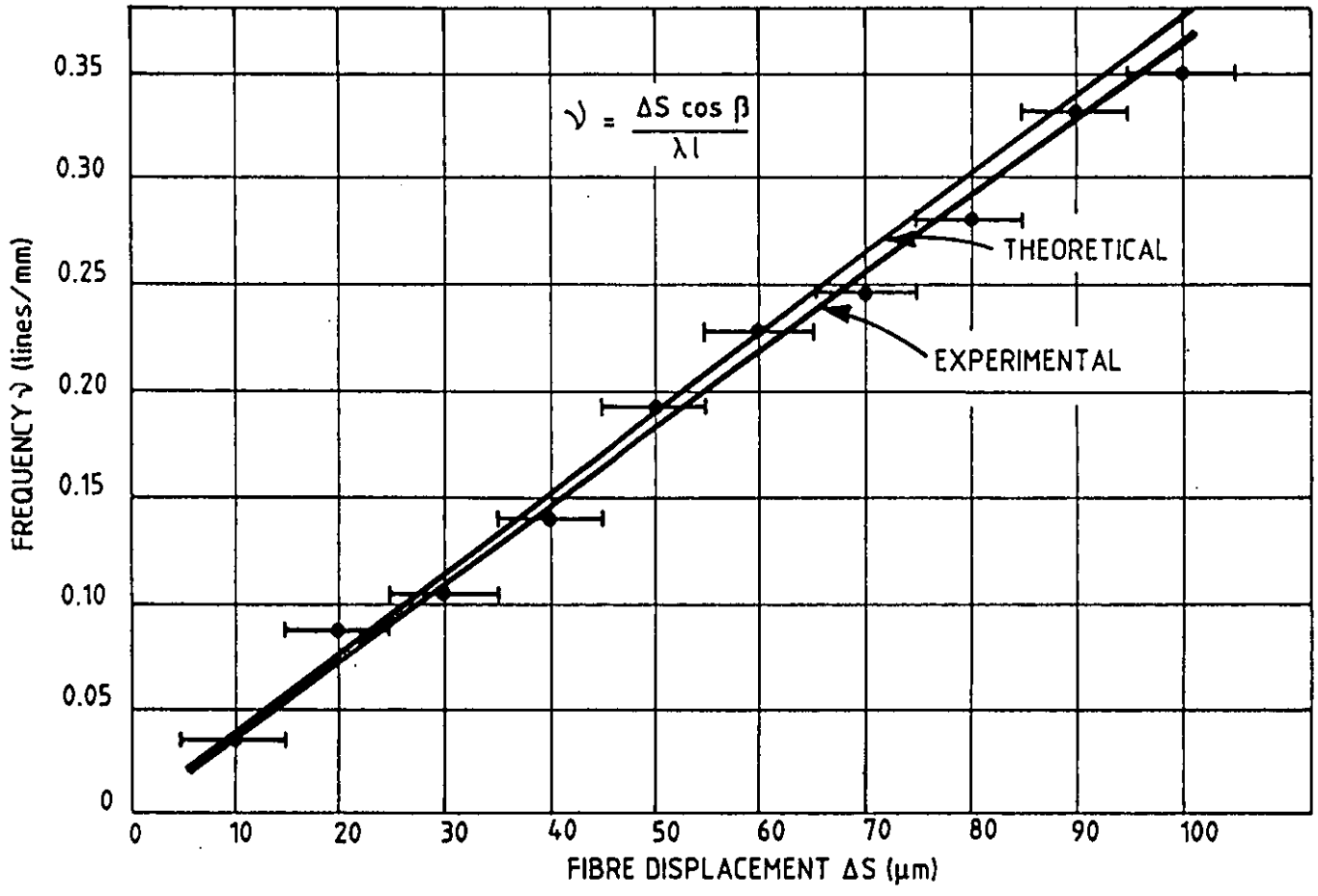

Figure 4.5
Fringe frequency against source displacement.

fibre optics were also used for reference and object beam delivery. Each fibre end is mounted on an x-y translation stage, adjustable by micrometer control, as shown in Fig. 4.6. At their original positions, the two fibre systems remain static, and the arrangement may be used for conventional ESPI displacement or vibration work. For contouring measurement, it is only necessary to slightly displace each micrometer setting in order to obtain the source movements described by equation (4.1), and therefore generate depth contour fringes.

4.3.1 Phase-stepping in ESC

It is not the objective of the present work to discuss the different fringe analysis methods for data reduction. It is possible to find in the literature excellent reviews showing techniques and applications of automatic and interactive fringe pattern analysis [Reid (1986/87)]. Among several of these, the phase shift methods introduced in the early 80's [Hariharan, et al. (1983)] now have become useful tools for data extraction from a interferometric fringe pattern. By applying discrete shifts to the position of the fringes, this technique achieves good accuracy and resolution in measurement [Creath (1988)].

The arrangements of Figs. 4.1 and 4.6 allow computer analysis of the surface shape from the phase information contained in the fringe patterns. This is done by using phase stepping techniques [Creath (1985) and Robinson & Williams (1986)]. For instance, a piezo translator (PZT) shifts a mirror in any one arm of the setup, thus altering the optical path length and hence the phase of the interference fringes. Alternatively, since optical fibres are used, the phase could be stepped by wrapping one of them around a PZT cylinder and stretching it [Mercer &

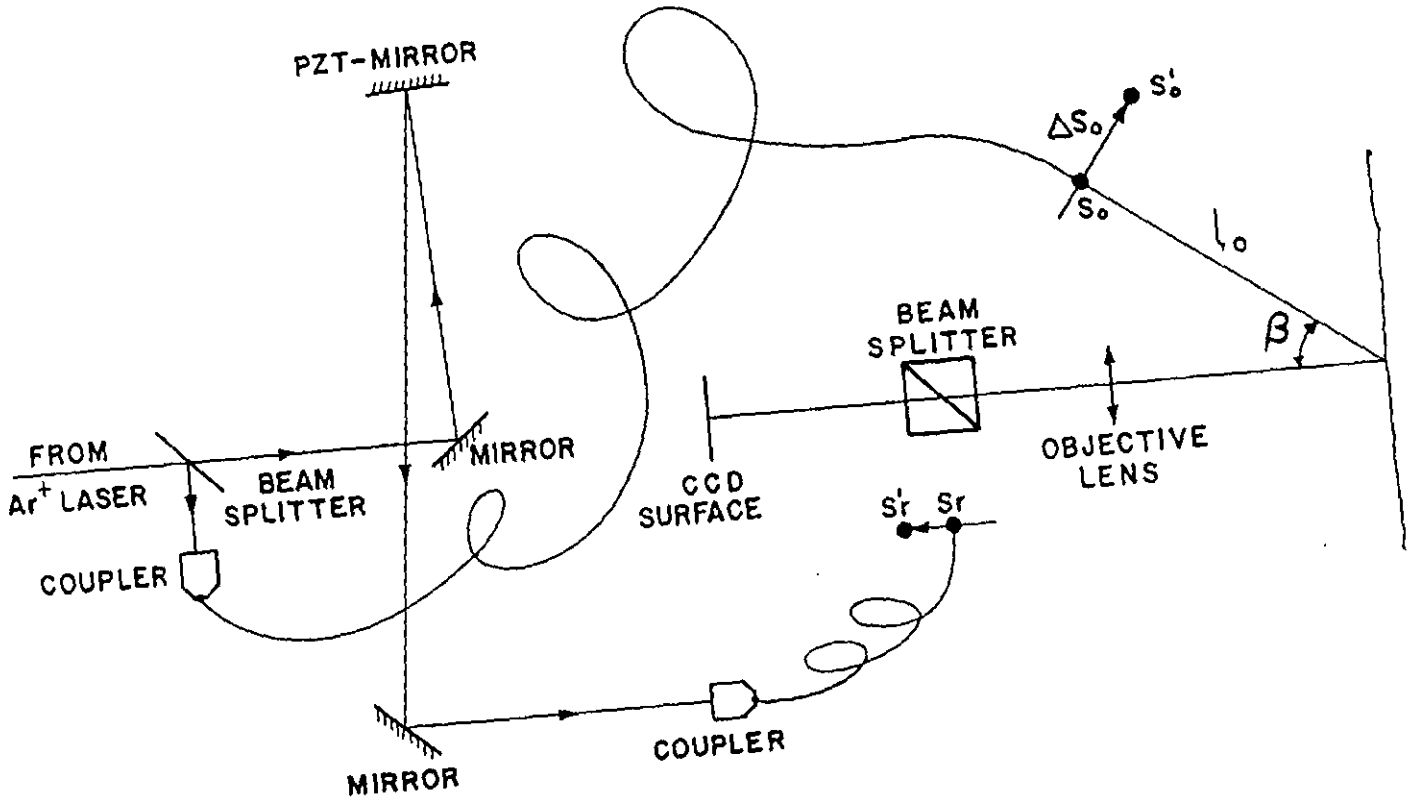

Figure 4.6
Experimental setup of the out-of-plane sensitive ESC system.

Beheim (1990), Dobbins, et al., Maas (1991), and Joenatan & Khorana (1992)]. Three phase shifted fringe patterns may thus be combined in a quasi-heterodyne fashion to obtain a phase map of the surface shape. The result is that removal of ambiguities between 'hills' and 'valleys' is achieved, and also the possibility of interpolation between fringe centres.

Fig. 4.7 shows depth contour fringes, the equivalent phase map (obtained by phase stepping with the PZT mirror), and the computed wire-frame surface isometric. These have been obtained (using the apparatus of Fig. 4.6) by consecutively stepping the reference beam path length with the PZT. The target surface examined was a 50 mm diameter metal sphere.

The phase map in figure 4.7 shows evidence of considerable speckle noise, even after smoothing the target speckled fringe pattern by local mask filters. Such noise represents a significant contribution in error to the overall accuracy of the technique. Other noise contributions arise from errors in the number of phase steps and from reduced fringe visibility due to smoothing. Estimations of such error contributions have been made [Kerr, et al. (1990)] using ESPI and computer generated data with Fourier filtering applied as a smoothing routine.

Errors due to reduced signal-to-noise ratio are the most significant, with a standard deviation of around 4° of phase for a 20% additive noise contribution. For errors in the applied phase step, an error standard deviation of around 1° of fringe phase is introduced for every 1° of error in the shifted phase. A reduction of 20% in fringe visibility contributes less than 1° of phase error standard

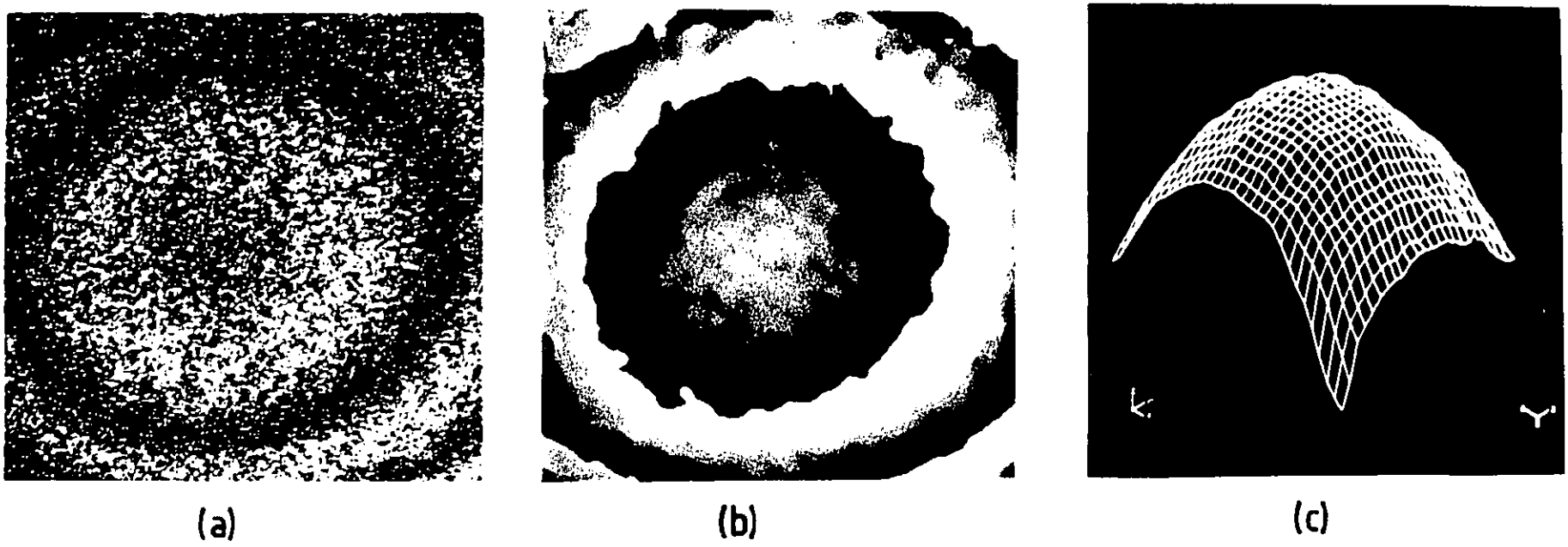

Figure 4.7
Out-of-plane sensitive ESC contour data from a spherical surface: (a) Depth contours; (b) unwrapped phase map; (c) wiremesh isometric.

deviation. For the phase shift and signal-to-noise ratio cases, the error functions are approximately linear.

The above errors are cumulative, and the final accuracy depends on optimally setting up the apparatus, as well as the correct choice of smoothing filters. For example, a reduction in the signal-to-noise ratio of 20% would correspond, in the case of the fringe pattern of figure 4.7, to an error standard deviation of around 0.05 mm, for a fringe interval of 3 mm, representing an error of 2%.

4.3.2 Shape and displacement information

With the aim of demonstrating its usefulness in engineering measurements, the experimental out-of-plane ESC arrangement was used in order to determine shape and deformation of a diffuse target surface. A 15 mm radii and 120 mm long cylindrical bar, made of bakelite, was clamped as shown in Fig. 4.8. The surface can be deformed by an induced force through a micrometric screw in the direction of the viewing system.

Initially, for absolute shape determination, the undeformed target was illuminated by an argon ion laser working at λ = 514 nm. The target (S_o) and reference (S_r) wavefronts were delivered by optical fibres mounted in micro-position stages as shown in Fig. 4.6. The illumination source made an angle $\beta = 15^\circ$ with the viewing axis and was at a distance l_o = 400 mm from the target surface. The reference beam, in line with the viewing axis, was at a distance l_r = 160 mm from the photosensitive surface of the CCD camera. Depth contours appearing on the target surface were obtained by transverse displacement of object and reference sources. Fig. 4.9 shows the contour map obtained with ΔS_o = 80 μm and ΔS_r = 50 μm. Data

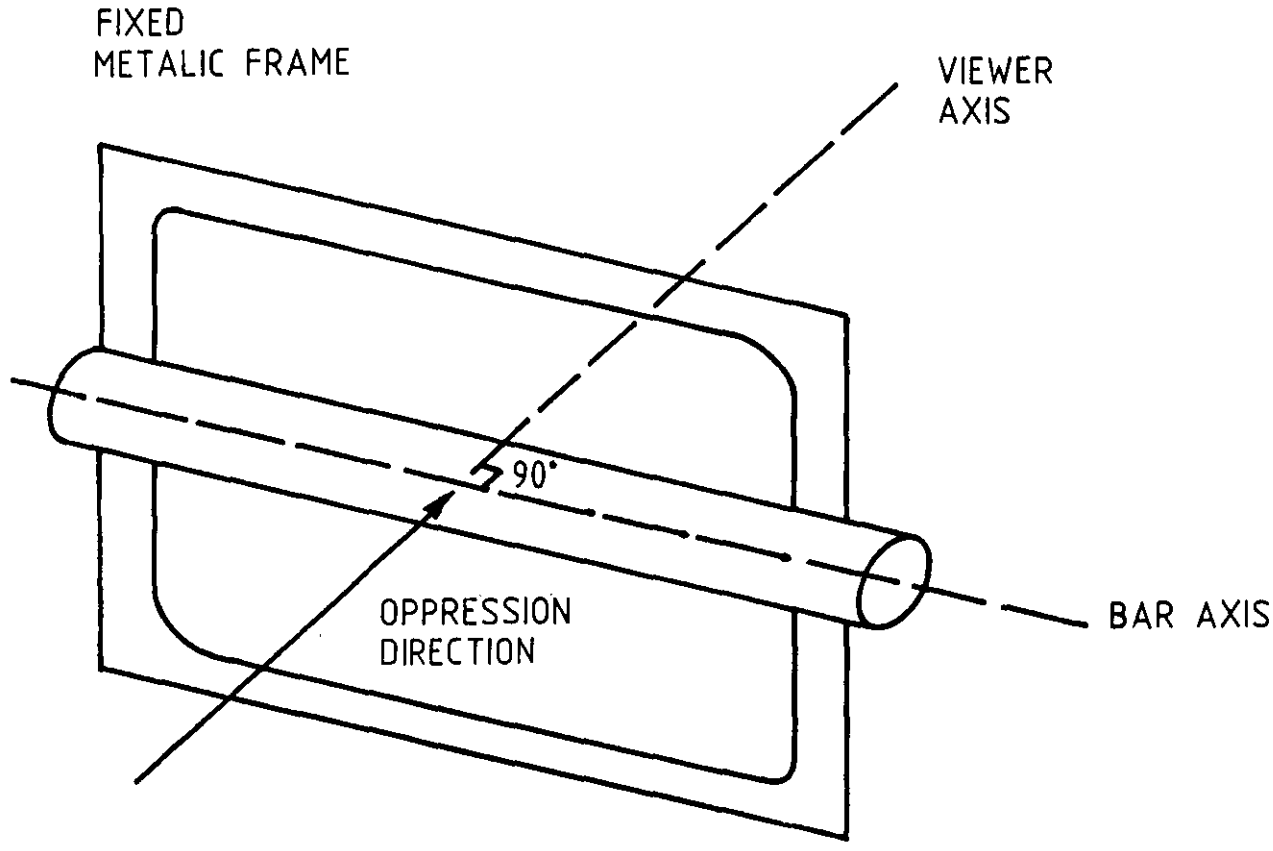

Figure 4.8
Cylindrical bar used for shape and displacement measuring employing the out-of-plane ESC apparatus.

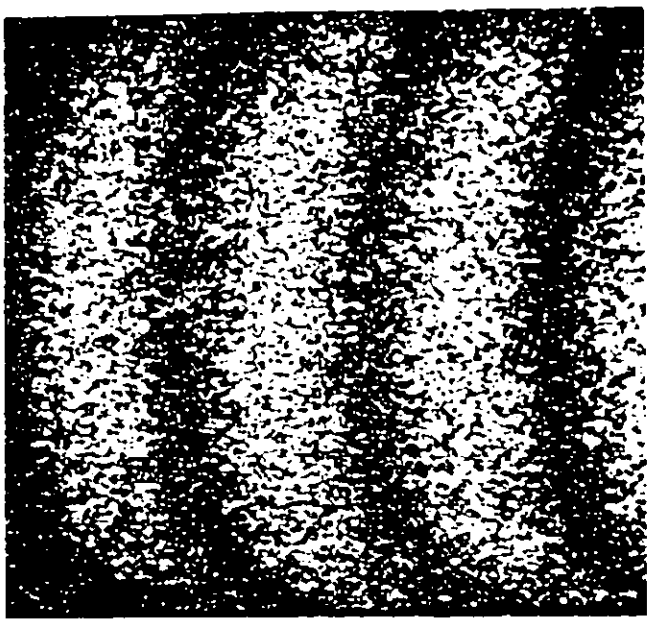

Figure 4.9
Depth contours produced by the out -of- plane sensitive E S C system on the cylindrical bar. Object and reference source displacements were 80 and 50 microns, respectively.

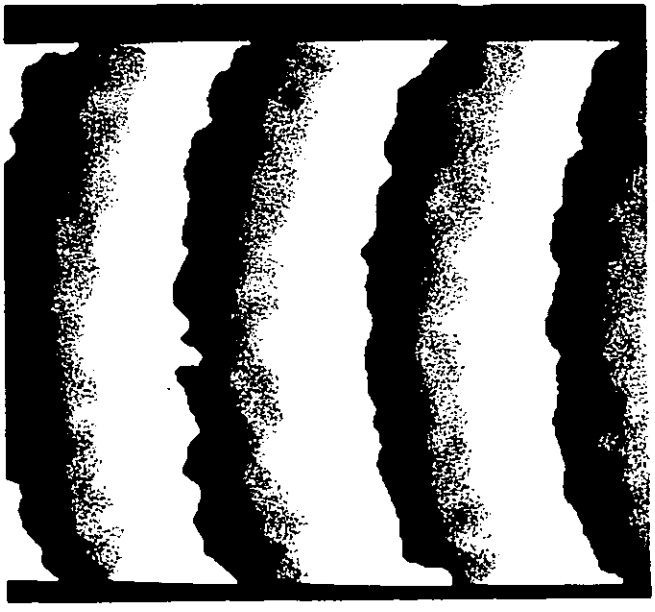

Figure 4.10
Unwrapped phase map obtained by the phase-stepping method.

reduction by using phase stepping gives the phase map and isometric plot shown in figures 4.10 and 4.11 respectively.

In order to obtain deformation measurement by using the same hardware as in figure 4.6, the bar was bent by a force from a screw contacting it from behind and along the viewing axis. A displacement contour map of the bar is shown in Fig. 4.12. The displacement given by the micrometer screw was 10 μm. The phase map and isometric plot of the calculated displacement by the phase-stepping technique are shown in Fig. 4.13 and 4.14, respectively. Parameters of the experimental setup were the same as in shape determination.

The results obtained above show that the ESC method is capable of measuring both shape and deformation by using the same experimental setup. The ultimate limitations to this technique are pixels with low intensity modulation as the phase is changed, and pixels having decorrelation of the speckles between data recorded before and after deformation, or between illuminating or reference sources displacements. In the next section, decorrelation problems of the ESC technique are analysed.

4.4. Decorrelation problems

The basic principle of an ESPI system is that small surface displacements produce a change in the relative phase of the object and reference wavefronts interfering. This phase change is proportional to the size of the displacement and will cause a spatial variation in the correlation of speckle patterns as observed before and after displacement. Speckle pattern correlation fringes are observed when the two patterns are subtracted or added. A basic assumption of the theory is that the fine-scale

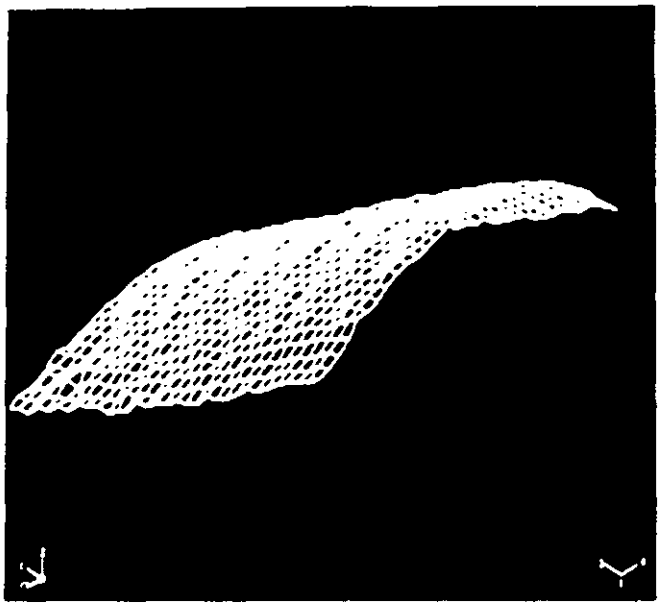

Figure 4.11
Three-dimensional plot showing the shape information.

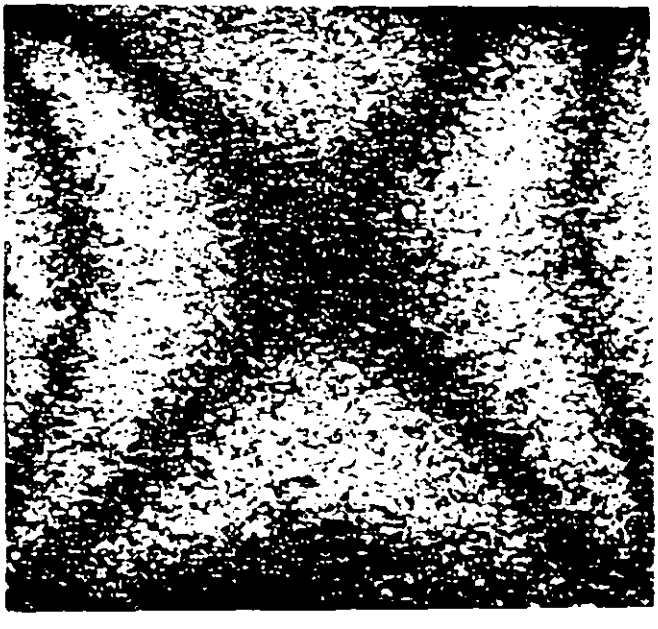

Figure 4.12
Out-of-plane displacement contours obtained when the bar of Fig. 4.8 is deformed. This case corresponds to a displacement of ten microns.

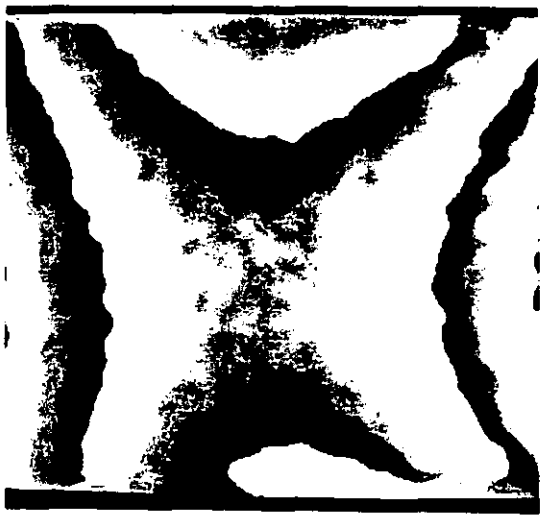

Figure 4.13
Unwrapped phase map obtained from out-of-plane displacement contours.

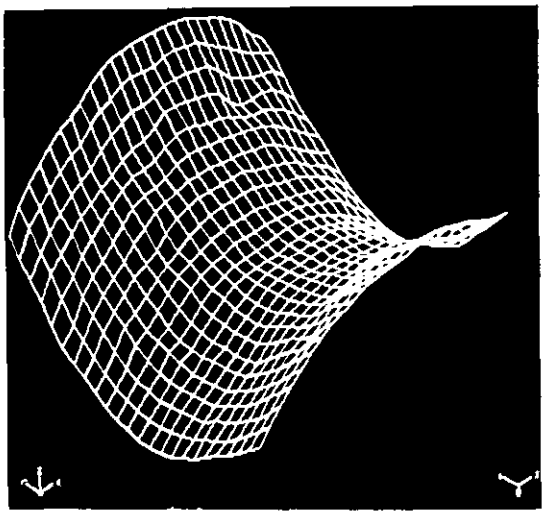

Figure 4.14
Three-dimensional plot showing the deformation information.

detail of the speckle patterns remain unchanged throughout. However, a loss in correlation fringe visibility will result if a change in this detail takes place, i.e. if a degree of speckle pattern decorrelation occurs between the two displacement states. For more on these decorrelation problems in ESPI the author refers the reader to Jones & Wykes (1977), Wykes (1977), and Owner-Petersen (1991), for instance.

All reported research on decorrelation basically study it as due to surface displacement or wavelength change. In the case of ESC, the decorrelation effects are produced by source shifts. They may be equivalent to surface displacements. However it is necessary to give some indication on the decorrelation consequences in the ESC system in order to understand its limitations and measurement range.

As can be seen from equation (4.5), the number of fringes on the target surface can be chosen by shifting one or both of the sources. In the out-of-plane ESC arrangement, it is possible to count up to 20 fringes on the monitor screen for the case of a 110 μm object source displacement and 57X57 mm^2 target surface dimension. With $\beta = 20^{\circ}$, $l_o = 575$ mm, $l_r = 160$ mm, and $\lambda = 514$ nm; the maximum depth interval calculated via equation (4.3) is 7.5 mm. For this number of fringes, the visibility is too low and the noise is increased considerably, effects produced by decorrelation. This situation may affect the accuracy in shape measurement as is mentioned above (section 4.3.1). Then, it is recommended to reduce the fringe number on the target surface.

The resolution limit of the particular micrometer

employed was ± 10 μm. Two fringes appear on a flat surface when the object illumination beam is displaced by that limit. Thus, this could be the smallest number of contours that is possible to detect, imposing a inferior limit of measurement. Of course, it is possible to use a more sensitive micrometer in order to increase the contour measuring range. This may be a differential micrometer whose resolution is ± 1 μm.

From this analysis, it can be seen that the measurement range of this particular ESC system is from 7.5 mm to 0.75 mm. The sensitivity, however, can be adjusted by changing the setup parameters.

Another important point that is necessary to mention here is the reference to object intensity ratio. It has been demonstrated, for ESPI, that maximum fringe contrast is obtained when this ratio is 2 [Jones & Wykes (1981)]. However, when the reference beam is displaced in the ESC system, fringe visibility is reduced substantially. Some qualitative judgment is needed to obtain reasonable fringe visibility on the monitor screen. This may be achieved by reducing the intensity of the reference beam. In this case, the best ratio found was 1. All the experimental results shown above were made by using this reference to object intensity ratio.

4.5 Conclusions

It has been shown that it is possible to obtain shape and displacement information from a diffuse target, using ESPI optical configurations identical to those commonly used for displacement measurement techniques. The patterns produced may be treated as though they are equivalent to simple projected fringes, and the analysis thus constructed

fits well with experimental data. The dual fibre method allows control over the orientation of the contour planes, which may be varied according to the relative source displacements.

The shape information produced provides important engineering data, and when combined with displacement amplitude, realizes the full potential of the ESPI system, permitting simultaneous measure of shape and deformation of the target surface. The depth contour fringes produced are easy to visualize in real time, and phase information may be extracted using conventional phase shifting techniques. Control of the contour interval can be easily adjusted, allowing adjustment of the sensitivity of the ESC method.

CHAPTER 5

General remarks and conclusions

5.1 Introduction

The work described in this thesis presents some advances in the optical contouring field for determining shape and displacement of diffuse engineering surfaces based on moiré and speckle techniques. The main advantages of the methods are, that they are non-contact, easily implemented and that their measure range extends from a fraction of the wavelength used to illuminate to several millimeters. This thesis did not attempt to study the different mechanisms of fringe analysis for data reduction, but instead gave an analysis of the optical systems and studied the effect of the optical phenomena.

This investigation has demonstrated that a computer linked to optical contouring is a feasible tool for inspecting engineering surfaces in real time.

The purpose of this final chapter is to emphasize the author's particular contribution to progress in the optical contouring field. The final concluding remarks include summaries of these contributions and point out the merits and limitations of each technique investigated. A number of recommendations for future work are put forward as a result of the achieved improvements.

5.2 Concluding remarks

The information output from the computer linked to the optical contouring techniques investigated could be made to suit the particular application and produced data on the following levels:

(a) Shape determination,
(b) Surface inspection,
(c) The overall difference between components,
(d) Surface deformation measurement.

The techniques could also be applied to the accurate measurement of complex distortion of engineering surfaces produced by engine condition tests, or other kind of environments.

5.2.1 The techniques based on the Talbot effect

The possibility of using Talbot-projected fringes to determine three-dimensional shape of engineering objects has been demonstrated. The principle is based on encoding the target surface with a Talbot self-image of a linear grating. The decoding process is carried out by overlapping the image of the deformed grating on a reference grating. This produces moiré patterns that correspond to a contour map. Two approaches of this method were demonstrated. One used laser illumination to obtain the moiré pattern which was transformed to phase information by using a phase stepping algorithm. The phase map contained the shape information of the target. The second approach used white light to produce different coloured Talbot planes, giving coloured moiré fringes. Each colour was associated with a different plane on the diffuse target. Some of the advantages of the Talbot methods are:

- Relatively high sensitivity: The sensitivity of the method is enough to determine small deformations of quasi-plane engineering targets. The depth resolution of the of the order of 11 μm can be obtained for a grating of 150 lines per millimeter. It is possible to increase the

resolution by using as high a grating frequency as the optical viewing system can resolve. This Talbot projected system can be used with the modified camera proposed by Forno (1975), by which it is possible to resolve up to 300 lines per millimeter.

- Adjustable measurement range: Since the contour interval size depends strongly on the grating frequency, it is possible to choose the measurement range according to the resolution required. The system was capable of being used as an inspection system on a routine basis for test golf balls. The information produced by this system was sufficiently accurate that detailed information of the indentations on a golf ball were clearly determined.

- High mechanical stability: Inherently, like other projection moiré techniques, the requirements for stability and special work environments for these Talbot techniques do not pose any practical difficulties, e.g., unlike holographic interferometry or ESPI.

- Solved "concave-convex" dilemma: The natural ability of the phase-stepping methods to remove the sign ambiguity has been connected to the TPMT method, making it a powerful quantitative technique for absolute shape measuring.

- Non-conventional fringe processing: The coloured moiré fringes obtained by using white light illumination can be analysed employing modern colour frame grabber boards now available. These boards acquire colour frames, store them in onboard memory, and display them on a colour monitor at real-time video rates. The hue-saturation-intensity model is a far more natural way of describing colour. Thus, it should be possible to adapt colour measurement for depth

determination.

The use of colour in the displayed fringes is not only more pleasing, but it also provides more visual information. While the human eye can perceive only few gray levels, it has the ability to distinguish between thousands of colours. Thus, associating a colour to each point of a three dimensional object, it is possible to have a general idea of its shape.

The major inconvenience with the use of digital colour processing for data reduction is its expensive hardware and software compared with the traditional monochromatic scheme.

A general disadvantage with the Talbot techniques is the size of the object to be tested. The techniques suffer, similarly to that of shadow moiré contouring and sticked grating moiré interferometry, a limitation: to test small targets, i.e. as small as the size of the optical aperture or diameter of the collimating lens. But they may still be useful in coined process and small turbine blade testing.

5.2.2 The Electronic moiré contouring method

The potential of Electronic Moiré Contouring (EMC) used together with a phase-stepping method was demonstrated experimentally. Absolute and comparative shape measurements were carried out to simply and quickly capture and retrieve information. Extension of the EMC technique to surface deformation has shown that it can be used in a similar way to ESPI, but with reduced sensitivity. This is useful when measurement of large displacements or big targets are desired. Some advantages were found by using computer generated gratings when studying grid contour subtraction.

This was done in order to tune the contour interval and then to remove unambiguous data from targets which have discontinuities in their surface shape.

The EMC technique was evaluated in terms of its fringe contour visibility. Image subtraction obtained with the electronic device of the EMC system was compared with image subtraction carried out directly in the computer. Furthermore, this comparison was also made while varying the aperture of the viewing lens. The superiority in contrast from the electronic fringe demodulation was clearly noticed.

The EMC system would be well suited to routine applications since remote detection is made. Hence it would not be liable to damage while the surface is loaded or unloaded. If operating in a particularly harsh environment, the optics could be completely hermetically sealed from the surroundings making a compact and easy to maintain device.

5.2.3 The Electronic speckle contouring method

The possibility of obtaining shape and displacement information from a engineering target using ESPI optical configurations identical to those for displacement measurement techniques was shown. The patterns produced were treated as though they were equivalent to projected fringes. The subsequent analysis fitted well with experimental data. The in-plane sensitive ESC method allows control over the orientation of the contour planes, which were changed according to the relative source displacements.

The shape information produced provides important engineering data, and when combined with displacement

amplitude, realises the full potential of the ESPI system. The depth contour fringes produced are easy to visualise, and phase information may be extracted using conventional phase measurement techniques.

A brief analysis with respect to decorrelation effects produced in the out-of-plane ESC system was made. The main decorrelation problem originated when the reference fibre was displaced, though it was to tune the optical system to obtain a better fringe visibility. Reference to object illumination ratio was found to be one in order to obtain the highest fringe contrast.

The applications described in the present work have been chosen to demonstrate the benefits of the specific innovations introduced in the ESC technique. The results of the improved optical design have already been highlighted as well as the novel theoretical interpretation of ESC fringes. However it is necessary to mention that many of the traditional applications of holographic interferometry and ESPI could be performed with ESC. Nondestructive testing; vibration evaluation of turbine blades, loudspeakers, and metal diaphragms has been popular applications as is the loading of metal strips and plates.

Electronic Speckle Contouring was compared and contrasted with Electronic Moiré contouring, and showed some significant advantages:

1. Shape and deformation can be performed on the same instrument as displacement in-plane or out-of-plane sensitive instrument, with a programmable grid spacing.

2. ESC does not suffer from diffractive blurring, moreover

the grid can intersect at a choice of orientations.

3. High resolution measurement.

Limitations to ESC compared with EMC are:

1. Fringes have low signal to noise ratio due to the speckle.

2. Decorrelation problems beyond 110 μm source displacement or 20 fringes on the monitor screen.

3. Interferometric stability of the apparatus is required, though not to the extent of that required for holography.

4. Small field of illumination such as only small objects can be tested.

5.3 Future work

With a pressing need for increased productivity and delivery of end products of uniform quality, industry is turning more and more toward computer-based automatic inspection and measurement. At the present time, most automatic inspection and measuring tasks are carried out by special-purpose machines designed to perform predetermined functions in a control and manufacturing process. The inflexibility and generally high cost of these machines, have led to a broad-based interest in the use of optical techniques capable of performing a variety of functions in more flexible working environment and lower cost.

New optical contouring configurations that combine optoelectronic devices and computer generated gratings

should provide more efficient solutions for surface inspection. Research efforts should be directed towards application of coordinate and movement sensors in order to achieve inspection of complex geometries in connection with shape and high amplitude vibration measurements. It should also involve general multiaxis manipulation with continuous path computer control for phase stepping and contour generation in moiré and ESC, respectively.

The field of view of the optical contouring systems was limited to test small targets. Where quantitative metrology of big targets is important, this disadvantage may be overcome by using proper optical objectives including zooms, wide angle, and macro lenses.

Particular attention must be given to the design and production of digital spatial filters. That will require a thorough study of the possibility to use adaptive filtering in fringe pattern analysis or include such filtering process into the optoelectronic hardware.

Colour processing is now possible in real time with cheap boards available in the market. Future investigation should be done in digital image processing in white light colour, specially for a quick inspection applying the Talbot effect.

All the techniques analysed in this work show experimental results without actual real figures. All are given, for example, in "normalized" units. Then, a rigorous calibration scheme must be carried out.

Finally, it is the opinion of the author that calibration problems exist in most of the optical measuring

techniques proposed up to date. These have been designed without a rigorous control process in order to have confidence in the measurements. National and international standards institutions must pay attention to controlling the spread out of new optical techniques and instruments, or at least, each worker should indicate that his measurement technique is in process of calibration.

5.4 Closure

A number of innovations in the optical contouring field were presented and discussed. The examples illustrate a range of optical inspection problems which can now be tackled. For an entire success, however, the techniques should be capable of performing more reliably and with more confidence than a human inspector.

Ease of calibration should also be part of any optical inspection and measuring system, reducing time for full industrial evaluation. The utilization of optical systems is becoming more widespread with the availability of more sensitive, faster and cheaper components, and with related CCD-based capture and computer information processing systems. They have also become more readily available to industry which will increasingly turn to designers for assistance in producing solutions for their inspection problems.

Finally, it is necessary to say that up to date artificial intelligent can not replace all the skills of a human, since knowledge is based upon observation and measurement. With this in mind there will be a great future for optical inspection in industry.

APPENDIX A

The Talbot effect

This appendix is essentially devoted to give a theoretical concept for the special application concerned with the Talbot-projected moiré methods, discussed in chapter 2 of this thesis.

Consider that a monochromatic plane wave is incident on a Ronchi grating placed on a x-y plane whose lines are parallel to the y-axis. The field behind this grating is

$$g_1(x,y,0) = \sum_{n=-\infty}^{\infty} C_n \exp(2\pi i n x/p), \qquad (A.1)$$

where p is the period of the grating, C_n is the nth coefficient of the Fourier series. The angular plane wave spectrum at the grating is given by the Fourier transform of the equation (A.1) as

$$\tilde{g}_1(f_x,f_y;0) = \sum_{n=-\infty}^{\infty} C_n \, \delta(f_x - n/p)\delta(f_y). \qquad (A.2)$$

The propagation of the angular plane wave spectrum is formulated by the Rayleigh-Sommerfeld theory [Goodman pp. 48-54 (1968)] as

$$\tilde{g}_1(f_x,f_y;z) =$$

$$\tilde{g}_1(f_x,f_y;0)\exp\left[2\pi i\left(1 - \lambda^2(f_x^2 + f_y^2)\right)^{1/2} z/\lambda\right]. \qquad (A.3)$$

Correspondingly, the angular plane wave spectrum at a distance z from the grating becomes

$$\tilde{g}_1(f_x,f_y;z) = \sum_{n=-\infty}^{\infty} C_n\, \delta(f_x - n/p)\,\delta(f_y)$$

$$X\ \exp\left[2\pi i\left(1 - \lambda^2 n^2/p^2\right)^{1/2} z/\lambda\right], \qquad \text{(A.4)}$$

and the optical field can be expressed as

$$g_1(x,y;z) = \sum_{n=-\infty}^{\infty} C_n\, \exp(2\pi i n x/p)$$

$$X\ \exp\left[2\pi i\left(1 - \lambda^2 n^2/p^2\right)^{1/2} z/\lambda\right]. \qquad \text{(A.5)}$$

Assuming that the grating is coarse enough such that $p >> |n\lambda|$, it is possible to approximate that

$$\left(1 - \lambda^2 n^2/p^2\right)^{1/2} = 1 - \frac{1}{2}\,\lambda^2 n^2/p^2. \qquad \text{(A.6)}$$

Eq. (A.5) then becomes

$$g_1(x,y;z) = \exp(2\pi i z/\lambda)$$

$$X \sum_{n=-\infty}^{\infty} C_n\, \exp(2\pi i n x/p)\, \exp(-i\pi n^2 \lambda z/p^2). \qquad \text{(A.7)}$$

Now, consider that an identical grating placed at a distance z from the first grating. Amplitude transmittance of this grating can be expressed as

$$g_2(x,y) = \sum_{m=-\infty}^{\infty} C_m\, \exp(2\pi i m x/p). \qquad \text{(A.8)}$$

After passing through the second grating, the field behind this grating becomes

$$p(x,y;z) = g_1(x,y;z)g_2(x,y) \qquad (A.9)$$

And the total intensity

$$P = \iint |p(x,y;z)|^2 \, dxdy. \qquad (A.10)$$

According to the Parseval's theorem [Goodman pp. 10 (1968)], the total intensity can also be expressed as

$$P = \iint |\tilde{p}(f_x,f_y;z)|^2 \, df_x df_y, \qquad (A.11)$$

where $\tilde{p}(f_x,f_y;z)$ is the Fourier transform of $p(x,y;z)$ and can be expressed as

$$\tilde{p}(f_x,f_y;z) = \tilde{g}_1(f_x,f_y;z) * \tilde{g}_2(f_x,f_y), \qquad (A.12)$$

where * denotes a convolution operation and $\tilde{g}_2(f_x,f_y)$ is the Fourier transform of $g_2(x,y)$. By substituting Eq. (A.4) with the approximation of Eq. (A.6) and the Fourier transform of Eq. (A.8) into Eq. (A.12), it yields

$$\tilde{p}(f_x,f_y;z) = \exp(2\pi iz/\lambda)$$

$$X \sum_{n=-\infty}^{\infty} \sum_{m=-\infty}^{\infty} C_n \exp(-i\pi n^2\lambda z/p^2)$$

$$X \, C_m \, \delta\left(f_x - (n-m)/p\right) \delta(f_y). \qquad (A.13)$$

The total intensity becomes

$$P = \iint \left| \sum_{n=-\infty}^{\infty} \sum_{m=-\infty}^{\infty} C_n\, C_m \exp(-i\pi n^2 \lambda z/p^2) \right.$$

$$\left. X\ \delta\left(f_x - (n-m)/p\right)\ \delta(f_y) \right|^2 df_x df_y. \qquad \text{(A.14)}$$

It is apparent from this equation that the total intensity P is maximum when

$$z = \Delta_k = k\ 2p^2/\lambda, \qquad \text{(A.15)}$$

where **k** is an integer. This condition is known as **Talbot distance.**

In order to illustrate Eq. **(A.14)** more clearly, a model of cosine grating is applied. The amplitude transmittance of a cosine grating is

$$g(x,y) = 1 + \tfrac{1}{2} \exp(2\pi i x/p) + \tfrac{1}{2} \exp(-2\pi i x/p). \qquad \text{(A.16)}$$

This equation can be expressed in the form of equation **(A.1)** where

$$C_o = 1, \qquad C_1 = C_{-1} = \tfrac{1}{2};$$

$$C_n = 0, \quad \text{for} \quad |n| \neq 1, \quad n \neq 0. \qquad \text{(A.17)}$$

With the same approximation applied on Eq. **(A.8)**, the total intensity becomes

$$P = A + \cos(\pi \lambda z/p^2) \qquad \text{(A.18)}$$

where **A** is an arbitrary constant. It is apparent again from

Eq. (A.18) that the total intensity P is maximum when

$$z = \Delta_k = k\ 2p^2/\lambda.$$

The distance Δ_k is again the Talbot distance as stated previously in Eq. (A.14).

APPENDIX B

Theory of ESC

In this appendix, the theoretical aspects of contour generation by Electronic Speckle Contouring (ESC) are derived for the general case of moving source illumination [Kerr et al. (1991) and Rodriguez-Vera et al. (1992)].

Fig. B1 shows a basic in-plane sensitive ESC optical arrangement, where the two-dimensional case is considered. A diffuse target surface represented by $z = f(x)$ is illuminated by two coherent, spherical beams given by

$$U_1 = A_1 \exp\left\{i[\phi_{s1}(x,z) + \vec{K}_1 \circ \vec{r}_1]\right\}, \qquad (B.1)$$

and

$$U_2 = A_2 \exp\left\{i[\phi_{s2}(x,z) + \vec{K}_2 \circ \vec{r}_2]\right\}, \qquad (B.2)$$

where A_1 and A_2 are the complex amplitudes of the illuminating beams, $\phi_{s1}(x,z)$ and $\phi_{s2}(x,z)$ are the random phases of the speckle patterns, and the distances r_1 and r_2 are measured from the source points $S_1(x_1,z_1)$ and $S_2(x_2,z_2)$ to an target point $P(x,z)$ whose position vector $\vec{r}$ lyes in the reference x-z plane. The position vectors of S_1 and S_2 are $\vec{I}_1$ and $\vec{I}_2$.

The wave vectors $\vec{K}_1$ and $\vec{K}_2$ are defined as $|\vec{K}_1| = |\vec{K}_2| = k = 2\pi/\lambda$. The z-axis is chosen as the observation line, with a TV camera recording the intensity distribution across the target surface. The output from the camera is processed by subtraction unit, and the 'real-time' image displayed on a TV monitor. The illumination at point P due

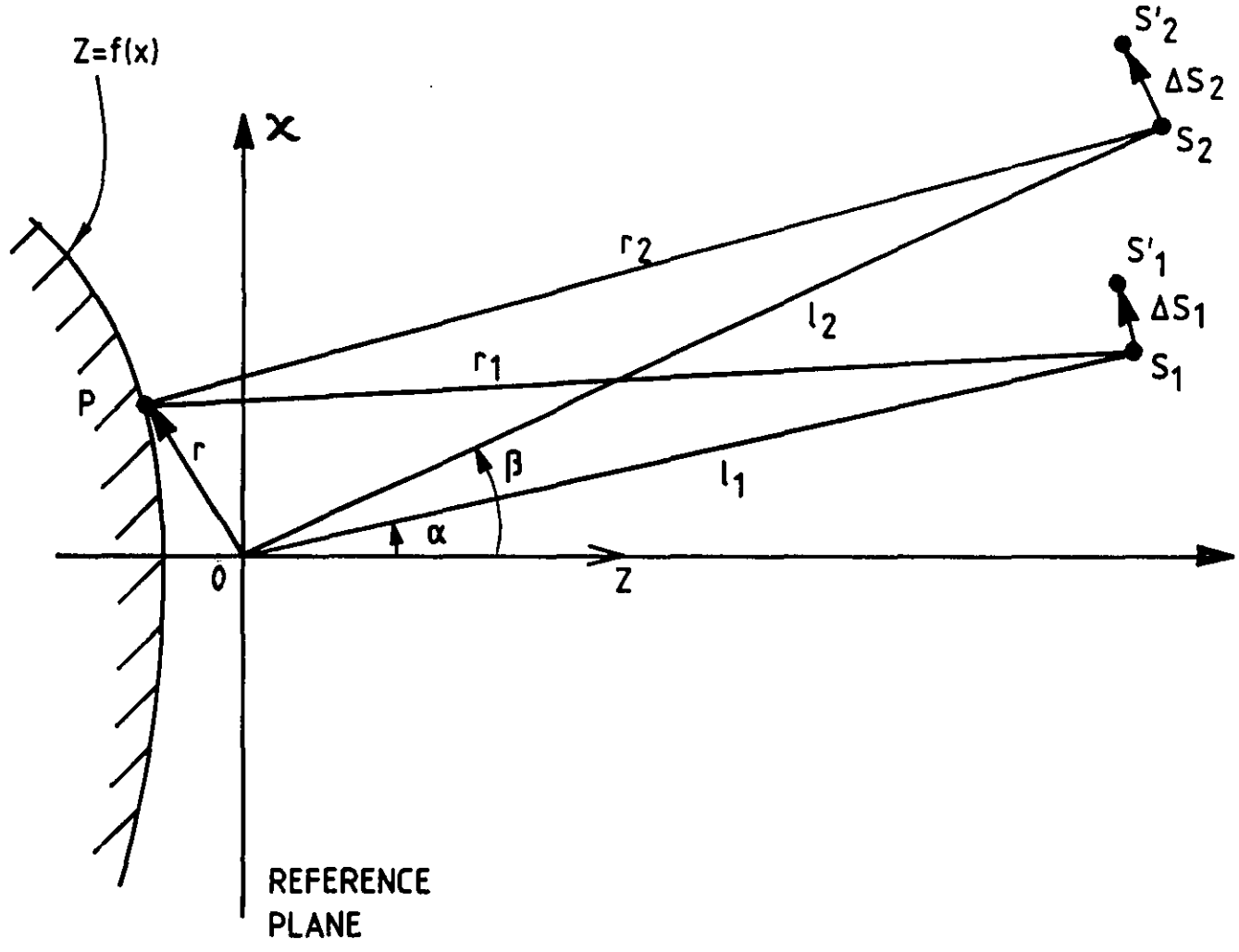

Figure B1
General optical geometry of the dual-beam ESC arrangement.

to the two light beams will have an intensity:

$$I(x) = |U_1 + U_2|^2 = |U_1|^2 + |U_2|^2 + U_1 U_2^* + U_1^* U_2$$

$$= I_1 + I_2 + 2\sqrt{I_1 I_2}\cos\varphi, \qquad \text{(B.3)}$$

where

$$\varphi = \left[(\phi_{s1} - \phi_{s2}) + (\vec{K}_1 \circ \vec{r}_1) - (\vec{K}_2 \circ \vec{r}_2)\right]. \qquad \text{(B.4)}$$

If a displacement of one or both of the illumination sources is introduced, the distances r_1 and r_2 and wave vectors $\vec{K}_1$ and $\vec{K}_2$ change. Assuming the random speckle field remains constant, the intensity at P becomes:

$$I'(x) = I_1 + I_2 + 2\sqrt{I_1 I_2}\cos\varphi', \qquad \text{(B.5)}$$

with

$$\varphi' = \left[(\phi_{s1} - \phi_{s2}) + (\vec{K}'_1 \circ \vec{r}'_1) - (\vec{K}'_2 \circ \vec{r}'_2)\right], \qquad \text{(B.6)}$$

and where $\vec{r}'_1$, $\vec{r}'_2$, $\vec{K}'_1$ and $\vec{K}'_2$ are associated with the new source positions $S'_1(x'_1, z'_1)$ and $S'_2(x'_2, z'_2)$ respectively.

The difference between equations (B.3) and (B.5) rests on the change in intensity at the point P, is produced by the ESPI subtraction electronic hardware, and is given by:

$$I - I' = 2\sqrt{I_1 I_2}\left(\cos\varphi - \cos\varphi'\right)$$

$$= 4\sqrt{I_1 I_2}\ \sin(\phi_s - \Delta'/2)\ \sin(\Delta/2), \qquad \text{(B.7)}$$

where

$$\phi_s = \phi_{s2} - \phi_{s1}, \qquad \text{(B.8)}$$

$$\Delta' = (\vec{K}_1 \circ \vec{r}_1 - \vec{K}_2 \circ \vec{r}_2) + (\vec{K}'_1 \circ \vec{r}'_1 - \vec{K}'_2 \circ \vec{r}'_2), \qquad \text{(B.9)}$$

$$\Delta = (\vec{K}_1 \circ \vec{r}_1 - \vec{K}_2 \circ \vec{r}_2) - (\vec{K}'_1 \circ \vec{r}'_1 - \vec{K}'_2 \circ \vec{r}'_2). \qquad \text{(B.10)}$$

The first term in Eq. (B.7) contains mainly the random speckle noise while the second represents the fringe pattern. Equations (B.9) and (B.10) represent the phase shift due to the change in illumination. The output voltage from the camera for a given point (x,y) will be proportional to the intensities i.e., $V_1 \propto I_1$ and $V_2 \propto I_2$. The difference between the two voltages is displayed on the TV monitor as fringes on the target surface surface. These fringes may be interpreted as Young's fringes produced from the two source positions.

Assuming that the target in Fig. B1 is illuminated initially by two point sources, S_1 and S_2, the respective wave vectors have the form:

$$\vec{K}_1 = k\,\frac{\vec{r}_1}{|\vec{r}_1|}\ ;\ \vec{K}_2 = k\,\frac{\vec{r}_2}{|\vec{r}_2|}. \qquad \text{(B.11)}$$

Using these in Eq. (B.10), we obtain

$$\Delta = k[(r_1 - r_2) - (r'_1 - r'_2)]. \qquad \text{(B.12)}$$

If it is assumed that the target dimensions are much

smaller than its distance to the illuminating points S_1, S_2, S'_1 and S'_2, it is possible to use the approximation:

$$r_1 = \left[(x_1 - x)^2 + (z_1 - z)^2\right]^{1/2}$$

$$\propto l_1 + \frac{r^2}{2l_1} - \frac{x_1 x}{l_1} - \frac{z_1 z}{l_1}, \qquad \text{(B.13)}$$

where l_1 and r are the source distance to the origin of a reference plane, and (the magnitude) the position vector from this origin to the point P, respectively. With corresponding expressions for r_2, r'_1, and r'_2, and substituting into equation (B.12) we obtain

$$\Delta = k\left[(l_1 - l'_1) + \frac{r^2}{2}\left(\frac{1}{l_1} - \frac{1}{l'_1} \right) - (l_2 - l'_2) \right.$$

$$- \frac{r^2}{2}\left(\frac{1}{l_2} - \frac{1}{l'_2} \right) + x\left(\frac{x_2}{l_2} - \frac{x_1}{l_1} + \frac{x'_1}{l'_1} - \frac{x'_2}{l'_2} \right)$$

$$\left. - z\left(\frac{z_1}{l_1} - \frac{z_2}{l_2} - \frac{z'_1}{l'_1} + \frac{z'_2}{l'_2} \right) \right]. \qquad \text{(B.14)}$$

The sources S_1 and S_2 are now moved to S'_1 and S'_2. Let the orthogonal source displacements, with respect to the $\vec{I}_1$ and $\vec{I}_2$ directions, be ΔS_1 and ΔS_2 respectively. These subtend angles to the z-axis $\Delta\alpha$ and $\Delta\beta$. From Fig. B1 we can see that:

$$\sin \alpha = \frac{x_1}{l_1} \qquad \sin \beta = \frac{x_2}{l_2}$$

$$\cos \alpha = \frac{z_1}{l_1} \qquad \cos \beta = \frac{z_2}{l_2}$$

$$\sin(\alpha + \Delta\alpha) = \frac{x_1'}{l_1'} \qquad \sin(\beta + \Delta\beta) = \frac{x_2'}{l_2'}$$

$$\cos(\alpha + \Delta\alpha) = \frac{z_1'}{l_1'} \qquad \cos(\beta + \Delta\beta) = \frac{z_2'}{l_2'}$$

Substituting these expressions into Eq. (B.14) and taking the approximation for small source displacements:

$l_1 \simeq l_1'$; $l_2 \simeq l_2'$; $\cos\Delta\alpha = \cos\Delta\beta \simeq 1$; $\sin\Delta\alpha \simeq \frac{\Delta S_1}{l_1}$; and

$\sin\Delta\beta \simeq \frac{\Delta S_2}{l_2}$ we have

$$\Delta = k\left[x\left(\frac{\Delta S_1}{l_1}\cos\alpha - \frac{\Delta S_2}{l_2}\cos\beta \right) \right.$$

$$\left. - z\left(\frac{\Delta S_1}{l_1}\sin\alpha - \frac{\Delta S_2}{l_2}\sin\beta \right) \right]. \qquad \text{(B.15)}$$

The conditions for the formation of maximum brightness fringes are governed by Eq. (B.7), with $\Delta = 2n\pi$. Thus equation (B.15) now becomes

$$x\left(\frac{\Delta S_1}{\lambda l_1}\cos\alpha - \frac{\Delta S_2}{\lambda l_2}\cos\beta \right)$$

$$- z\left(\frac{\Delta S_1}{\lambda l_1}\sin\alpha - \frac{\Delta S_2}{\lambda l_2}\sin\beta \right) = n, \qquad \text{(B.16)}$$

where n is an integer number. It defines the fringe order. Equation (B.16) represents a set of fringes which appear to the observer as if two linear gratings had been projected on the target surface. The equation contains the depth information of the target in contour lines, whose depth interval is given by the quantity:

$$\Delta z = \left(\frac{\Delta S_1}{\lambda l_1} \sin \alpha - \frac{\Delta S_2}{\lambda l_2} \sin \beta \right)^{-1}. \qquad \text{(B.17)}$$

In order to understand the physical significance of these general equations, several special cases were studied in chapter 4 of this thesis.

APPENDIX C

Symbol list

A_1, A_2 Amplitude distribution of Illumination wave.

$\hat{A}(f_x, f_y)$ Fourier transform of $A(x,y)$.

B Fringe brightness.

BS Beam splitter.

C_n n-th coefficient of a Fourier series.

D Aperture diameter of the viewing system.

f Focal length of the viewing system.

f_f Frequency of fringes in a contour map.

f_x, f_y Spatial coordinates in the Fourier domain.

$f(x,z)$ Mathematical target surface representation.

$f^{\#}$ f-number (= f/D).

f_f Spatial frequency of a contour pattern.

$\mathcal{F}\{\ \}$ Fourier transform of { }.

G_1, G_2 Linear gratings.

$g(x,y,z)$ Amplitude distribution of a grating.

$\tilde{g}(x,y,0)$ Fourier transform of $g(x,y,0)$.

$I_i(x,z)$ i-th Intensity of a fringe pattern distribution.

Im{ } Imaginary part of the complex in { }.

$\vec{k}_1, \vec{k}_2$ Wave vectors.

L Lens.

$\vec{I}_1$, $\vec{I}_2$ Position source vectors.

n Fringe order (integer number).

O(x,z) Amplitude distribution of an target surface.

$p(x,y;z)$ Amplitude distribution produced by the light field behind of two gratings placed in tandem.

$\tilde{p}(f_x,f_y)$ Fourier transform of $p(x,y)$.

P Total intensity produced by the field behind of two gratings placed in tandem.

p Period of a grating.

R(x,z) Reflectivity function characteristic of a target surface.

Re { } Real part of the complex in { }.

$\vec{r}_1, \vec{r}_2$ Position vectors.

S_1, S_2 Illumination sources.

S_1', S_2' Displaced illumination sources.

t Time.

U_1, U_2 Spherical wavefronts.

V Translation speed of a fringe pattern.

w Object surface dimensions.

(x,y,z) Rectangular Cartesian coordinates.

α, β, θ Angular magnitudes.

Δ_k k-th Talbot distance.

$\Delta S_1, \Delta S_2$ Transversal source displacements.

Δz Depth contour.

ε Depth of field of the viewing system.

ϕ_{s1}, ϕ_{s2} Random phases of the speckle patterns.

λ Wavelength of light employed.

ν Frequency of a grating.

ω Oscillation frequency of a fringe pattern.

APPENDIX D

Publications

List of publications arising from the work presented in this thesis:

KERR, D., RODRIGUEZ-VERA, R., and MENDOZA-SANTOYO, F., (1991).
Surface Contouring Using Electronic Speckle Pattern Interferometry, SPIE Proc. **1554A**, pp. 668-679.

RODRIGUEZ-VERA, R., KERR, D., and MENDOZA-SANTOYO, F., (1991).
3-D Contouring of Diffuse Objects by Talbot-Projected Fringes, J. Mod. Opt. **38**, pp. 1935-1945.

RODRIGUEZ-VERA, R., KERR, D., and MENDOZA-SANTOYO, F., (1991).
Three-Dimensional Contouring of Diffuse Objects Using Talbot Interferometry, SPIE Proc. **1553**, pp. 55-65.

RODRIGUEZ-VERA, R., KERR, D., and MENDOZA-SANTOYO, F., (1992).
Electronic Speckle Contouring, J. Opt. Soc. Am. **A9**, pp. 2000-2008.

RODRIGUEZ-VERA, R. and KERR, D., (1992).
Electronic Moiré Contouring (EMC), Proc. 6th. FASIG Meeting, 14-17 September, Leeds, UK, pp. 31-39.

RODRIGUEZ-VERA, R. and KERR, D., (1992).
Shape and Deformation Measurements of Diffuse Objects by Electronic Moiré Contouring, Proc. 1st. Iberoamerican Meeting on Optics, 21-23 September, Barcelona, Spain, pp. 604-605.

RODRIGUEZ-VERA, R. and KERR, D., (1992).
Extraction of Shape and Deformation Using Electronic Speckle Contouring, to be published in SPIE Proc. on International Symposium on Optical Instrumentation and Applied Science, San Diego 11-16 July (1993).

References

ABRAMSON, N., (1976).
Sandwich Hologram Interferometry. 3: Contouring, Appl. Opt. 15, 200.

AGGARWAL, A.K., GIGLIO, M., MUSAZZI, S., and PERINI, U., (1984).
Remote Surface Contouring Using a Cross-Correlation Speckle Technique, Appl. Opt. 23, 2348.

ANDREEV, A.M., VANYAN, A.R., GINZBURG, V.M., PRESNYAKOV, Y.P., and N.M. RAMISHVILI, (1989).
Analysis of the Surface-Shape Determination Technique for a Liquid Deformed by a Stationary or Variable Force Based on the Self-Imaging Effect, Opt. Spectrosc. 66, 789.

ANDRESEN, K. and KLASSEN, D., (1986/87).
The Phase Shift Method Applied to Cross Grating Moiré Measurements, Opt. Lasers Eng. 7, 101.

ASUNDI, A. and YUNG K.H., (1991a).
Phase-Shifting and Logical Moiré, J. Opt. Soc. Am. 8A, 1591.

ASUNDI, A. and YUNG K.H., (1991b).
Logical Moiré and Its Application, Exp. Mech. 31, 236.

ASUNDI, A. and DOBBINS, B.M., (1992).
Digital Moiré of Moiré, Exp. Tech. 16, 13.

ASUNDI, A., (1993).
Moiré Methods Using Computer-Generated Gratings, Opt. Eng. 32, 107.

BENOIT, P. and MATHIEU, E., (1974).
Real Time Contour Line Visualization of an Object, Opt. Comm. 12, 175.

BERGQUIST, B.D. and MONTGOMERY, P., (1985).
Contouring by Electronic Speckle Pattern Interferometry (ESPI), Proc. SPIE 599, 189.

BROOKS, R.E. and HEFLINGER, L.O., (1969).
Moiré Gauging Using Optical Interference Patterns, Appl. Opt. 8, 935.

BURCH, J.M., (1963).
The metrological Applications of Diffraction Gratings, in: *Progress in Optics*, E. Wolf, Ed., Vol. II, North-Holland, Amsterdam.

BUTTERS, J.N. and LEENDERTZ, J.A., (1971).
Holographic and Video Techniques Applied to Engineering Measurement, Meas. Control 4, 349.

BUTTERS, J.N. and LEENDERTZ, J.A., (1974).
Component Inspection Using Speckle Pattern, Proc. of The Technical Program of Electro-Optics Conf. Brighton, (Kiver Publications), pp. 43-50.

BUTTERS, J.N., JONES, R., McKECHNIE, S., and WYKES, C., (1980).
Measurement Techniques for Quality Assurance and Control, Conf. Proc. Electro-Optics/Laser International'80 UK, H.G. Jerrard, Ed. Brighton 25-27 March, pp. 139-156.

CHANG, M. and WAN, D.S., (1991).
On-Line Automated Phase-Measuring Profilometry, Opt. Lasers Eng. 15, 127.

CHAVEL, P. and STRAND, T.C., (1984).
Range Measurement Using Talbot Diffraction Imaging of Gratings, Appl. Opt. 23, 862.

CHIANG, F.P. and WILLIAMS, JR., R.C., (1985).
Simultaneous Generation of 3-D Displacement Contours of a Fracturing Specimen Using Moiré, Eng. Fracture Mech. 22, 731.

CLINE, H.E., LORENSEN, W.E., and HOLIK A.S., (1984).
Automatic Moiré Contouring, Appl. Opt. 23, 1454.

CREATH, K., (1985).
Phase-Shifting Speckle Interferometry, Appl. Opt. 24, 3053.

CREATH, K., (1988).
Phase-Measurement Interferometry Techniques, in: *Progress in Optics*, E. Wolf, Ed., Vol. XXVI, North-Holland, Amsterdam.

CREATH, K., (1989).
Holographic Contour and Deformation Measurement Using a 1.4 Million Element Detector Array, Appl. Opt. 28, 2170.

CREATH, K. AND MORALES, A., (1992).
Contact and Noncontact Profilers, in: *Optical Shop Testing*, D. Malacara, Ed. John Wyley & Sons, Inc. New York. Chapter 17, pp. 687-714.

DAI, Y.Z. and CHIANG, F.P., (1991).
Contouring by Moiré Interferometry, Exp. Mech. 31, 76.

DENBY, D., QUINTANILLA, G.E., and BUTTERS, J.N., (1975).
Contouring by Electronic Speckle Pattern Interferometry, Proc. of the Strathclyde Conference (Cambridge University Press), pp. 171-197.

DESSUS, B. and LEBLANC, M., (1973).
The 'Fringe Method' and Its Application to the Measurement of Deformations, Vibrations, Contour Lines and Differences of Objects, Opto-electronics 5, 369.

DESSUS, B., GERARDIN, J.P., and MOUSSELET, P., (1975).
Une 'Methode des Franges' en Temps Reel et ses Applications Industrielles: Deformations, Vibrations, Courbes de Niveau, Opt. Quant. Electron. 7, 15.

DOBBINS, B.N., HE, S.P., KAPASI, S., WANG, L.S., BUTTON, B.L., and WU, X.P., (1991).
Application of Phase-Stepping Speckle Interferometry to Shape and Deformation Measurement of a 3D Surface, Proc. SPIE **1554A**.

DOTY, J.L., (1983).
Projection Moiré for Remote Contour Analysis, J. Opt. Soc. Am. **73**, 366.

DURELLI, A.J. and PARKS, V.J., (1970).
Moire Analysis of Strain, Prentice-Hall, Inc., Englewood Cliffs, N.J.

FORNO, C., (1975).
White-Light Speckle Photography for Measuring Deformation, Strain, and Shape, Opt. Laser Tech. 7, 217.

GANESAN, A.R. and SIROHI, R.S., (1988).
New Method of Contouring Using Digital Speckle Pattern Interferometry (DSPI), SPIE **954**, 327.

GASVIK, K.J., (1983).
Moiré Technique by Means of Digital Image Processing, Appl. Opt. **22**, 3543.

GASVIK, K.J. and FOURNEY, M.E., (1986).
Projection Moiré Using Digital Video Processing: A Technique for Improving the Accuracy and Sensitivity, J. Appl. Mech. **53**, 652.

GASVIK, K.J., HOVDE, T., and VADSETH, T., (1989).
Moiré Technique in 3-D Machine Vision, Opt. Lasers Eng. **10**, 241.

GOODMAN, J.W., (1968).
Introduction to Fourier Optics, McGraw-Hill, New York.

GREIVENKAMP, J.E. and BRUNING J.H., (1992).
Phase Shifting Interferometry, In *Optical Shop Testing*, D. Malacara, Ed. Wiley Series in Pure and Applied Optics, John Wiley & Sons, New York., Chapter 14.

HALIOUA, M. AND LIU, H.C., (1989).
Optical Three-Dimensional Sensing by Phase Measuring Profilometry, Opt. Lasers Eng. **11**, 185.

HARIHARAN, P., OREB, B.F., and BROWN, N., (1983).
Real-Time Holographic Interferometry: A Microcomputer System for the Measurement of Vector Displacements, Appl. Opt. 22, 876.

HILDEBRAND, B.P. and HAINES, K.A., (1967).
Multiple-Wavelength and Multiple-Source Holography Applied to Contour Generation, J. Opt. Soc. Am. 57, 155.

HORMIERE, J. and MATHIEU, E., (1976).
Reference Plane Orientation Using Optoelectronic Methods in Moiré Contour Lining, Opt. Comm. 19, 37.

HOVANESIAN, J.D. and HUNG, Y.Y., (1971).
Moiré Contour-Sum Contour-Difference, and Vibration Analysis of Arbitrary Objects, Appl. Opt, 10, 2734.

HUNG, Y.Y., (1978).
Displacement and Strain Measurement, in: *Speckle Metrology*, R. K. Erf, Ed. Academic Press, New York. Chapter 4, pp. 51-71.

IDESAWA, M., YATAGAI, T., and SOMA, T., (1977).
Scanning Moiré Method and Automatic Measurement of 3-D Shapes, Appl. Opt. 16, 2152.

INDEBETOUW, G., (1978).
Profile Measurement Using Projection of Running Fringes, Appl. Opt. 17, 2930.

JAISINGH, G.K. and CHIANG, F.P., (1981).
Contouring by Laser Speckle, Appl. Opt. 20, 3385.

JIN, G.C., and TANG, S., (1989).
Automated Moiré Contouring of Diffuse Surfaces, Opt. Eng. 28, 1211.

JOENATHAN, C., PFISTER, B., and TIZIANI, H.J., (1990).
Contouring by Electronic Speckle Pattern Interferometry Employing Dual Beam Illumination, Appl. Opt. 29, 1905.

JOENATHAN, C. and KHORANA, B.M., (1992).
Phase-Measuring Fiber Optic Electronic Speckle Pattern Interferometer: Phase Step Calibration and Phase Drift Minimization, Opt. Eng. 31, 315.

JONES, R. and BUTTERS, J.N., (1975).
Some Observations on the Direct Comparison of the Geometry of Two Objects Using Speckle Pattern Interferometric Contouring, J. Phys. E: Sci. Instrum. 8, 231.

JONES, R. and WYKES, C., (1977).
De-correlation Effects in Speckle-Pattern Interferometry 2. Displacement Dependent De- correlation and Applications to the Observation of Machine-Induced Strain, Opt. Acta 24, 533.

JONES, R. and WYKES, C., (1978).
The Comparison of Complex Object Geometries Using a Combination of Electronic Speckle Pattern Interferometric Difference Contouring and Holographic Illumination Elements, Opt. Acta 25, 449.

JONES, R. and WYKES, C., (1981).
General Parameters for the Design and Optimization of Electronic Speckle Pattern Interferometers, Opt. Acta, 28, 949.

JONES, R. and WYKES, C., (1983).
Holographic and Speckle Interferometry, Cambridge University Press, London.

JOYEUX, D. and SABBAN, Y.C. (1982).
High Magnification Self-Imaging, Appl. Opt. 21, 625.

JUTAMULIA, S., LIN, T.W., and YU, F.T.S. (1986).
Real-Time Color-Coding of Depth Using a White-Light Talbot Interferometer, Opt. Comm. 58, 78.

KAFRI, O. and GLATT, I., (1985).
Moiré Deflectometry: A Ray Deflection Approach to Optical Testing, Opt. Eng. 24, 944.

KAFRI, O. and GLATT, I., (1990).
The Physics of Moire Metrology, Wiley Series in Pure and Applied Optics, John Wiley & Sons, New York.

KERR, D., F. MENDOZA SANTOYO, and TYRER, J.R., (1990).
Extraction of Phase Data from Electronic Speckle Pattern Interferometric Fringes Using a Single Phase Step Method: A Novel Approach, J. Opt. Soc. Am. 7A, 820.

KERR, D., RODRIGUEZ-VERA, R., and MENDOZA- SANTOYO, F., (1991).
Surface Contouring Using Electronic Speckle Pattern Interferometry, Proc. SPIE 1554A, 668.

LEENDERTZ, J.A., (1970).
Interferometric Displacement Measurement on Scattering Surfaces Utilizing Speckle Effect, J. Phys. E: Sci. Instrum. 3, 214.

LEGER, J.R. and SNYDER, M.A., (1984).
Real-Time Depth Measurement and Display Using Fresnel Diffraction and White-Light Processing, Appl. Opt. **23**, 1655.

LIVNAT, A. and KAFRI, O., (1983).
Finite Fringe Shadow Moiré Slope Mapping of Diffusive Objects, Appl. Opt. **22**, 3232.

LOHMANN, A.W. and SILVA, D.E., (1971).
An Interferometer Based on the Talbot Effect, Opt. Comm. **2**, 413.

MALACARA, D., Ed., (1992).
Optical Shop Testing, Wiley Series in Pure and Applied Optics, Second Edition, New York.

MAKOVSKI, A., RAMSEY, S.D., and SCHAEFER, L.F., (1971).
Time-Lapse Interferometry and Contouring Using Television Systems, Appl. Opt. **10**, 2722.

MASS, A.A.M., (1991).
Shape Measurement Using Phase Shifting Speckle Interferometry, Proc. SPIE **1553**.

MEADOWS, D.M., JOHNSON, W.O., and ALLEN, J.B., (1970).
Generation of Surface Contours by Moiré Patterns, Appl. Opt. **9**, 942.

MENDOZA SANTOYO, F., SHELLABEAR, M.C., and TYRER, J.R., (1991).
Whole Field In-plane Vibration Analysis Using Pulsed Phase-Stepped ESPI, Appl. Opt. **30**, 717.

MERCER, C.R. and BEHEIM, G., (1990).
Fiber-Optic Projected-Fringe Digital Interferometry, Proc. Conf. on Hologram Interferometry and Speckle Metrology, SEM Publishing, Baltimore, USA. November 5-8, pp. 210-216.

MERTZ, L., (1983).
Real-Time Fringe-Pattern Analysis, Appl. Opt. 22, 1535.

MILES, C.A. and SPEIGHT, B.S., (1975).
Recording the Shape of Animals by Moiré Method, J. Phys. E: Sci. Instrum. 8, 773.

MONTGOMERY, P.C., (1987).
Forward Looking Innovations in Electronic Speckle Pattern Interferometry, Ph.D. thesis. University Of Technology, Loughborough, Leics. England.

MOORE, D.T. and TRUAX, B.E., (1979).
Phase-Locked moiré fringe analysis for automatic contouring of diffuse surfaces, Appl Opt. 18, 91.

MORSHEDIZADEH, M.R. and WYKES, C.M., (1989).
Optical Measurement of Surface Form Using Computer-Generated Referencing, J. Phys. E: Sci. Instrum. 22, 88.

MURAKAMI, K. and MURAKAMI, Y., (1978).
A Study on the Moiré Topography (An Accurate Theory and the Applicable Limit of the Divergent Light Ray Method), Bull. JSME 21, 788.

NISHIJIMA, Y. and OSTER, G., (1964).
Moiré Patterns: Their Application to Refractive Index and Refractive Index Gradient Measurements, J. Opt. Soc. Am. 54, 1.

OWNER-PETERSEN, M., (1991).
Decorrelation and Fringe Visibility: On the Limiting Behavior of Various Electronic Speckle-Pattern Correlation Interferometers, J. Opt. Soc. Am. **8A**, 1082.

PATORSKI, K., (1989).
The Self-Imaging Phenomenon and Its Applications, in: *Progress in Optics*, E. Wolf, Ed., Vol. XXVII, North-Holland, Amsterdam.

PIRODDA, L., (1982).
Shadow and Projection Moiré Techniques for Absolute or Relative Mapping of Surface Shapes, Opt. Eng. **21**, 640.

POST D., (1982).
Developments in Moiré Interferometry, Opt. Eng. **21**, 458.

POST, D., (1985).
Moiré Interferometry for Deformation and Strain Studies, Opt. Eng. **24**, 663.

QUAN, C. and BRYANSTON-CROSS, P.J., (1990).
Double-Source Holographic Contouring Using Fibre Optics, Opt. Laser Tech. **22**, 255.

RASTOGI, P.K., (1984).
Comparative Holographic Moiré Interferometry in Real Time, Appl. Opt. **23**, 924.

RASTOGI, P.K. and PFLUG, L., (1990).
A Fresh Approach of Phase Management to Obtain Customized Contouring of Diffuse Object Surfaces of Broadly Varying Depths Using Real-Time Holographic Interferometry, J. Mod. Opt. **37**, 1233.

RASTOGI, P.K. and PFLUG, L., (1991).
A Holographic Technique Featuring Broad Range Sensitivity to Contour Diffuse objects, J. Mod. Opt. **38**, 1673.

RASTOGI, P.K. and PFLUG, L., (1992).
Holographic Moiré Phase Reinforcement Procedure to Obtain Variable Sensitivity Surface Topographic Mapping: Extension to Phase Stepping, Opt. Laser Tech. **24**, 203.

REID, G.T., (1984).
Moiré Fringes in Metrology, Opt. Lasers Eng. **5**, 63.

REID, G.T., RIXON, R.C., and MESSER, H.I., (1984).
Absolute and Comparative Measurements of Three-Dimensional Shape by Phase Measuring Moiré Topography, Opt. Laser Tech. **16**, 315.

REID, G.T., (1986/87).
Automatic Fringe Pattern Analysis: A Review, Opt. Lasers Eng. **7**, 37.

REID, G.T., RIXON, R.C., MARSHALL, S.J., and STEWART, H. (1986).
Automatic On-Line Measurements of Three-Dimensional Shape by Shadow Casting Moiré Topography, Wear **109**, 297.

REID, G.T., RIXON, R.C., and STEWART, H., (1987).
Moiré Topography With Large Contour Intervals, Proc. SPIE **814**, 307.

ROBINSON, D.W., (1981).
High Resolution Moiré Contouring by a Hybrid Technique Combining Light and Electron Optics, Opt. Laser Tech. **13**, 145.

ROBINSON, D.W., (1983).
Automatic Fringe Analysis with a Computer Image-Processing System, Appl. Opt. 22, 2169.

ROBINSON, D.W. and WILLIAMS, D.C., (1986).
Digital Phase Stepping Speckle Interferometry, Opt. Comm. 57, 26.

RODRIGUEZ-VERA, R., KERR, D., and MENDOZA-SANTOYO, F., (1991a).
3-D Contouring of Diffuse Objects by Talbot-Projected Fringes, J. Mod. Opt. 38, 1935.

RODRIGUEZ-VERA, R., KERR, D., and MENDOZA-SANTOYO, F., (1991b).
Three-Dimensional Contouring of Diffuse Objects Using Talbot Interferometry, Proc. SPIE 1553, 55.

RODRIGUEZ-VERA, R., KERR, D., and MENDOZA-SANTOYO, F., (1992).
Electronic Speckle Contouring (ESC), J. Opt. Soc. Am. A9, 2000.

RODRIGUEZ-VERA, R. and KERR, D., (1992a).
Electronic Moiré Contouring (EMC), Proc. 6th. FASIG Meeting, 14-17 September,Leeds, UK. pp. 31-39.

RODRIGUEZ-VERA, R. and KERR, D., (1992b).
Shape and Deformation Measurements of Diffuse Objects by Electronic Moiré Contouring, Proc. 1st. Iberoamerican Meeting on Optics, 21-23 September, Barcelona, Spain. pp. 604-605.

ROSVOLD, G.O., (1990).
Fast Measurements of Phase using a PC-based Frame Grabber and Phase Stepping Technique, Appl. Opt. 29, 237.

ROWE, S.H. and WELFORD, W.T., (1967).
Surface Topography of Non-Optical Surfaces by Projected Interference Fringes, Nature 216, 786.

SCIAMMARELLA, C., (1982).
Holographic Moiré, an Optical Tool for the Determination of Displacements, Strains, Contours, and Slopes of Surfaces, Opt. Eng. 21, 447.

SERVIN, M. RODRIGUEZ-VERA, R., CARPIO, M. and MORALES, A. (1990).
Automatic Fringe Detection Algorithm Used for Moiré Deflectometry, Appl. Opt. 29, 3266.

SHAMIR, J., (1973).
Moiré Gaugin by Projected Interference Fringes, Opt. Laser Tech. 5, 78.

SHAPIRA, I. and VOLOSHIN A.S., (1992).
Fractional Moiré Fringe Analysis by Optimization, Opt. Eng. 31, 838.

SHUPE, D. and GORMAN, R.P., (1979).
Moiré Inspection of Multicomponent Assemblies, Appl. Opt. 18, 4046.

SUGANUMA M. and YOSHIZAWA, T., (1991).
Three-Dimensional Shape Analysis by Use of Projected Grating Image, Opt. Eng. 30, 1529.

TAKASAKI, H. (1970).
Moiré Topography, Appl. Opt. 9, 1457.

TAKEDA, M., INA, H., and KOBAYASHI, S., (1982).
Fourier-Transform Method of Fringe-Pattern Analysis for Computer-Based Topography and Interferometry, J. Opt. Soc. Am. 72, 156.

TAKEDA, M. and MUTOH, K., (1983).
Fourier Transform Profilometry for the Automatic Measurement of 3-D Object Shapes, Appl. Opt. 22, 3977.

TANG, S. and HUNG, Y.Y., (1990).
Fast Profilometer for the Automatic Measurement of 3-D Object Shapes, Appl. Opt. 29, 3012.

TATAM, R.P., DAVIES J.C., BUCKBERRY C.H., and JONES, J.D.C., (1990).
Holographic Surface Contouring Using Wavelength Modulation of Laser Diodes, Opt. Laser Tech. 22, 317.

THALMANN R. and DANDLIKER, R., (1985).
Holographic Contouring Using Electronic Phase Measurement, Opt. Eng. 24, 930.

THEOCARIS, P.S., (1969).
Moire Fringes in Strain Analysis, Pergamon Press, London.

TOYOOKA, S. and IWAASA, Y., (1986).
Automatic Profilometry of 3-D Diffuse Objects by Spatial Phase Detection, Appl. Opt. 25, 1630.

VARMAN, P.O., (1984).
A Moiré System for Producing Numerical Data of the Profile of a Turbine Blade Using a Computer and Video Store, Opt. Lasers Eng. 5, 41.

VARNER, J.R., (1974).
Holographic and Moiré Surface Contouring, in *Holographic Nondestructive Testing*, R.K. Erf, Ed., Academic Press, New York, Chapter 5.

WASOWSKI, J., (1970).
Moiré Topographic Maps, Opt. Comm. 2, 321.

WINTHER, S. and SLETTEMOEN, G.A., (1984).
An ESPI Contouring Technique in Strain Analysis, Proc. SPIE 473, 44.

WOMACK, K.H., (1984).
Interferometric Phase Measurement Using Spatial Synchronous Detection, Opt. Eng. 23, 391.

WYKES, C., (1977).
De-correlation Effects in Speckle-Pattern Interferometry 1. Wavelength Change Dependent De-correlation with Application to Contouring, Opt. Acta 24, 517.

YOKOZEKI, S. and SUZUKI, T., (1971).
Shearing Interferometer Using the Grating as the Beam Splitter, Appl. Opt. 10, 1575.

YOKOZEKI, S., (1982).
Moiré Fringes, Opt. Lasers Eng. 3, 15.

YONEMURA, M., (1982).
Holographic Contour Generation by Spatial Frequency Modulation, Appl. Opt. 21, 3652.

YOSHINO, Y., TSUKIJI, M., and TAKASAKI, H., (1976).
Moiré Topography by Mean of a Grating Hologram, Appl. Opt. 15, 2414.

ZOU, Y., DIAO, H., PENG, X., and TIZIANI, H. (1992a).
Geometry for Contouring by Electronic Speckle Pattern Interferometry Based on Shifting Illumination Beams, Appl. Opt. 31, 6616.

ZOU, Y., DIAO, H., PENG, X., and TIZIANI, H. (1992b).
Contouring by Electronic Speckle Pattern Interferometry with Quadruple-Beam Illumination, Appl. Opt. 31, 6599.